The Initiation of Action Potentials and the Passive Electrical Properties of Identified Snail Neurones

Alan Robert Kay

A dissertation submitted for the degree of Doctor of Philosophy in the University of Cambridge

Darwin College

March 1984

The Initiation of Action Potentials and the Passive Electrical Properties of Identified Snail Neurones

Alan Robert Kay

A dissertation submitted for the degree of Doctor of Philosophy in the University of Cambridge

Darwin College

March 1984

The Initiation of Action Potentials and the Passive Electrical Properties of Identified Snail Neurones

Alan Robert Kay

Two aspects of neuronal function were investigated: the passive electrical properties of neuronal membranes and the initiation of action potentials.

The passive electrical properties of a neurone, together with its morphology, determine the efficiency of synaptic current transfer to the impulse initiation zone. A general analysis was made of the problems of estimating the electrical properties of a neurone from the measured input impedance with the aid of equations for the input impedance. These equations were used to quantify the error resulting from an idealization of the neurones structure. Furthermore, frequency and time domain methods for electrotonic parameter estimation were contrasted and frequency domain methods were shown to be less susceptible to error.

Frequency domain methods were applied to the problem of estimating the electrotonic parameters of some identified neurones of the garden snail. The membrane time constants for the group of neurones studied had an average value of 43 ms.

The nonlinear properties of snail neurones were characterised by measuring the harmonic content of the voltage response to a sinusoidal current input. The model so deduced accounted for the response of neurones for inputs with peak-to-peak amplitudes up to 2 nA, but the form of the input showed a strong dependence on the DC bias of the input.

In the second part of this thesis stochastic and deterministic signals were used to characterise and model the dynamics of spike initiation. Neurones were stimulated with Gaussian white noise current signals. Records of the action potentials evoked, together with the input noise allowed measurement of the characteristics of the current trajectories that lead to the initiation of action potentials. These records were analysed in the framework of Wiener's theory of nonlinear systems, to obtain a model of the current-to-spike transformation. The models were similar in form to that of a low-pass filter in cascade with a threshold device and predicted 60 to 80 % of the observed action potentials. The spiking behaviour evoked by step current inputs was contrasted with that produced by Gaussian white noise and the dynamics of the neurone were shown to depend on the form of the input used.

for my parents

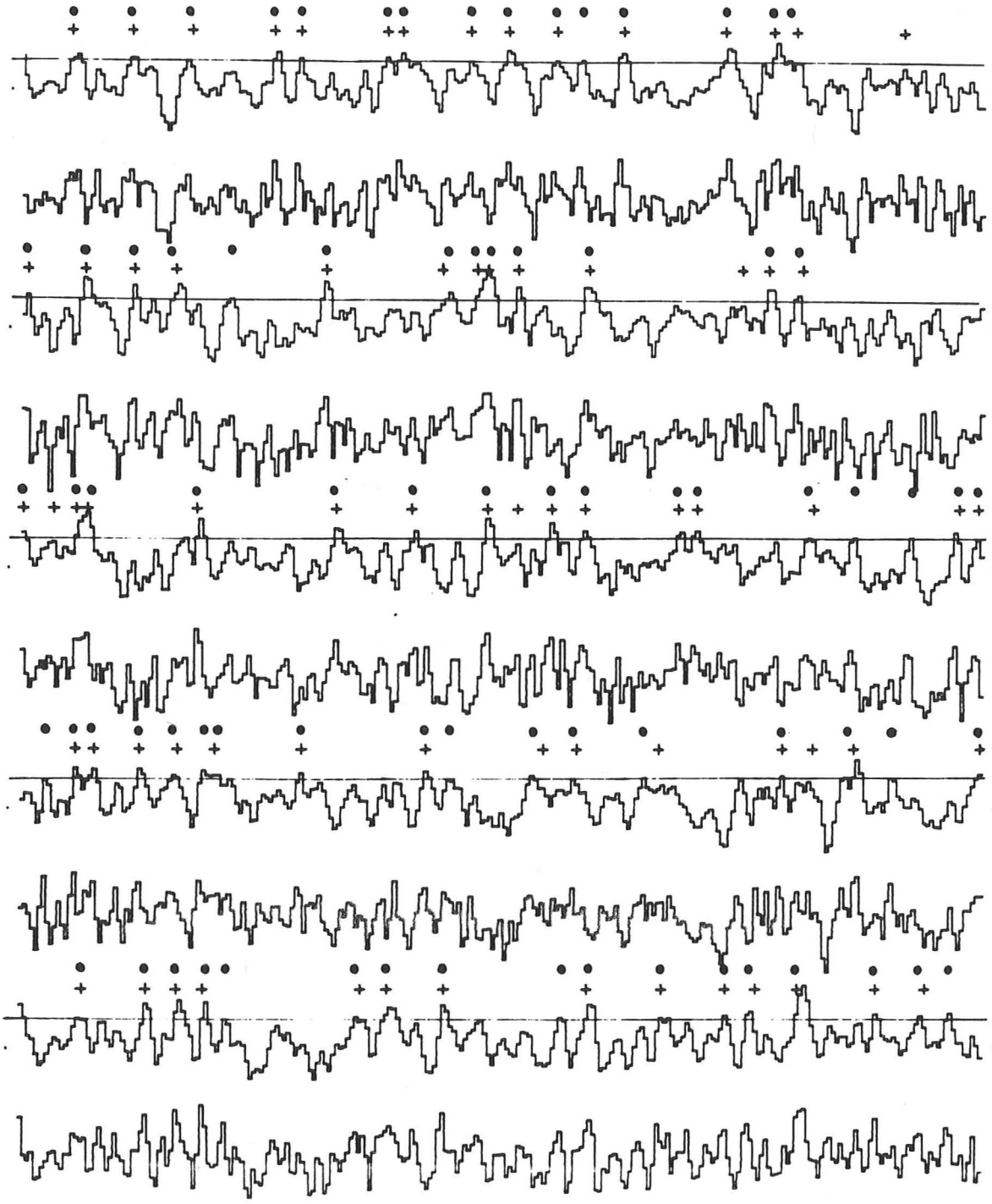

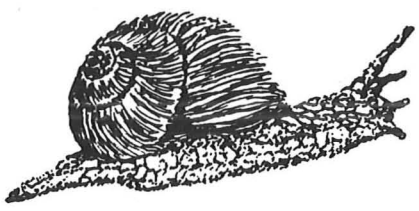

TABLE OF CONTENTS

PREFACE

This thesis describes work carried out between October 1979 and November 1982 in the Department of Zoology in Cambridge University. This dissertation is the result of my own work and includes nothing which is the outcome of work done in collaboration. I am grateful to Professor G. Horn for making the facilities of the Department freely available to me and to the Cambridge Philosophical Society for a Studentship.

I thank my supervisor, Dr. Malcolm Burrows for his support. I am also grateful to Dr. John Art, Dr. Josephine Gibson, Dr. Ken Machin and Dr. Alan Watson for their close reading of parts of this thesis. Thanks also go to Steve Buckingham, Rob Elson, Dr. Bob Meech, Dr. Claire Rind, Dr. Melody Siegler and Dr. Branwyn Watkins for valuable discussions. I am much indebted to Dr. P. J. W. Rayner (Dept. Engineering) for suggesting the use of Goertzel's algorithm. I would like to thank Dr. Roger Moreton and Dennis Unwin for their invaluable advice on computers and electronics.

I would also like to thank Dr. Brad Amos, Peter Barlow, Neil Maskell, Frances Pang and Ray Symonds. for their assistance. Thanks also to Ron Hughes and Mandy Randall for their help in the library.

I owe a special debt to Harriet Snape who hunted not only the snails, but also the syntactic snarls.

SYMBOLS

a = cable radius

C_m = capacitance per unit area of membrane (F cm^{-2})

c_m = $2\pi a C_m$ = membrane capacitance per unit length of cable

f = frequency (Hz.).

G_s = conductance of soma

$i(t)$ = current

$I(s)$ = Laplace transform of current.

j = $(-1)^{1/2}$

$K_{ij}(j\omega)$ = transfer impedance between points j and i on cable.

$k_{ij}(t)$ = Fourier transform of $K_{ij}(j\omega)$.

P = power of GWN signal

R_i = intracellular resistivity.

r_a = $R_i/\pi a^2$ = intracellular resistance to axial flow of current along a cable

R_m = resistance of unit area of membrane (Ω cm^2).

r_m = $R_m/2\pi a$ = membrane resistance of unit length.

s = Laplace transform variable.

t = time

$v(t)$ = transmembrane potential

$V(s)$ = Laplace transform of $v(t)$

Z = r_a/γ = characteristic impedance of cable

γ = $(1+j\omega\tau_m)^{1/2} / \lambda$ = propagation constant

λ = $(r_m/r_a)^{1/2}$ = space constant.

ω = $2\pi f$ = angular frequency (rad/sec).

ϱ = $\varrho_\infty \tanh(L)$

ϱ_∞ = $1/(r_a \lambda G_s)$.

σ_x = standard deviation of GWN signal

τ_m = $R_m C_m$ = membrane time constant.

ABBREVIATIONS

ACT = Average current trajectory

B&C = Butz and Cowan (1974)

GWN = Gaussian white-noise

Lpr = Left parietal

Rpr = Right parietal

CHAPTER 1

INTRODUCTION

1.1. NEURONES AND NETWORKS

It is a commonplace assumption that the operation of a neuronal network can in principle be explained in terms of the properties of the component neurones and their interactions. Any assay of this supposition is crucially dependent on the way in which the neurones are represented; an elaborate representation might render the test impracticable, while a simpler one might omit features essential to the networks operation. This thesis is an attempt to model the input-output characteristics of identified molluscan neurones.

It is difficult to avoid the conclusion that any such representations must be mathematical, for the simple reason that there is no other way of predicting the operation of a complex interconnected network. Even a verbal description would have to be transformed into some form of mathematical formalism, however primitive, to predict the working of a neuronal network.

A related problem is that of locating the appropriate level at which to base the neuronal representation. For example, it would be inappropriate to attempt to reconstitute the input-output properties of a neurone from the quantum mechanics of its component molecules. It may seem more fitting to deduce a neurone's dynamics from the kinetics of the component ionic channels. Even this project would be daunting: not only would it be necessary to measure the kinetics of all types of channels in the neurone and reveal the neurone's morphology, but it would also be necessary to measure the detailed density distribution of

all channel types (Skaugen & Walloe, 1979). Furthermore mathematical models at this level of representation prove to be very time- consuming to solve (Joyner et al. 1978).

These considerations drive one back to what is essentially a classical neurophysiological method (Lapique, 1907; Lucas, 1917), namely the search for purely phenomenological models of neuronal activity. For example, spike initiation might be represented as a integrator circuit in cascade with a threshold device. This model has no direct relationship to the structure of the neurone; it simply attempts to reproduce the input-output properties of the neurone.

1.1.2. MODELLING NEURONES

Some theoretical treatments of neural systems assume that their function derives principally from the connectivity of the neurones, while all the component neurones are treated as simple stereotyped units (Conrad et al., 1974; Amari, 1974). Often the neurone is modelled as a threshold device that responds to the instantaneous value of the sum of the inputs - the so-called "logical neurone" (McCulloch & Pitts, 1943). McCulloch and Pitts (1943) demonstrated that any process that can be described by an algorithm can be emulated by a machine composed of logical neurones. It is, however, likely that for any given process there will be many different ways of realising the circuitry using logical neurones. It is therefore hazardous to attempt to derive the neuronal basis of behaviour simply from a system's input-output properties.

Neurones are much more complex than the logical neurone model would suggest. Besides omitting the important category of

all channel types (Skaugen & Walloe, 1979). Furthermore mathematical models at this level of representation prove to be very time- consuming to solve (Joyner et al. 1978).

These considerations drive one back to what is essentially a classical neurophysiological method (Lapique, 1907; Lucas, 1917), namely the search for purely phenomenological models of neuronal activity. For example, spike initiation might be represented as a integrator circuit in cascade with a threshold device. This model has no direct relationship to the structure of the neurone; it simply attempts to reproduce the input-output properties of the neurone.

1.1.2. MODELLING NEURONES

Some theoretical treatments of neural systems assume that their function derives principally from the connectivity of the neurones, while all the component neurones are treated as simple stereotyped units (Conrad et al., 1974; Amari, 1974). Often the neurone is modelled as a threshold device that responds to the instantaneous value of the sum of the inputs - the so-called "logical neurone" (McCulloch & Pitts, 1943). McCulloch and Pitts (1943) demonstrated that any process that can be described by an algorithm can be emulated by a machine composed of logical neurones. It is, however, likely that for any given process there will be many different ways of realising the circuitry using logical neurones. It is therefore hazardous to attempt to derive the neuronal basis of behaviour simply from a system's input-output properties.

Neurones are much more complex than the logical neurone model would suggest. Besides omitting the important category of

nonspiking neurones (Bush & Roberts, 1981), the logical neurone model also does not account for the nonlinear interaction between converging synaptic inputs. Furthermore, it reduces spike initiation to a simple threshold crossing event, whereas the multiplicity of complex time dependent phenomena associated with spike initiation (eg. adaptation, accommodation, rebound excitation, plateauing and spike failures), suggests a need for more elaborate models.

This thesis attempts to characterise the input-output properties of some identified snail neurones by finding mathematical functions that map the input in the form of synaptic current, into an output in the form of spikes or synaptic potentials. It is not possible to measure directly the overall input-output function, because the voltage at all points in the neurone cannot be sampled. This problem can be circumvented by representing the overall neuronal input-output function as a cascade of operationally separable process, each represented by a single input-output function, termed here a *transfer function*.

Following Calvin and Graubard (1979) four types of transfer functions are defined, as follows;

(1) The *Synaptic* transfer function describes the transformation of presynaptic voltage into postsynaptic current. It encompasses all processes, from the initiation of neurotransmitter release to the postsynaptic conductance change, and should include all time dependent effects like facilitation and depression.

(2) The *Electrotonic* transfer function transforms current injected at one site on the dendrite to voltage at another in the same neurone. To take into account interaction between synapses, all synaptic sites should be linked by transfer functions to all

others. Furthermore, the spike initiation zone should be linked by electrotonic transfer functions to all synaptic input and output sites, to include the effect of the retrograde invasion of the action potential.

(3) The *Spike initiation* transfer function converts current at the spike initiation zone into action potentials. This transfer function may be represented as a simple threshold device or it may be a more complex function of the input current.

(4) The *spike propagation* transfer function describes the transformation of action potentials at the impulse initiation zone into action potentials at the nerve terminals. In the simplest case it is a time delay element. In more complex cases, it may be necessary to take into account changes in the propagation velocity resulting from the interaction between spikes (Swadlow et al, 1980).

Figure 1 illustrates how a simple neuronal network can be represented by the four transfer functions. In subsequent chapters it is shown how the transfer functions can be represented mathematically.

1.1.3. TWO CAVEATS

It should be noted that although it may be possible to predict the operation of a neuronal network from the properties of its parts, such a simulation of a system does not necessarily disclose its function. For example, a computer simulation of a radio may correctly predict the voltage at all points in the circuit, but it would leave someone ignorant of electromagnetic radiation no wiser as to what a radio actually does. Considerations of this kind reinforce Marr and Poggio's (1977)

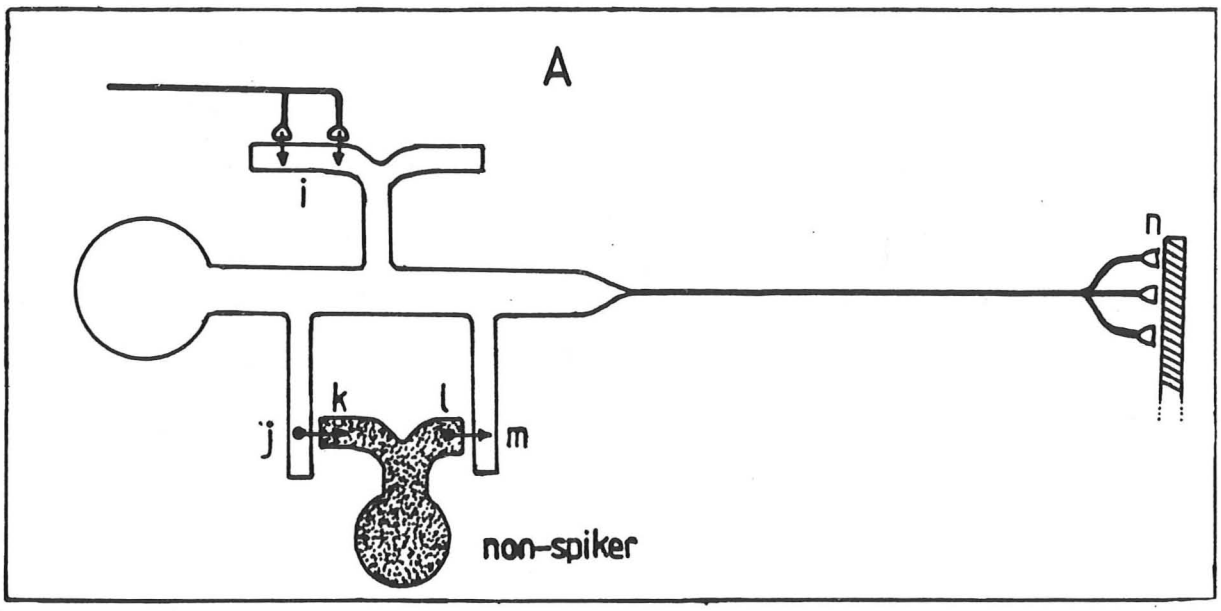

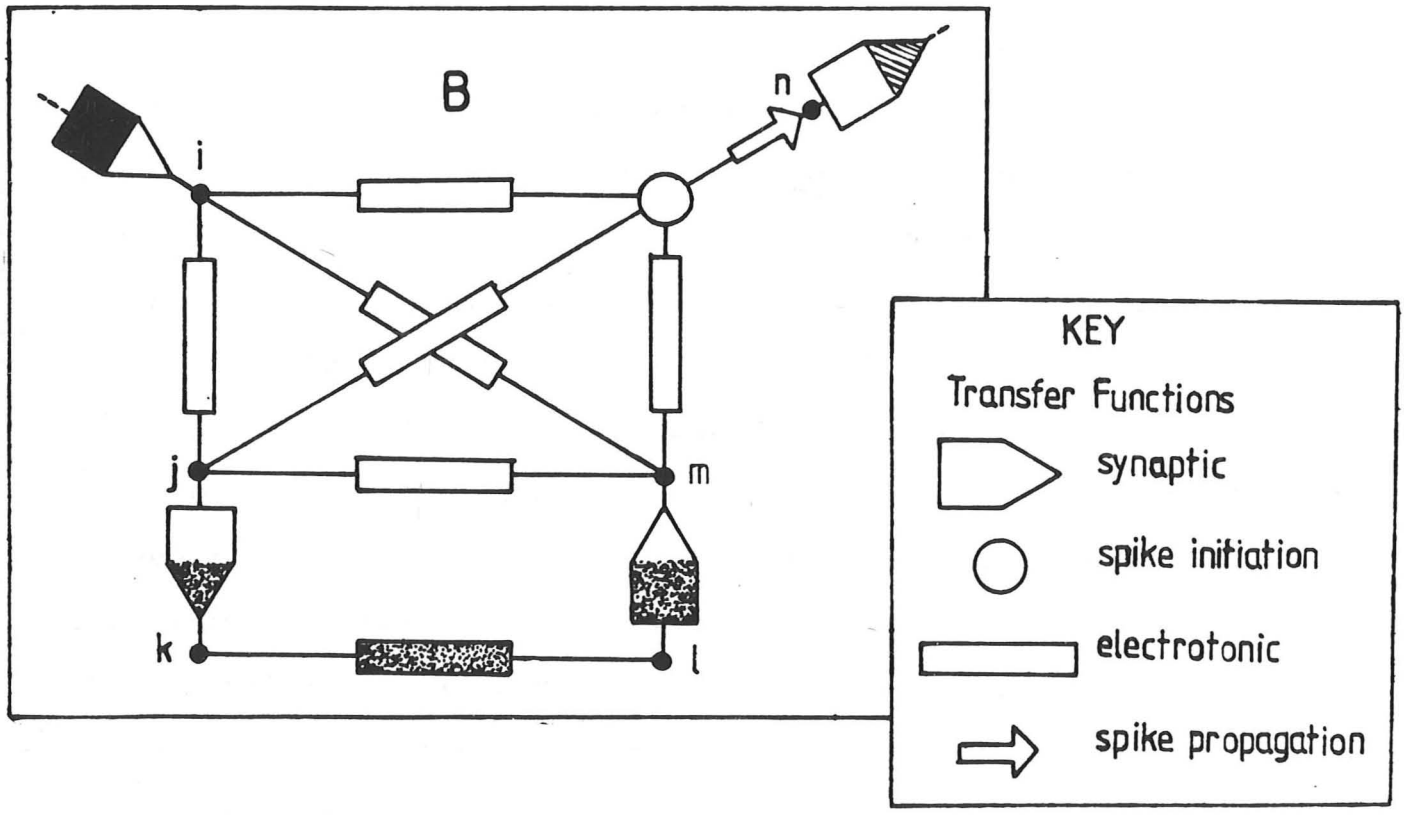

Figure 1.1 (A) Hypothetical neuronal circuit. (B) Representation of the neuronal circuit depicted in A, using transfer functions. (Synaptic transfer functions have been divided into a postsynaptic and presynaptic elements. Shading indicates the correspondence of the parts in figures A and B.)

plea for a multiplicity of approaches to neural systems, at both the whole system and at the neuronal level.

Only deterministic neuronal representations will be considered in this work; however it should be recognized that neurones are intrinsically stochastic and that this may contribute in a significant way to the sort of operations the neuronal networks can perform (Holden, 1976). For example, it has been shown for learning automata, constructed from logical neurones, that a certain class of problems can be solved by stochastic automata, but not by deterministic ones (Mars & Poppelbaum, 1981).

1.2. OUTLINE OF THESIS

With the development of techniques for reliably staining neurones, it has become routine to reveal a neurone's morphology and to measure its physiological properties. The literature is replete with detailed drawings of identified neurones in invertebrate ganglia (eg. molluscs; Winlow & Kandel, 1976 ; Haydon & Winlow, 1981 : arthropods; Siegler & Burrows, 1979 ; Sigvardt et al. 1982), but morphology alone does not disclose the strength of the electrical coupling between various parts of a neurone. However, from a knowledge of the resistance and capacitance of the neurone's membrane it is possible to translate these details of morphology into predictions about the attenuation of synaptic potentials between any two points on the dendritic tree.

The first part of this work considers the general problem of estimating the passive electrical properties of neurones. In chapters 2 and 3, equations representing the electrical properties of neurones are derived, that are then used to develop

techniques for measuring the electrical properties of neurones. Particular attention is given to estimating the reliability of these techniques. The methods so developed are applied in chapter 4 to the measurement of the passive electrical properties of some identified snail neurones. In chapter 5 a method is devised for quantifying the nonlinear properties of neuronal membranes.

The second part of this thesis is devoted to the phenomenological characterization of spike initiation. Both deterministic and noise signals are used, to probe the process of spike initiation, and to aid in the formulation of models of the input current-to-spike transformation.

1.3. SYSTEM IDENTIFICATION

Much of this thesis is concerned with the formulation and verification of models. As both these processes are complex and hazardous, this section attempts to clarify the activity of model building.

The relationship of models to reality is complex, and in practice bears little resemblance to the simple inductivist view that theories derive in some straightforward way from observations. There is inevitably a complex interplay of theory and observations, the one conditioning the other. However I shall not dwell on the origins of models, as this is largely a question of creativity, but in what follows I shall examine the various stages in the verification of a model.

Following the terminology of Eykhoff (1974), the mathematical representation of a system is referred to as a *model*, and the total process of establishing and confirming a model is called *System Identification*.

1.3.1. WHY MODEL?

There are two main reasons for wanting to model a system,

1.3.1.1. *System Representation.* One may need a compact mathematical model that replicates the input-output dynamics of the system, either as an aid to understanding the nature of the transformation performed on the input, or as an element in the simulation of some larger system. For example, accurate representations of the dynamics of single neurones could be useful in the understanding of the operation of neuronal networks.

When attempting to reproduce the dynamics of a system, the form of the mathematical equations need have no direct relationship to the structure of the system: the model is judged solely on the grounds of its ability to reproduce the input-output dynamics of the system.

1.3.1.2. *Parameter Estimation.* Alternatively a model may be used to estimate aspects of the system which are not open to direct measurement. For example, a model of a neurone's passive electrical properties provides a link between the measured input impedance and the unit membrane resistance, a quantity that cannot be measured directly in a nonspace-clamped neurone (Jack, Noble & Tsien 1975).

Models used for parameter estimation, if accurate, should reproduce the system's input-output dynamics. However, for the reliable estimation of the system's parameters, the assumptions underlying the derivation of the model should be tested independently, since a correspondence between the input-output properties of the system and the model is not in general an

adequate test of these assumptions.

1.3.2. MODEL SPECIFICATION

Calculating the response of a given mathematical model to any input is straightforward, if one is prepared to accept a numerical solution. However, the inverse problem of specifying the form of the model given the input-output data of the system, is far more difficult. Indeed it is not possible to deduce a model of the system that has a direct relationship to its internal structure by using an algorithmic procedure, operating simply on the input and output of the system (Marmarelis & Marmarelis, 1978). Models that mirror the internal structure of the system can only be derived from prior information about the structure of the system.

These considerations lead to a distinction between two sorts of models, nonparametric and parametric models:

1.3.2.1 *Nonparametric models*. No assumptions are made about the internal structure of the system (ie. it is treated as a 'black box'), and the system's input-output properties are modelled as a series approximation, which has no direct relationship to the structure of the system. This form of model is often part of a system identification procedure which prescribes the form of the input and a method for estimating the terms of the series approximation. An example of this form of procedure is described in more detail in chapter 6.

1.3.2.2. *Parametric* models are derived from information, or from a conjecture, about the structure of the system, rather than directly from the input-output properties of the system. An example of this class of model is encountered in cable theory in which information about a neurone's shape and electrical

properties, together with the laws of electrical current flow, are used to derive a partial differential equation linking current input and voltage output (Jack, Noble & Tsien, 1975).

1.3.3. PARAMETER ESTIMATION

Assuming that the form of a parametric model is known and that there is no simple algebraic relationship between the system parameters and the system output, the parameters can be estimated by minimizing the difference between the output of model and the response of the system. The difference between the model and the system output is quantified by an error statistic, normally taken to be the sum of squares of the difference between the model ouput and the measured output (Grove et al.,1980). This process of parameter estimation can be visualized by considering a two parameter model: if the error statistic is plotted as a function of the two parameters, a surface in three-dimensional space is obtained, and if a unique solution exists, the surface has a global minimum.

The shape of the error surface is dependent not only on the form of the model, but also on the type of input used to perturb the system. Therefore the choice of input signal can influence the variance of the estimated parameters (Swanson, 1977), and can also influence the rate of convergence of the routine that searches for the solution (Nicola et al., 1980).

1.3.4. ERRORS OF PARAMETER ESTIMATION

Once a model has been selected, it may seem natural to pass on immediately to parameter estimation. However, if the estimated parameters are to have any meaning, the structure of the model itself ought to be explored beforehand. Three possible sources of

error in parameter estimation are considered in the following subsections.

1.3.4.1 SYSTEM IDENTIFIABILITY

The models encountered in biological problems are often rate or diffusion equations, and there is often no simple algebraic relationship between the system's output and the model's parameters. It is not always obvious from the form of the mathematical model, whether or not a unique parameter set exists. A model is said to be *structurally identifiable* if a unique parameter set does exist (Bellman & Astrom, 1970)

Parameter estimation should not be attempted with a model that is not structurally identifiable, because although it may be possible in this case to estimate a set of parameters, there may be infintely many parameters consistent with the data. (Swanson (1977) and Zierler (1981) give examples from the biological literature where this error has been committed.)

The problem of deciding whether or not a model is structurally identifiable is complex: even the simplest case, that of linear systems, poses considerable problems for mathematicians (Nguyen & Wood, 1982). Some specific examples of structural identifiability are raised in chapters 2 and 4.

1.3.4.2. PARAMETER SENSITIVITY

Structural identifiability is concerned with the idealized situation where the data is free from noise. Noise will have the effect of decreasing the accuracy of the estimated parameters. The relationship between the noise and the accuracy of the parameters is determined by the nature of the model , and it is as well to investigate this relationship prior to parameter estimation, because it might be that the parameters to be

estimated are so sensitive to noise as to render their measurement meaningless (Grove et al., 1980).

The effect of noise can to a certain extent be minimized by an appropriate choice of the form of the input signal, because as was mentioned above, the shape of the error surface, and consequently the parameter's variance, is partially determined by the form of the input (Swanson, 1977).

1.3.4.3. MODELLING ERRORS

Simplifying assumptions are often introduced into a model to render the mathematical equations more tractable. If the correspondence of the assumptions to the system is poor, the estimated parameters will be in error. This so-called modelling error can be calculated if the detailed version of the model can be solved. Examples of such calculations are given in chapter 2.

CHAPTER 2

FREQUENCY DOMAIN ELECTROTONIC THEORY

2.1. INTRODUCTION

The input impedance measured from the vantage point of the soma contains information about the cell's electrical properties and shape. In this chapter the influence of neuronal morphology and electrical properties on the input impedance are explored using analytic expressions for the input impedance derived by the method of Butz and Cowan(1974) (see below). These equations are also used to define the theoretical limits to the reliable estimation of the electrotonic properties of a neurone from the measured input impedance.

The view from the soma will be pursued because it is often the only site from which reliable recordings may be made. In addition, when estimating electrotonic parameters, it is essential to know the location of the electrode, and this, in most cases, is only possible for the soma.

2.1.1. LINEARITY IN THE FREQUENCY DOMAIN

A system is linear if, for all possible sinusoidal inputs, the steady-state response is a sine wave with the same frequency as the input. The output may have a different amplitude and its phase may be shifted with respect to the input. In addition the ratio of the input to output amplitude must be independent of the input amplitude. If the output contains frequency components that were not present in the input, then the system is nonlinear.

Measurement of the magnitude and phase of the ouput over a range of frequencies defines the transfer function (or impedance

if the input is current and the output voltage), which provides a complete description of the system, in that it can be used to calculate the response to any input. The transfer function, because it is represented as a function of frequency, is termed a 'frequency domain' representation. An alternative complete description of a linear system is provided in the time domain by the response of the system to a unit impulse input. The time and frequency domain representation of the systems are equivalent in that they are Fourier transforms of one another (Bracewell, 1965), however parameter estimation often proves simpler and more reliable when the system is represented in the frequency domain (Diamond & Machen, 1983).

2.1.2. ORGANIZATION OF CHAPTER

This chapter is divided into three sections. The first part describes a method for translating the neurone's morphology into an algebraic representation of its linear electrotonic properties. In part two the frequency domain behaviour of some simple circuits are described and these are then used to facilitate the understanding of more complex electrotonic structures. In the third section the input impedance expressions ar used to explore the influence of data accuracy and modelling errors on parameter estimation.

2.2. THE BUTZ & COWAN GRAPHICAL CALCULUS

Butz and Cowan (1974, abbreviated as B&C) developed a graphical calculus for deriving the transfer impedance between any two points on a linear dendritic tree. The current-to-voltage transfer function $K_{ij}(s)$, relates the voltage output at site i, to the current input at site j, as follows:

$$V_i(s) = K_{ij}(s) I_j(s) \qquad (1)$$

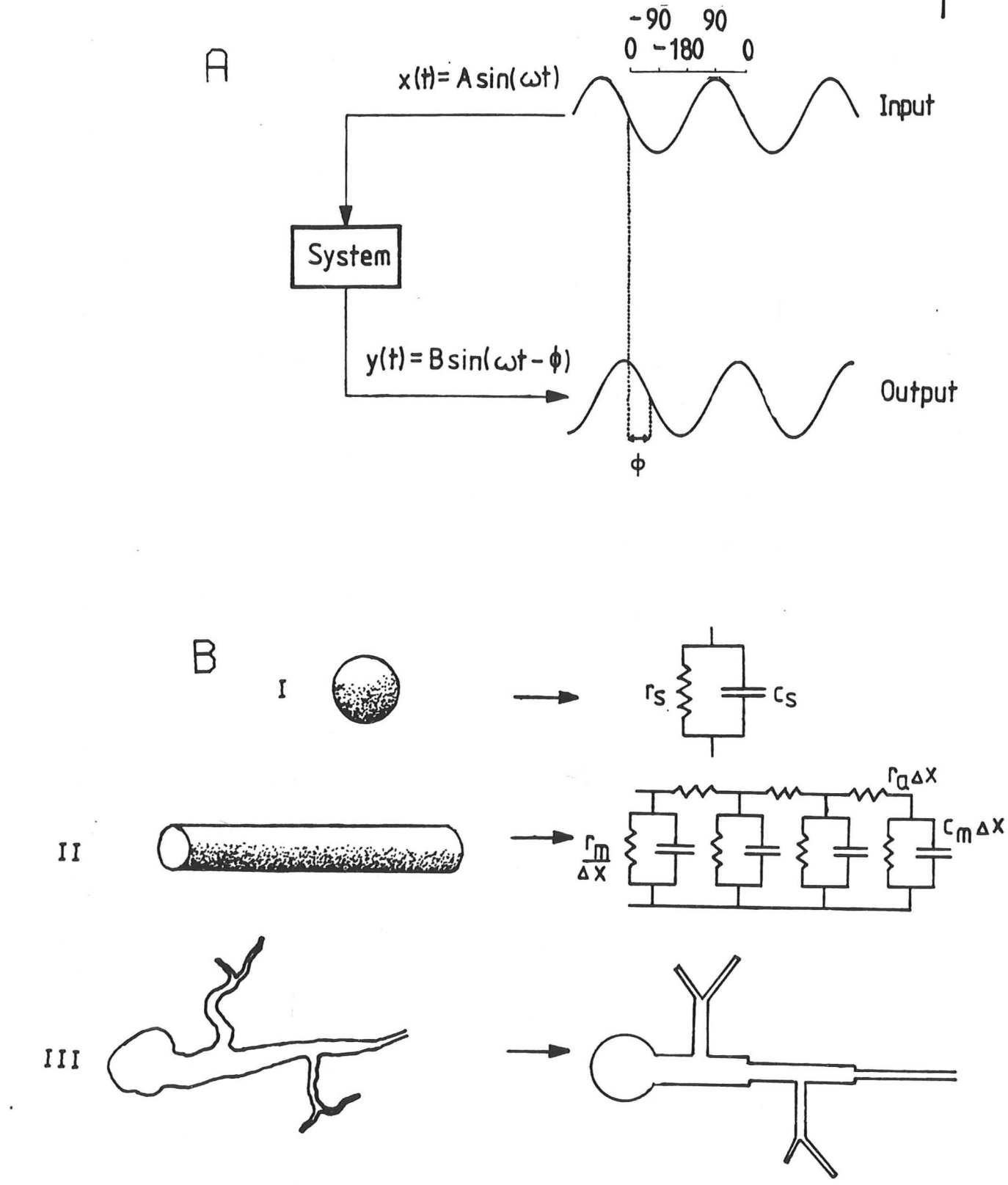

Figure 2.1. (A) The input-output relationship of a linear system. (B) Some simple electrotonic objects and their equivalent circuits. The membrane of all structures has a unit resistance, R_m, and capacitance per unit area of C_m. (Δx=length increment) (I) isopotential soma of radius b, $r_s=R_m/4\pi b^2$ & $c_s=4\pi b^2 C_m$. (II) finite cable of radius a, $r_m=R_m/2\pi a$, $r_a=R_a/\pi a^2$ & $c_m=2\pi a C_m$. (III) Hypothetical neurone approximated by a structure composed of cylinders.

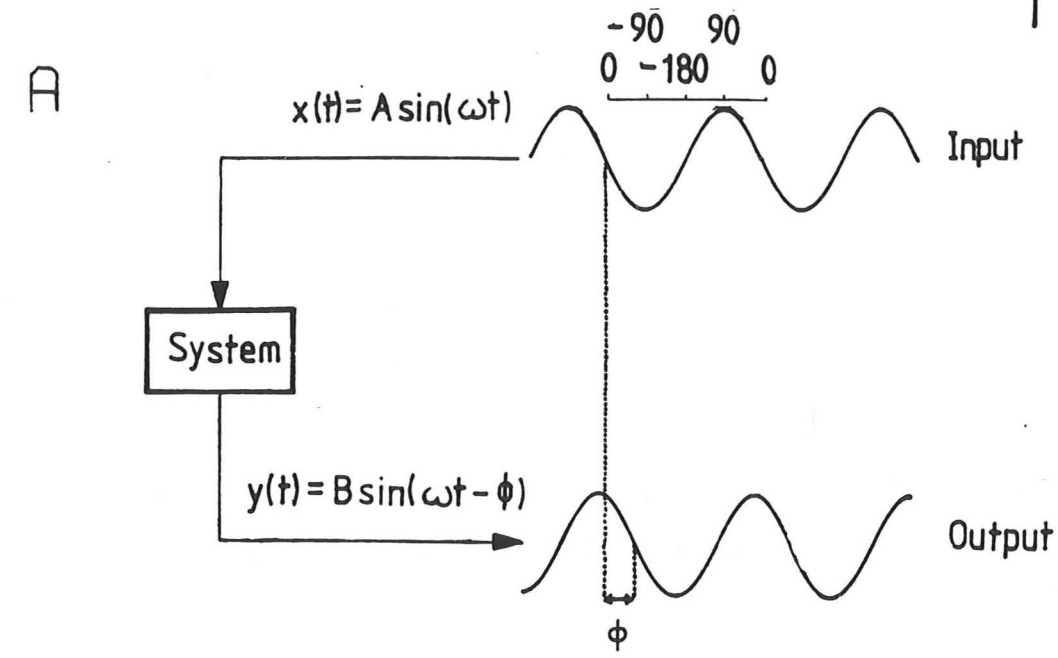

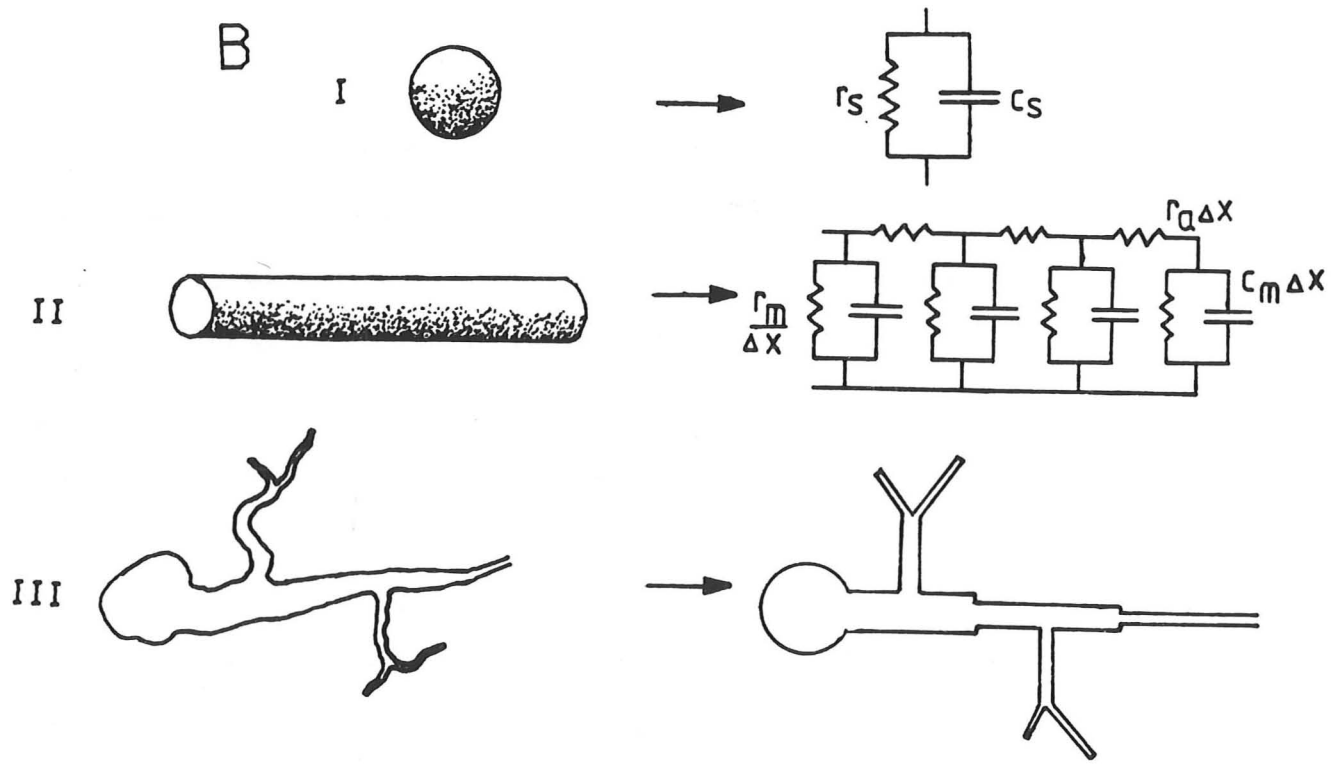

Figure 2.1. (A) The input-output relationship of a linear system. (B) Some simple electrotonic objects and their equivalent circuits. The membrane of all structures has a unit resistance, R_m, and capacitance per unit area of C_m. (Δx=length increment) (I) isopotential soma of radius b, $r_s=R_m/4\pi b^2$ & $c_s=4\pi b^2 C_m$. (II) finite cable of radius a, $r_m=R_m/2\pi a$, $r_a=R_a/\pi a^2$ & $c_m=2\pi a C_m$. (III) Hypothetical neurone approximated by a structure composed of cylinders.

where $V_i(s)$ and $I_j(s)$ are the Laplace transforms of the voltage and current respectively and s is the Laplace transform variable. (s can be replaced by $j\omega$, where $j = (-1)^{1/2}$ and ω is the frequency in radians per second (Bendat & Piersol, 1971).

The transfer impedance is a complex function, its magnitude is the ratio of the amplitude of the output sinusoid to that of the input. The phase of the transfer impedance is the phase shift between an output and input at frequency ω. These relationships for a linear system are displayed in fig 1A.

The time domain expression equivalent to equation 1 is,

$$v_i(t) = \int_0^{\infty} k_{ij}(\tau) i_j(t-\tau) d\tau \qquad i(t)=0 \text{ for } t \leq 0 \qquad (2)$$

where the lower case letters are the Laplace transforms of the equivalent symbols in equation 1. As a mathematical expression, this is clearly more difficult to evaluate than the frequency domain equivalent, equation 1. In addition, it is only possible to invert $K_{ij}(j\omega)$ for some simple symmetrical trees dendritic (Jack & Redman, 1971; Horwitz, 1981 & 1983) . On the other hand $K_{ij}(j\omega)$ can be found analytically for an arbitrarily complex dendritic tree.

In the derivation of the graphical calculus Butz and Cowan drew on the standard assumptions of linear cable theory. These assumptions have been discussed and justified by Rall (1977) and Jack, Noble & Tsien (1975), and will hence only be reproduced here. The assumptions are,

(1) The unit membrane can be represented by a linear impedance.

(2) The intracellular medium provides a purely ohmic resistance

to current flow.

(3) The extracellular resistance is negligible.

These assumptions imply that a dendritic process with uniform diameter, much less than the space constant, can be represented by a one-dimensional cable (see fig.1B II), while a cell body with a diameter much less than the space constant can be represented by an isopotential compartment (see fig.1B I)

The B&C method can be applied to any dendritic tree that can be approximated by a structure composed of cylinders with uniform electrotonic properties (see fig 1B III). In this exposition of the method the unit membrane is assumed to be a resistance and capacitance in parallel (R-C), however in appendix A the method is generalized to include the case of an arbitrary membrane impedance. In the B&C calculus the unit membrane impedance may be non-uniform and there are no restrictions on the radii at branch points.

The B&C procedure translates a diagram of a dendritic tree into a transfer impedance connecting any two points on the tree. The elements of the calculus, termed here 'building blocks', are two components of trees, namely, branches (unbifurcated cable) and triads (bifurcated cable). The building blocks are treated as algebraic entities that are manipulated according to a set of rules, the end result of which is a symbolic equivalent of the transfer impedance. The building blocks are then replaced by their mathematical equivalents to produce the input impedance in its analytic form.

The B&C method will be given in full because a few innovations to the method have been introduced and an error in the original paper has been corrected.

2.2.1. THE BUILDING BLOCKS

The building blocks and their various manifestations are defined in the following table . When using the B&C method it is only necessary to remember the symbolic representation.

NAME		SYMBOL	MATHEMATICAL REPRESENTATION
Branch	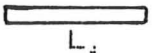	$[L_i]$	$Z_i \sinh(\gamma L_i)$
Triad	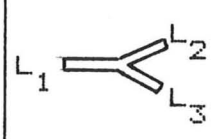	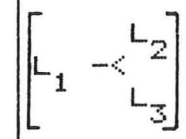	$Z_1 Z_2 [L_1] [L_2]^* [L_3]^*$ $+ Z_1 Z_2 [L_1]^* [L_2] [L_3]$ $+ Z_2 Z_3 [L_1] [L_2] [L_3]$

Where: $Z_i = r_a / \gamma$ = characteristic impedance of cylinder i

$r_a = R_i / \pi a^2$

$\gamma = (1+j\omega\tau m)^{1/2} / \lambda$ = propagation constant

a = cable radius

$\lambda = (R_m a / 2 R_i)^{1/2}$ = length constant

R_i = intracellular resistivity.

$\tau m = Rm.Cm$ = membrane time constant

Rm = Unit membrane resistance

Cm = capacitance per unit area of membrane

l_i = Physical length of cylinder i

$L_i = l_i / \lambda_i$ = Dimensionless electrotonic length of cylinder i

* - Denotes an operation, 'complementation' which has the effect of changing all occurrences of sinh to cosh and vice versa.

It is assumed that for each segment the following parameters are known; L,a,Rm,Cm and Ra.

2.2.2. BRANCH TERMINATIONS

To derive the transfer impedance of a dendritic tree it is

necessary to specify the impedance at the termination of all branches. Within the B&C calculus there are three ways of terminating a branch. Firstly the termination may be a parallel R-C circuit, which is termed a 'leaky' termination and is represented in diagrams by '-O'. Then there are two special cases of the leaky termination: the 'closed-circuit' termination, with the resistance and capacitance both zero (represented as an unadorned branch tip '-') and the 'open-circuit' termination, with an infinite resistance at the tip (represented in diagrams by '⊣').

A leaky termination may be used to represent an isopotential soma or a branch terminated with a disk of membrane having the same impedance as the rest of the cable. Whenever a tip is designated a leaky termination, all the symbolic representations of the branch (eg. [x]) must be replaced by [O-x] where the mathematical equivalent of this term is,

$$[O\text{-}x] \equiv Z\sinh(\gamma x) + Z_o\cosh(\gamma x) \qquad (3)$$

Where $Z_o = 1/(sC_o+G_o)$; G_o = Conductance of the tip and C_o = Capacitance of the tip.

Additional configurations may be derived from the basic building blocks by the introduction of the notion of a 'virtual branch'. This is a branch with zero length and, where appropriate, a closed tip. The virtual branch is denoted by a dashed line. Consider the representation of cables that undergo a diameter change and a trifurcation respectively:

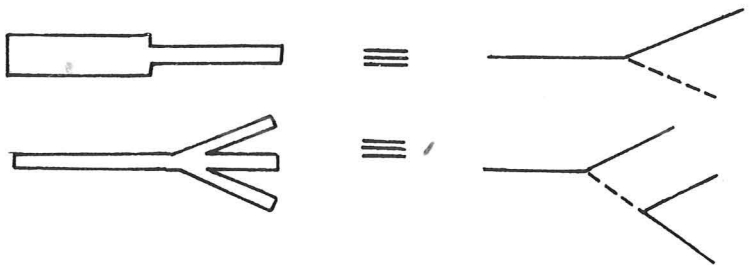

It is important for the derivation of the transfer function, to hang onto the virtual branch until the derivation is completed, and only then can it be eliminated by substituting L=0.

In what follows the B&C calculus is represented as a set of rules in the form of a flow chart on the left-hand side of the page and on the right-hand side of the page the appropriate manipulations are performed on a dendritic tree.

2.2.3. THE RULES

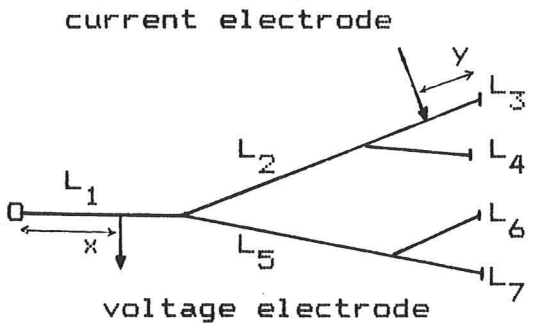

Draw a 'stick' representation of the neurone. Denote tip conditions and position of soma . Position recording and current passing electrodes.

Assume initially that all tips that do not have a leaky termination, have a closed-circuit termination

The numerator and denominator of the transfer impedance are derived in turn.

NUMERATOR

Delete branches on the direct line between the two electrodes. The numerator is composed of the product of two terms:

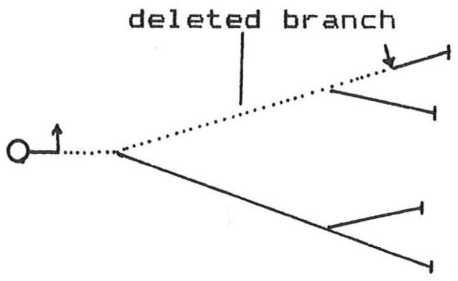

(i) The product of all characteristic impedances (Z_i) of branches that lie on a deleted branch point. A given branch may be represented no more than twice in this term.

$$Z_1 Z_2^2 Z_4 Z_5 Z_3$$

(ii) The product of the symbols of all the remaining bits of the tree. Symbols more complicated than the building blocks are simplified in the same way as those in the denominator, as demonstrated below.

$$[O\text{-}x]\left[L_5 -\!< \begin{matrix} L_6 \\ L_7 \end{matrix}\right][L_4][y]$$

DENOMINATOR

The denominator is the representation of the whole tree.

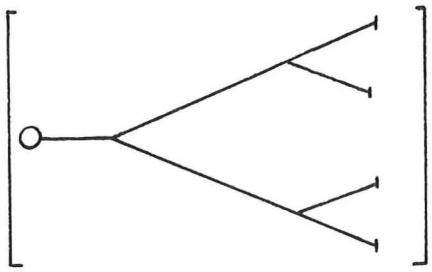

The denominator is simplified by taking the ' ⊛ ' product of all the component triads of the tree. Where ⊛ represents multiplication in the ordinary sense, save that when the same branch is involved in

$$\left[O\text{-}L1 < \begin{matrix} L_2 \\ L_5 \end{matrix}\right] \circledast \left[L2 -\!< \begin{matrix} L_3 \\ L_4 \end{matrix}\right] \circledast \left[L5 -\!< \begin{matrix} L_4 \\ L_7 \end{matrix}\right]$$

the operation the following conversion rule applies:

$\sinh(L)\ \sinh(L) \rightarrow \sinh(L)$

$\cosh(L)\ \cosh(L) \rightarrow \sinh(L)$

$\sinh(L)\ \cosh(L) \rightarrow \cosh(L)$

The transfer function at this stage is that for the tree with all tips having a closed-circuit termination. If there are any open-circuit terminations the following operations are performed:

All symbols in the numerator and denominator with open-circuit terminations are complemented the same number of times as there are open-circuit terminations in that term. If a branch in a triad is complemented, all terms in the mathematical representation are complemented.

$$\text{Numerator} = [0-x]\left[L5-\prec \begin{matrix} L_6^* \\ L_7^* \end{matrix}\right][L4\,]^*[y]^*$$

$$\text{Denominator} = \left[0-L_1-\prec \begin{matrix} L_2 \\ L_5 \end{matrix}\right] \circledast \left[L_2-\prec \begin{matrix} L_3^* \\ L_4^* \end{matrix}\right] \circledast \left[L_5-\prec \begin{matrix} L_6^* \\ L_7^* \end{matrix}\right]$$

The derivation is now complete. The mathematical equivalents of the building blocks can now be substituted into the symbolic expression.

As explained above the magnitude and phase of the transfer function represents the attenuation and phase shift experienced

by an input sine wave . Such a magnitude-phase, or Bode plot can be obtained by encoding the transfer function in a computer language with a facility for handling complex numbers (eg. Fortran). The magnitude and phase can be calculated in the following way:

$$\begin{aligned} &\text{Let,} \quad X = \mathrm{Re}(K_{ij}(j\omega)) \\ &\qquad\quad Y = \mathrm{Im} (K_{ij}(j\omega)) \\ &\text{Then ;} \quad \text{Amplitude} = ((X)^2 + (Y)^2)^{1/2} \\ &\qquad\quad \text{Phase} \quad = \arctan (Y/X) \end{aligned} \tag{4}$$

Where Re and Im are operators that take the real and imaginary part of the operand respectively.

2.2.4. SOME USEFUL PROPERTIES OF TRANSFER IMPEDANCES

(1) The transfer impedance at $\omega=0$, $K_{ij}(0)$, is the transfer resistance between i and j for a D.C. input at j.

(2) For a tree-like structure (Koch et al., 1982)

$$K_{ij}(j\omega) = K_{ji}(j\omega) \tag{5}$$

(3) The current transfer between sites i and j for current input at j is,

$$I_j(j\omega) = (K_{ji}(j\omega)\ I_i(j\omega)) / K_{jj}(j\omega) \tag{6}$$

(4) The fraction of charge injected at site i reaching site j, (the charge factor, Q) is (Koch et al., 1982),

$$Q = K_{ji}(0) / K_{jj}(0) \tag{7}$$

(5) If, instead of an R-C circuit, the membrane is represented by an arbitrary linear circuit with admittance $y(j\omega)$, then all that needs to be changed in the B&C method is the definition of the propagation constant (for proof see appendix A):

$$\gamma = (r_a\ y(j\omega))^{1/2} \tag{8}$$

(6) A method for introducing synapses is given in appendix B.

2.2.5. A WORKED EXAMPLE

To illustrate the use of the B&C calculus I shall derive the transfer impedance for a lumped soma finite cable model (LSFC):

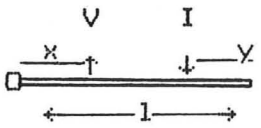

$$K_{ij}(j\omega) = [0-x][y]^{*}/[0-l]^{*}$$

$$= \frac{(Z \sinh(\gamma x) + Z_s \cosh(\gamma x))(Z \cosh(\gamma y))}{(Z \cosh(\gamma l) + Z_s \sinh(\gamma l))} \quad (9)$$

The input impedance at the soma can be found by moving both electrodes to the soma. (ie x=0 , y=l)

$$K_{ss} = 1/((1/Z_s) + (1/Z)\tanh(\gamma l)) \quad (10)$$

Rearranging equation (10),

$$K_{ss}(j\omega) = (1/G_s) / (1 + j\omega\tau_m + \rho_\infty(1+j\omega\tau_m)^{1/2}\tanh(\gamma l)) \quad (11)$$

Where $\rho_\infty = 1/(r_a \lambda G_s)$, is the ratio of the dendritic to somatic conductance, for an equivalent LSFC with a cable of semi-infinite length (Jack, Noble & Tsien, 1975)

The DC input resistance measured at the soma can then be found from this expression by setting $\omega=0$.

$$K_{ss}(0) = (1/G_s) / (1 + \rho_\infty \tanh (l/\lambda)) \quad (12)$$

2.3 THE FREQUENCY DOMAIN REPRESENTATION OF SOME ELECTROTONIC STRUCTURES

2.3.1. THE FREQUENCY DEPENDENT SPACE CONSTANT

The space constant, λ defines the steady-state voltage decrement with distance in an infinite cable; λ is the distance at which the voltage declines to exp(-1) of its value at the site of current injection. To extend the notion of a space constant to time varying signals, consider the transfer impedance of an infinite cable, with the current injected at site i, the measuring site j being at a distance x from the current source,

$$K_{ji}(j\omega) = Z \exp\left(-\gamma x\right) \quad \text{for } 0 < x \qquad (13)$$

Using equations 13 and 4, the ratio of the output to the input amplitude is,

$$V_j(\omega)/I_i(\omega) = \frac{R_a \lambda \exp\left(-(2)^{-1/2}((1+\omega^2\tau^2)^{1/2}+1)^{1/2}(x/\lambda)\right)}{(1+\omega^2\tau^2)^{1/4}} \qquad (14)$$

From this equation it follows that the amplitude of the output falls to exp(-1) of its value at x=0, when x is equal to the effective space constant, $\lambda'(\omega)$, defined as,

$$\lambda'(\omega) = \frac{(2)^{1/2}\,\lambda}{((1+\omega^2\tau^2)^{1/2}+1)^{1/2}} \qquad (15)$$

The complex space constant is an inverse function of frequency, so high frequency inputs are attenuated more strongly with distance than low frequency inputs.

The frequency dependence of the space constant proves useful in rationalising the frequency domain representation of the input impedance of neurones. In what follows the frequency domain behaviour of some simple electrotonic structures are exhibited and it is shown that the input impedance of more complex

electrotonic structures can be understood in terms of the response of these simple circuits, when account is taken of the frequency dependence of the space constant.

All input impedance plots are displayed as phase-magnitude plots and in all cases the magnitude has been normalized by the maximum value of the magnitude. The magnitude and frequency are both scaled logarithmically. Further the frequency in all plots designates dimensionless frequency, which is the product of the frequency in radians per second and the membrane time constant in seconds. The shapes of all phase-magnitude plots are thus rendered independent of the absolute value of the membrane time constant.

2.3.2. ISOPOTENTIALITY

The notion of isopotentiality recurs frequently in this work and consequently deserves some clarification. Any part of a neurone is isopotential if, when perturbed by a current input, voltage gradients do not develop within the defined area. Whether a given part of a neurone is isopotential will depend on the neurone's electrotonic structure and on the frequency components in the input. It is important to note that even though, for example, a soma may be isopotential, there may be voltage gradients between the dendrite and the soma; the neurone is then, as a whole, not isopotential. The distinction between the isopotentiality of the whole or part of a neurone is important because only when the neurone as a whole is isopotential, does the measured input impedance correspond to the unit membrane impedance. In a nonisopotential neurone the unit membrane impedance can only be measured through the intermediate of an

electrotonic model. It should also be noted that because of the frequency dependence of the space constant, a neurone may be isopotential at low frequencies but not at high frequencies (Eisenberg & Johnson, 1970).

2.3.3. THE ISOPOTENTIAL SOMA AND THE INFINITE CABLE

The parallel R-C combination is conventionally used to represent an isopotential soma (Jack, Noble & Tsien, 1975). The input impedance of an R-C circuit is,

$$K_{ii}(j\omega) = R / (1 + j\omega RC) \qquad (16)$$

The Bode plot (Fig. 2A) of the R-C circuit is characterized by an amplitude which decreases with a slope of -1 at high frequencies. The time constant of the circuit (τ=RC) can be measured directly from the gain-phase plot and it is equal to the inverse of the frequency (in rads/s) at which the gain falls to $(2)^{-1/2}$ of its initial value. The phase at very low frequency is zero and at a frequency of $.1/\tau$ it begins to lag the input, and decreases to a phase of -90^{o}, at a frequency of approximately $10/\tau$.

The input impedance of an infinite cable is:

$$Kii(j\omega) = ra\ \lambda / \quad (1+j\omega\tau)^{1/2} \qquad (17)$$

The magnitude decreases with a slope of -1/2, and the time constant is given by the inverse of the frequency (rads/s) at which the amplitude has fallen to $(2)^{-1/4}$ its original value (see fig. 2A). The phase shows a progressive lag with increasing frequency, but now tends to a limit of -45^{o}.

2.3.4. REFLECTIONS

The effect of introducing open-circuit terminations to a cable can be illustrated as follows. Consider a homogeneous infinite cable. If a step of current is applied, the steady state

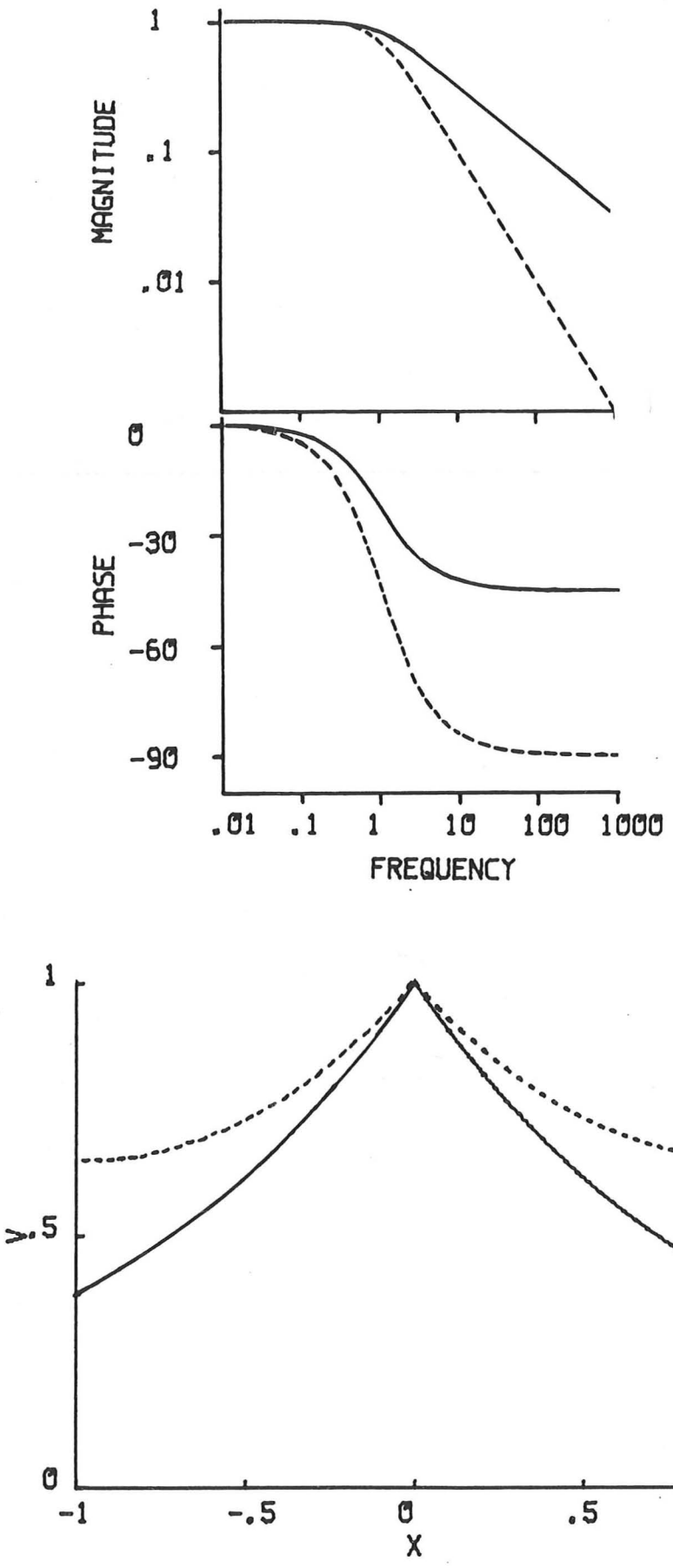

Figure 2.2. (A) Phase-magnitude plot of the input impedance of an infinite cable (——) and a parallel R-C circuit (-----).
(B) Comparison of the steady-state voltage distribution of an infinite cable (——) and a finite cable of length 2λ (-----) with open-circuit terminations.

distribution of voltage is given by (see fig. 2B):

$$v(x) = (r_a \lambda / 2) \exp (-x / \lambda) \qquad (18)$$

where x is the distance from the current electrode.

If the cable is cut at points λ and $-\lambda$, and the end points capped with infinite resistances, and a step of current applied to the middle of the cable, the steady state voltage distribution is for $0 < x < l$,

$$v(x) = \frac{Z \cosh (\gamma_o l) \cosh (\gamma_o (2l - x))}{\sinh (\gamma_o 2l)} \qquad (19)$$

where $\gamma_o = 1/\lambda$

In fig.2B the two distributions are plotted on the same axes and are clearly different. The voltage decays less rapidly with distance in the case of the terminated cable, because current is reflected back towards the electrodes by the terminating impedances. Such reflections will occur whenever two abutting regions of the cable have different characteristic impedances; this is termed an impedance mismatch (Dworsky, 1979). (The characteristic impedance of a cable is the input impedance of an equivalent infinite cable.)

2.3.5. FINITE CABLE WITH OPEN-CIRCUIT TERMINATIONS

The input impedance of a cable with open-circuit ends resembles at low frequencies a parallel R-C circuit, and at high frequencies an infinite cable (see fig. 3A). The shorter the cable, the higher the frequency at which this transition occurs. This shift in the electrotonic appearance of the cable with frequency can be explained in terms of the frequency dependence of the space constant as follows. The length constant is an inverse function of frequency, therefore at low frequencies the terminations appear to be closer to the electrodes than at high frequencies. This increases the amount of current reflected back to the stimulating electrode, making the voltage distribution within the cable uniform. The whole cable then resembles an isopotential compartment and consequently behaves like a parallel R-C circuit. At high frequencies the cable appears very long, and the terminations will have little effect, consequently the cable's response resembles that of an infinite cable.

2.3.6. FINITE CABLE WITH CLOSED-CIRCUIT TERMINATIONS

The input impedance of cable with closed-circuit terminations is almost indistinguishable from that of an infinite cable, in that its magnitude decreases with a slope of -1/2 and the phase tends at high frequencies towards -45^{o} (see fig. 3B). It is only distinguishable from the infinite cable at the frequencies where roll-off commences and by a transient phase roll-off past -45^{o}.

Unlike the infinite cable the time constant cannot be determined from the amplitude plot alone, as the frequency at which roll-off commences, increases as the length of the cable

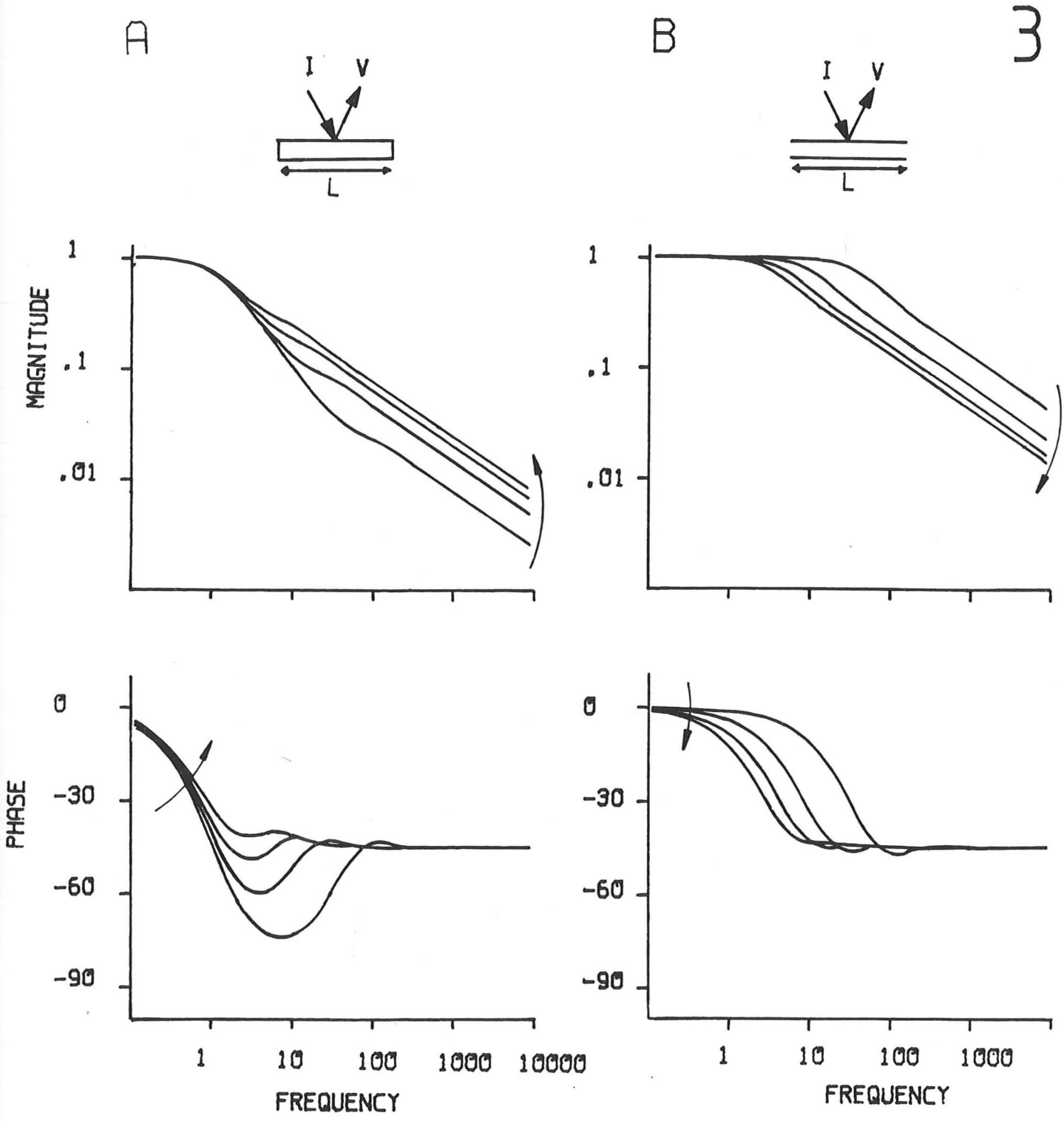

Figure 2.3. Input impedance of a finite cable with electrodes in the middle of the cable (A) open-circuit terminations (B) closed-circuit terminations. The length of the cable increases in the direction of the arrow; L = 0.5, 1, 1.5, 2λ. All impedance curves were traced by hand from computer generated plots.

decreases.

2.3.7. THE LUMPED SOMA FINITE CABLE MODEL (LSFC)

The simplest analogue of a neurone is a lumped soma attached in parallel to finite cable (the abbreviation LSFC refers, unless otherwise stated to the case where the cable has an open-circuit termination). The LFSC occupies a central role in practical cable theory for two reasons. Firstly it is probably the most complex model that can be used for electrotonic parameter estimation. The LSFC model has three unknown parameters (τ_m, ρ_∞ and L), while if a bifurcated cable is substituted for the cable the model now has seven unknown parameters. Given the limited precision of biological data and the number of unknown parameters, fitting the equations of this model would prove intractable for most optimization routines. Secondly, Rall (1962) has shown that if a dendritic tree satisfies certain conditions, the somatic input impedance is indistinguishable from that of an LSFC model. These conditions for a dendritic tree with a homogeneous unit membrane impedance are,

(1) The relationship of all parent branch diameters, d_j, to daughter branch diameters, $d_{(j-1)k}$, must obey the following equation,

$$\left(d_j \right)^{3/2} = \sum_k \left(d_{(j-1)k} \right)^{3/2} \qquad (20)$$

(2) All direct paths from the soma to the branch terminations must be of the same electrotonic length.

(3) All branch terminations must have the same impedance.

In fig.4 the input impedance of an LSFC model is plotted for different values of the dendritic to somatic conductance ratio

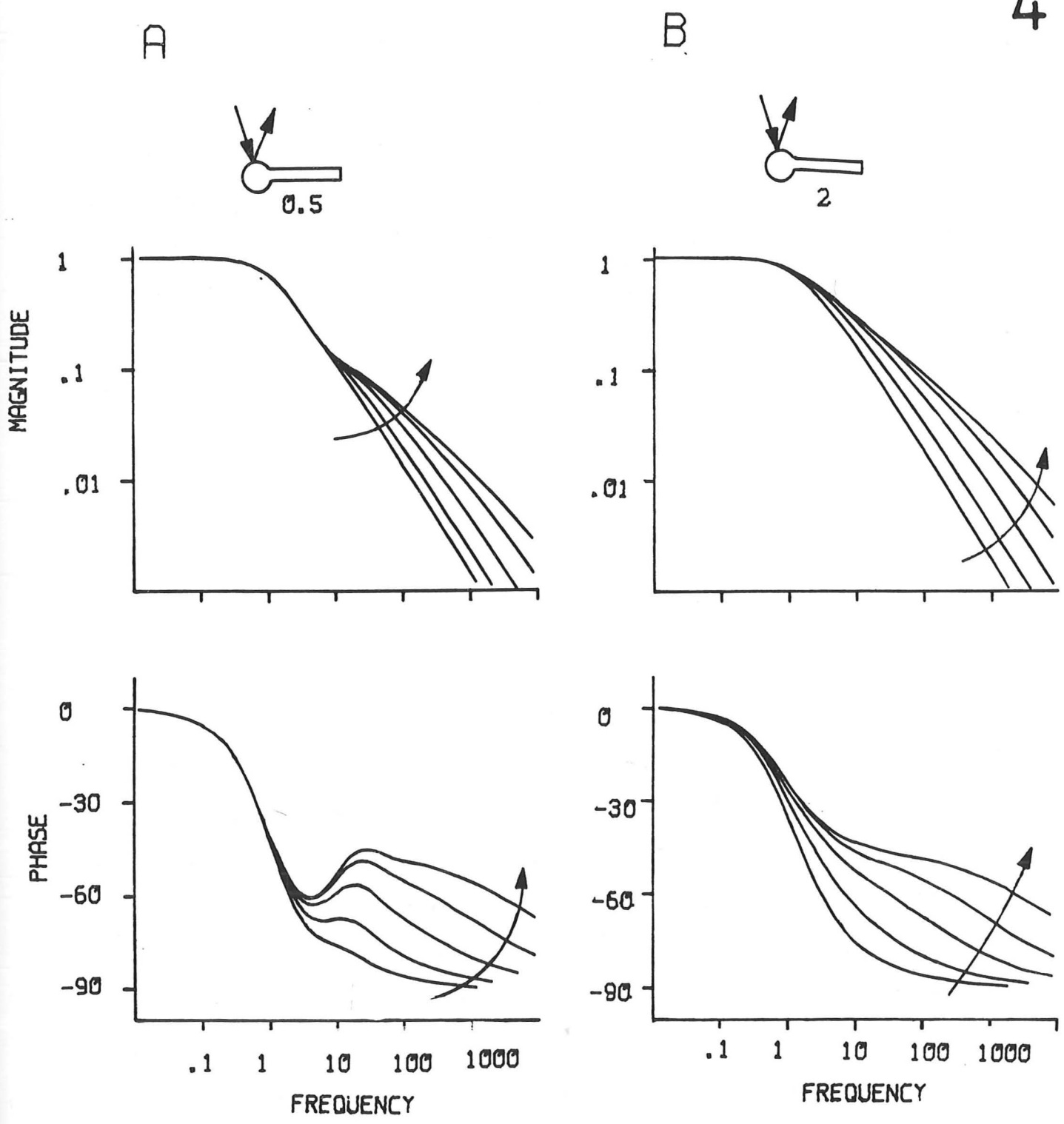

Figure 2.4. Somatic input impedance of an LSFC model (A) L=0.5λ (B) L=2.0λ ; e_{ω} increases in the direction of the arrow; 1, 3.16, 10., 31.6, 100.

ρ_∞. For low ρ_∞ the soma dominates the response and the presence of the cable cannot be detected. As ρ_∞ is increased the cable gives evidence of its presence, in the amplitude plot as an intermediate region with a slope of greater than -1, and in the phase plots as a tendency for the high frequency limit to shift toward -45^o. At very high ρ_∞ (> 100) the response is indistinguishable from that of a pure cable.

2.3.8 INHOMOGENEOUS LSFC

Most electrotonic models assume for reasons of parsimony that the unit membrane resistance is uniform. This is by no means necessary and it is possible that the soma and dendrites might have different unit resistances (Fatt, 1957). The B&C method can cope with membrane inhomogeneity and in fig 6. Bode plots of an LSFC model with different somatic and dendritic resistances are displayed.

The impedance of an inhomogeneous model differs from that of the homogeneous case, however whether one can detect a discontinuity in membrane resistance will depend on the model's parameters (ρ_∞ and L) , the difference between the somatic and dendritic resistance, and the accuracy of the experimental data. Although the precise range over which it is possible to distinguish between the somatic and dendritic resistance, has not been studied, the same method used in section 2.4. could be

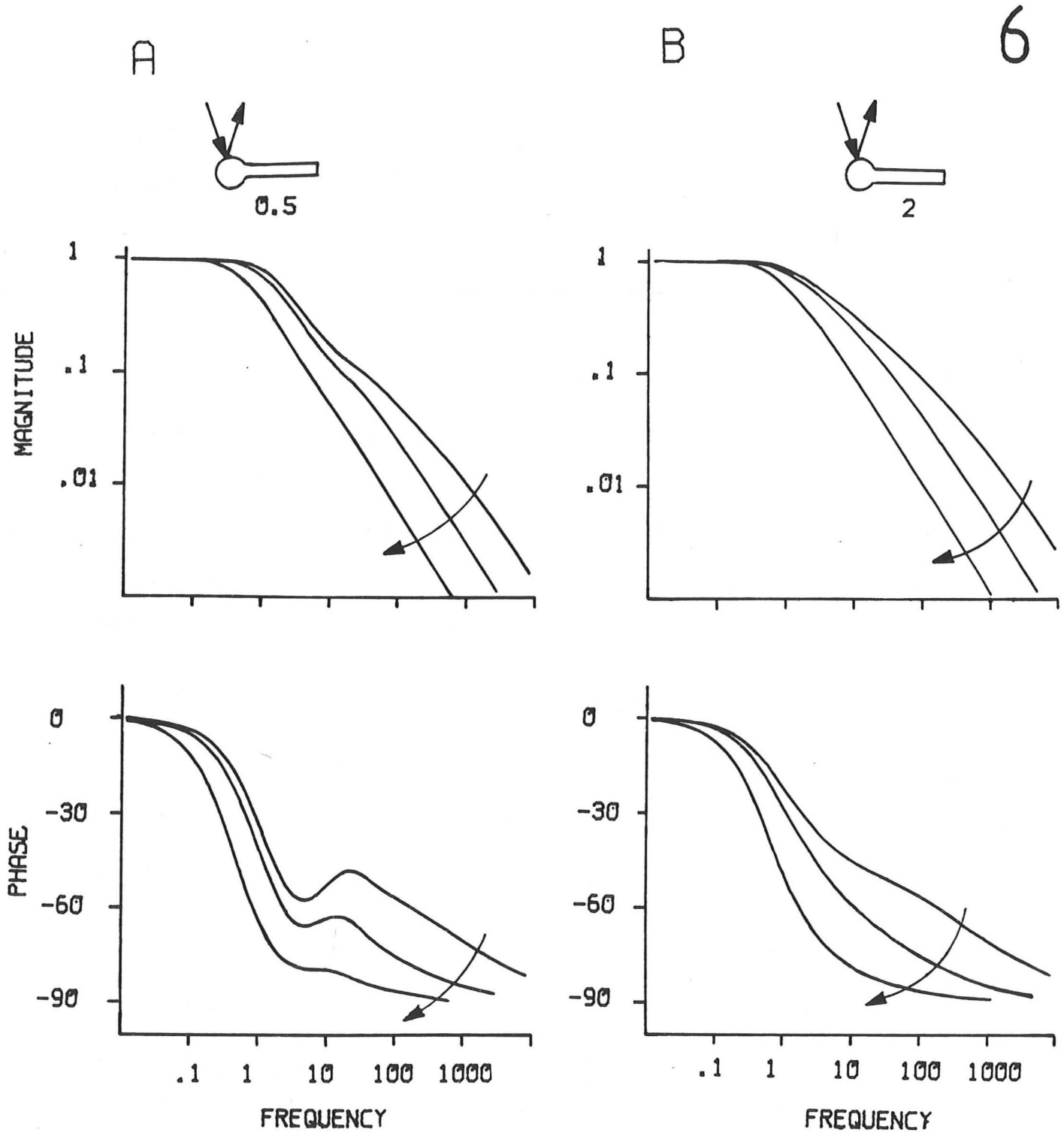

Figure 2.6. Input impedance of an LSFC model (ρ_∞=5) with different somatic time constants. (A) L=0.5λ (B) L=2λ. The somatic time constant, τ_s increases in the direction of the arrow; $\tau_s = 0.5\tau_m$, τ_m and $1.5\tau_m$.

employed for this purpose. It should be noted that input impedance measurements alone cannot distinguish between a reduced somatic time constant that is the result of a microelectrode induced leak or the result of the natural variation of the membrane time constant.

2.3.9. INDUCTANCE

Although there are no true inductive elements in biological systems, inductive-like responses may arise through the behaviour of voltage gateable channels (Chandler et al., 1962).

Consider a channel, which may be open or closed. Let p be the fraction of channels in the open state and α and β be the voltage dependent rate constants for the opening and closing reactions respectively. The reaction can be represented as:

$$(1 - p) \underset{\beta}{\overset{\alpha}{\rightleftharpoons}} p$$

By linearizing the rate equation about an average voltage $\bar{v}$, Chandler et al. (1962) were able to derive the small-signal admittance:

$$y(j\omega) = \bar{g} + G_o / (1 + j\omega / \omega_o) \qquad (21)$$

where: $G_o = (\partial p(\bar{v}) / \partial v)(\bar{v}-E_o)g_o$: $\omega_o = \alpha(\bar{v}) + \beta(\bar{v})$; E_o = electrochemical potential of the channel ; g_o = conductance of channel; $\bar{g} = g_o\, p(\bar{v})$; v = voltage change about $\bar{v}$

To estimate the effect of cable properties on the input impedance of an inductive-like system, the admittance represented by equation 21 is taken in parallel with a capacitance, and this combination is used as the unit membrane impedance of a finite cable.

The input impedance of this system is plotted in figure

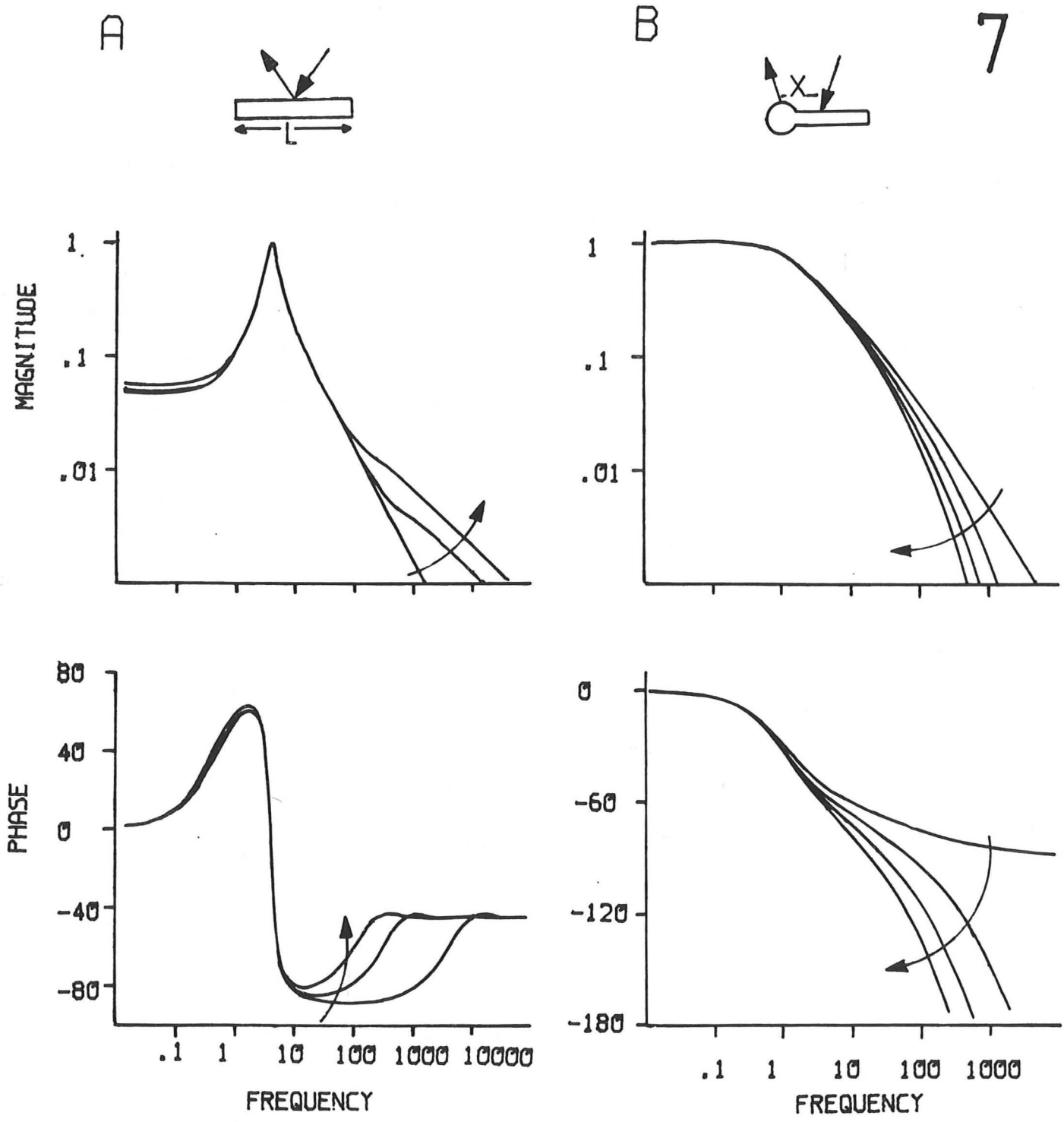

Figure 2.7. (A) Phase-magnitude plot of a finite cable with an inductive-like membrane (ω_o=100 rad s^{-1}; G_o=.01 mS), measured at the centre of the cable. The cable has open-circuit terminations. The length of the cable increases in the direction of the arrow; L= 0.125, 0.8, 1.5λ. The frequency is in rad s^{-1}. (B) Transfer impedance of an LSFC model (L=2; ρ_∞ = 5), with the current passing electrode in the soma and the voltage electrode a distance X from the soma; X increases in the direction of the arrow; X = 0.05, 0.1, 0.15 λ.

7A for a number of different cable lengths. The position of the resonance peak, determined by ω_o, is not affected by the length of the cable, however, increasing the cable length leads to a magnitude plot with reduced slope at high frequencies, tending for very long cables to the infinite cable limit of -1/2. The cable length also has a pronounced affect on the phase plots; increasing the cable length compresses the maximum phase excursions. This example illustrates again the importance of using an electrotonic model to deduce the unit membrane impedance of a nonisopotential system.

2.3.10. NON-ISOPOTENTIALITY

As the frequency of input to a neurone increases there must come a point where isopotentiality even within the soma breaks down, because the space constant declines with increasing frequency. Roberge et al (1977). have derived an approximate expression for this frequency for a homogeneous spherical soma,

$$f_{crit} = ((0.01\ \sigma/a)^2 - G_m^2)^{1/2} / 2\ \pi\ Cm \qquad (22)$$

where G_m=membrane conductivity per unit area ; a = cell radius ; Cm = membrane capacitance per unit area ; σ = conductivity of cytoplasm.

Using the average values found for *Helix aspersa* neurones in chapter 4 , $R_m = 5 \times 10^4\ \Omega\ cm^2$, a= 100 μm, and assuming σ = .01 mhos/cm and $C_m = 1 \mu F\ cm^2$, the critical frequency is 1591 Hz. This frequency is well beyond the highest frequency used to measure the input impedance (200 Hz.), so for the structures encountered in this study the effects of non-isopotentiality will be very small. It is nevertheless interesting to enquire how non-isopotentiality might manifest itself in the frequency domain. Initially a series approximation derived by Eisenberg and

Engel (1970) was used to simulate non-isopotentiality, but its convergence properties proved very poor. To simulate the effects of non-isopotentiality the LSFC model was used, with the input electrode in the soma and the output electrode in the proximal dendrite. (see fig. 7B). Non-isopotentiality manifests at high frequencies as an amplitude roll-off with upward convexity and a phase that rolls off past -90^{o}.

2.3.11. ELECTROTONICALLY INDISTINGUISHABLE CABLES

If the analytical impedances of two structures are equal, it is impossible from the input impedance alone to distinguish between the structures. If one is to decide between two possible forms, then either the experiment must be performed from a different locus, or details of the morphology must be obtained. For example it is not possible to distinguish between the following two configurations,

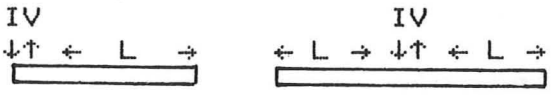

2.4. ELECTROTONIC PARAMETER ESTIMATION

In appendix E it is demonstrated that the LSFC model is structurally identifiable, it is hence licit to use this model to estimate the electrotonic parameters, τ, ρ_{∞} and L. These parameters can be estimated by sampling the input impedance at a range of logarithmically spaced frequencies and then adjusting the model parameters until the fit between the model and the data is optimal. The accuracy with which the parameters of the LSFC model can be determined is limited by the precision of data, the verity of the model and the value of the model parameters.

2.4.1 DISTINGUISHABLE ELECTROTONIC STRUCTURES

The range of electrotonic parameters consistent with the experimental error, can be calculated from the expression for the input impedance of an LSFC model. To implement this calculation, a criterion has to be established for deciding whether two electrotonic structures are distinguishable. Using the fact that the phase shift is very sensitive to variations in the electrotonic structure (Clausen et al., 1979), the difference between two impedances can be quantified by the statistic P, defined as,

$$P = 1/N \sum_{i=1}^{N} | \phi_i^{e} - \phi_i^{t} | \qquad (23)$$

where, N is the number of frequencies at which the impedance is measured and ϕ_i^{e} denotes the phase of the experimental and ϕ_i^{t} and theoretical impedances at the ith frequency. If the phase can only be determined with an accuracy of say $\pm$ 0.5^{o}, then the two impedances are distinguishable when P exceeds 0.5. (In all that follows the experimental error will be assumed to be $\pm$0.5^{o}, as this is the expected error with the method used in chapter 4).

2.4.2. PARAMETER ESTIMATION AND DATA ACCURACY

2.4.2.1 THE ERROR IN THE MEMBRANE TIME CONSTANT

To establish the range of the time constants consistent with a given experimental error, the following procedure was used. An LFSC model with time constant τ^{e} was used to generate the 'experimental' impedance. The phase was calculated at 10 logarithmically spaced frequencies, over the range $.1/2\pi\tau^{e}$ to $10/2\pi\tau^{e}$ Hz., where the impedance is maximally sensitive to frequency variations. The electrotonic length and e_{ω} were held

constant while the time constant, referred to as τ^t, was increased (decreased) in very small steps until the impedance was just indistinguishable from the experimental curve. In this way an upper (lower) bound was established for the time constant at a given experimental error.

The relative bounds on the time constant are independent of the absolute value of the time constant, but the error bounds increase with decreasing ρ_∞ (see fig. 8A). The electrotonic length does influence the error bounds, but only to a slight extent; for a given ρ_∞ the error associated with a long cable is greater than that with a short cable.

2.4.2.2. ERROR IN THE ESTIMATED CABLE LENGTH

The same technique was used to examine the effect of data accuracy and ρ_∞ on the ability to estimate correctly the length of the dendritic cable (L). An LSFC model with known ρ_∞, τ_m and L was used to generate the experimental impedance. Fixing the value of τ_m and ρ_∞, at the values used in the model, L was varied, until the impedance was just distinguishable from the experimental values. In this way an upper and lower bound for the electrotonic length was established. The bounds on the electrotonic length are influenced by the length of L and ρ_∞, but not by the absolute value of the membrane time constant. The error bounds on an LSFC model with two different lengths of cable are shown in figure , as a function of ρ_∞. The range of indistinguishable electrotonic lengths increases with decreasing ρ_∞ and with increasing L. From figure 8B it can be seen that for a typical physiological value of ρ_∞ equal to 5, it is not possible to distinguish between cables with lengths in the range 2 to infinity.

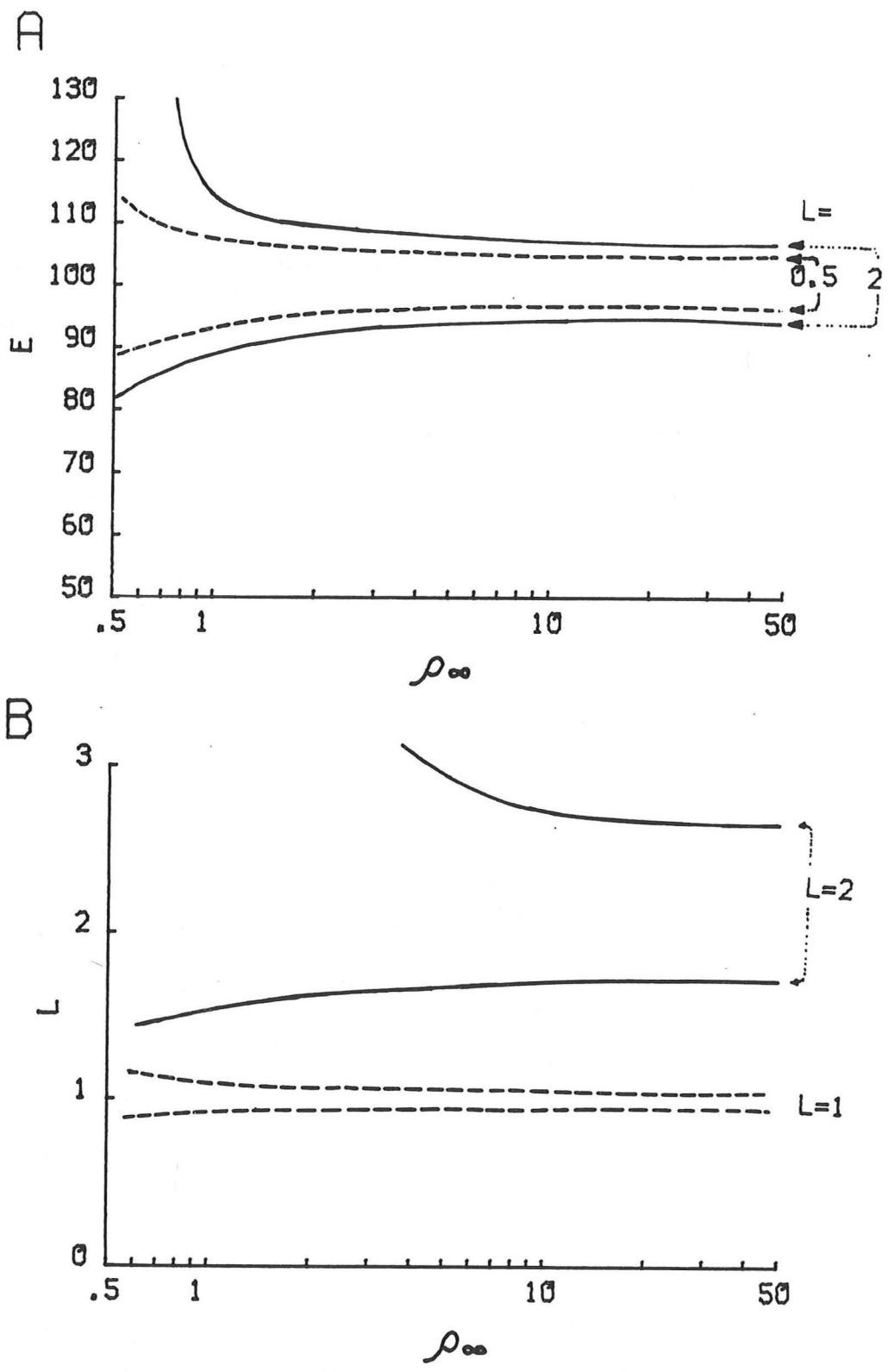

Figure 2.8. (A) The error bounds ($E= \tau^t/\tau^e$) on the membrane time constant of an LSFC model, as a function of θ_∞ for an experimental error of $\pm 0.5^o$ at two different cable lengths. (B) The error bounds of the electrotonic length (L) of an LSFC model as a function of θ_∞ for an experimental error of $\pm 0.5^o$.

The error bounds established in the last two sections should be regarded as minimal bounds, as perfect knowledge was assumed about two of the parameters. It is likely that if all parameters are allowed to vary, the error bounds will increase.

2.4.3 MODELLING ERRORS

2.4.3.1. SECONDARY BRANCH VISIBILITY

Real neurones seldom correspond morphologically to an LSFC model. In this section the effect of adding a single cable to an LSFC is examined. In particular, how small does the diameter of the appended branch have to be, for it to be undetectable from the soma?

The technique for investigating this is identical to that used in the last section. The radius, r_2 of the appended branch was reduced until the impedance was just indistinguishable from that of the LSFC model without a secondary branch. If r_2^* denotes the radius of the secondary branch when the model is just indistinguishable from the LSFC model, and r_1 is the radius of the primary branch, the 'visibility',V of the secondary branch can be defined as,

$$V (e_\infty, L_1, L_2) = r_1 / r_2^* \qquad (24)$$

The visibility is a function of e_∞, the primary branch length(L_1) and the appended branch length (L_2), but it is independent of the primary branch diameter and the membrane time constant. Moving an appended branch towards the soma increases its visibility, however if the branch is closer than 0.1λ the visibility diminishes as the branch is moved closer to the soma (see fig. 9). This paradoxical effect has its origins in the disappearance of the impedance mismatch at the bifurcation, when

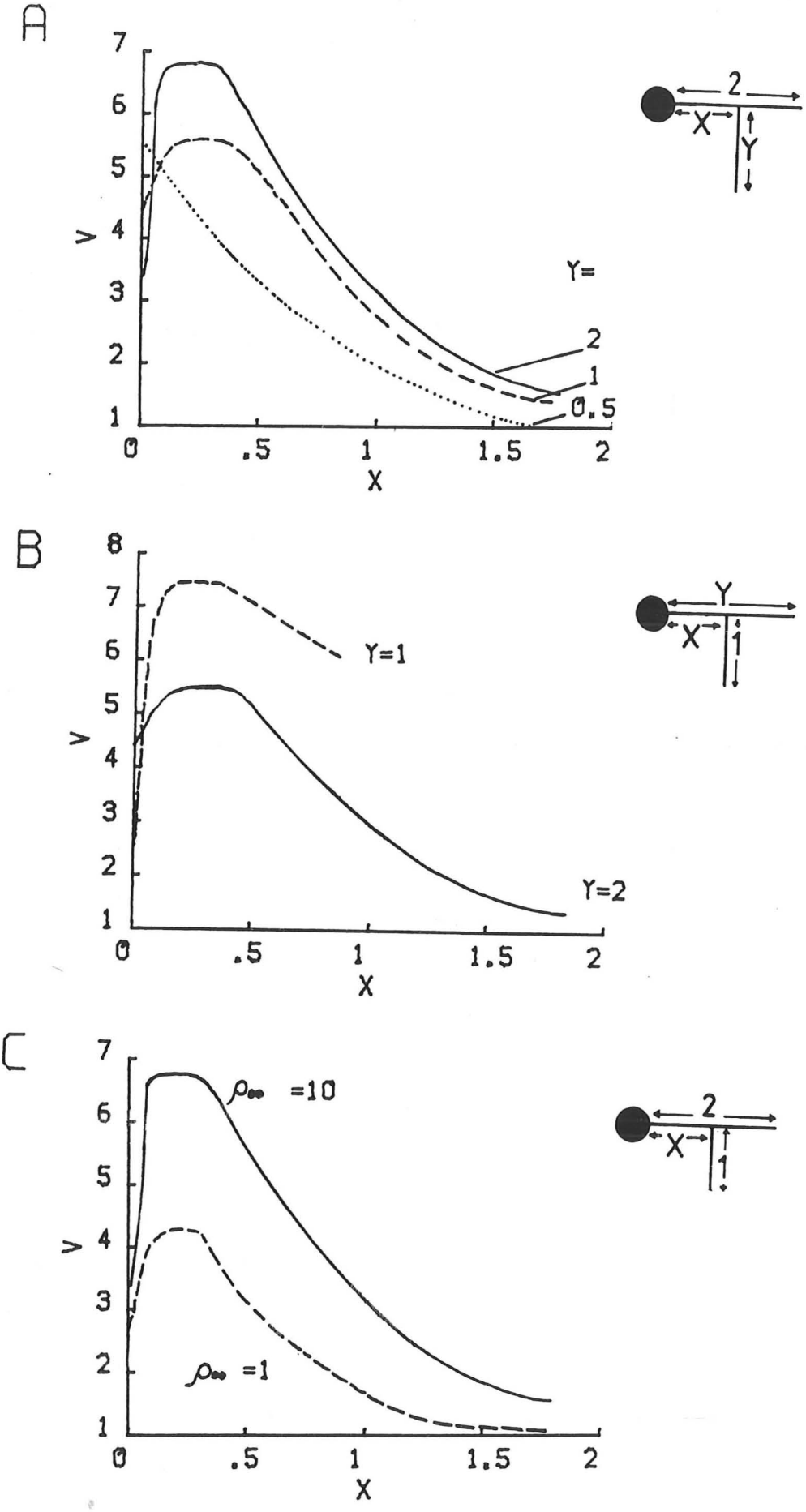

Figure 2.9. The visibility (V) of a secondary branch on an LSFC model as a function of the electrotonic distance from the soma (X). (A) The effect of primary branch length. (B) The effect of secondary branch length. (C) The effect of ρ_∞

the primary branch is so short as to be indistinguishable from the soma. The model neurone can then be approximated by a soma with two branches attached directly to the soma, and for the case when the two branches have the same electrotonic length the model is indistinguishable from an LSFC model.

If instead of a single appended branch, there were N branches, all attached at the same distance from the soma, then this cluster of branches will have the same electrotonic appearance as the original branch, if it has the same input impedance. This will be true if all branches in the cluster have the same electrotonic length as the original branch and if the relationship of the single branch diameter to that of the cluster obeys the 3/2 rule (equation 20).

2.4.3.2. PARAMETER ESTIMATION AND MODELLING ERRORS

Most methods for estimating the electrotonic properties of neurones are based on the assumption that the neurone can be represented by an LSFC model. The conditions under which the correspondence between a branched neurone and an LSFC is exact, have been discussed in section 2.3.7. However many neurones do not comply with this condition (Barrett & Crill, 1974; Christensen & Teubl, 1979). It is the object of this section to examine the effect of an erroneous assumption about the structure of the neurone on the estimated time constant (ie. a modelling error in the terminology of chapter 1). In particular how does the assumption of an LSFC model effect the estimation of the electrotonic parameters, when the neurone is in fact a bifurcated cable attached to a soma?.

The procedure for estimating the modelling error was as follows. The equation for the input impedance of a triad attached

to a lumped soma was used to calculate the 'experimental' impedance at 30 logarithmically spaced frequencies. In all cases the secondary branches were symmetrical. A nonlinear least squares routine (see chapter 4 for details) was used to fit an LSFC model to the data. The routine adjusted the value of the three parameters (τ_m, ρ_ω, L) of the LSFC model until an optimum fit between the experimental data and the LSFC model was achieved.

The results of parameter estimation, in the presence of modelling error are displayed in figures 10. The estimated time constant expressed as a fraction (E) of the true time constant and is plotted against the ratio (R) of the secondary branch radius to primary branch radius, since the error is independent of the absolute value of the time constant and the primary branch radius. The error in the estimate of the time constant does depend on ρ_ω , the ratio of the secondary to primary branch radius and the lengths of the secondary and primary branches. Errors in the estimated time constant occur for branch radii greater than and less than the impedance match radius (indicated by an arrow in figs. 10). The sudden increase in the estimated time constant in figure 10A occurs at the point where the appended cable appears to undergo a discontinuous transition from a finite to an infinite cable.

The error in the estimated membrane time constant as a function of the primary branch length is illustrated in figure 10B. The error is most significant for intermediate primary branch lengths (0.01 to 1 λ). At very high primary branch lengths the effect of the impedance mismatch becomes negligible.

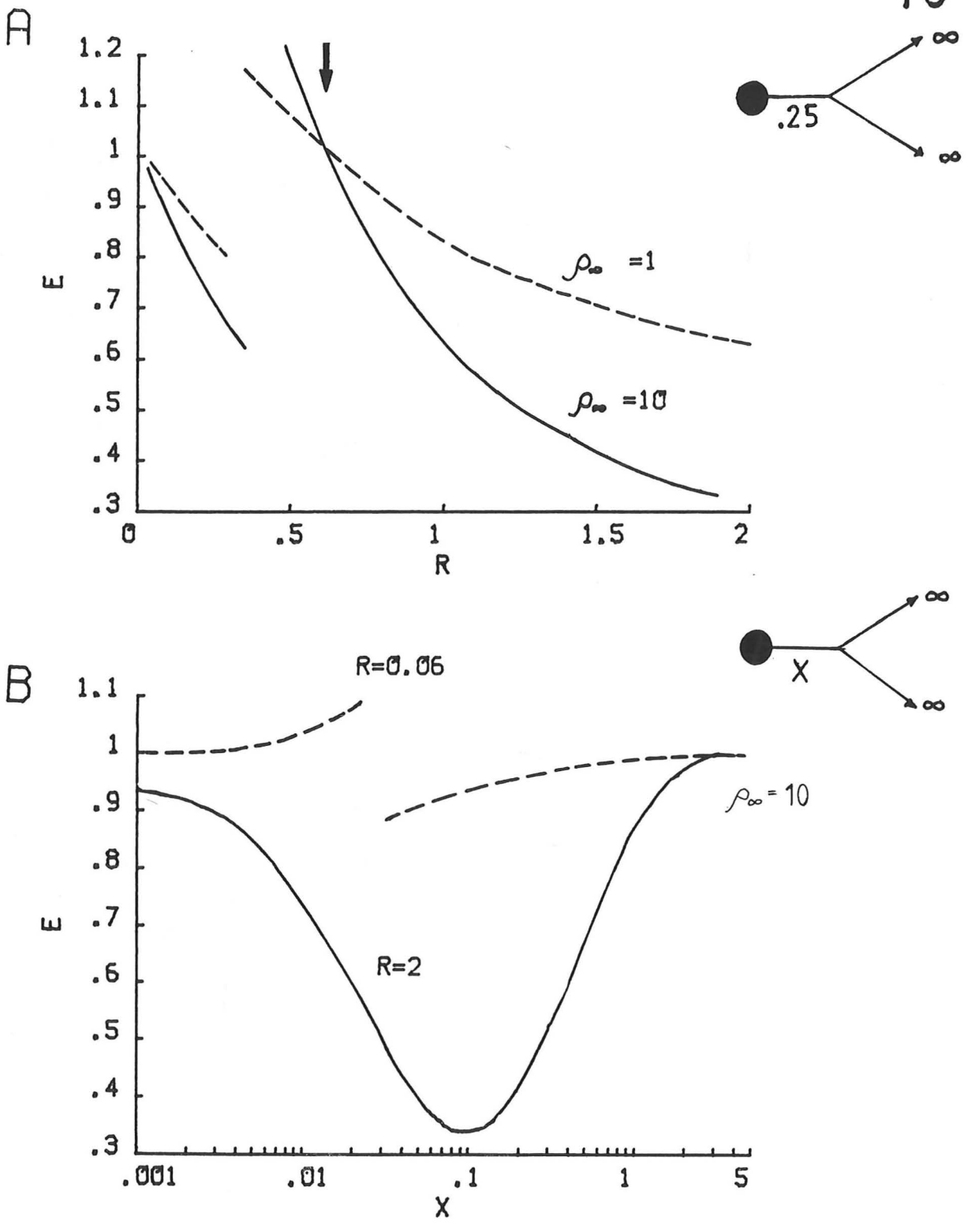

Figure 2.10. The error in the estimated time constant (E = τ_m(estimated)/τ_m(true)) incurred when fitting a lumped soma attached to a bifurcated cable with an LSFC model. (A) The error as a function of R (the ratio of the radius of the secondary branch to that of the primary branch), for secondary branches of infinite length, at two values of ρ_∞. The impedance match condition has been denoted by an arrow. (B) The error (E) as a function of the primary branch length, with the secondary branches of infinite length, and at two different values of R.

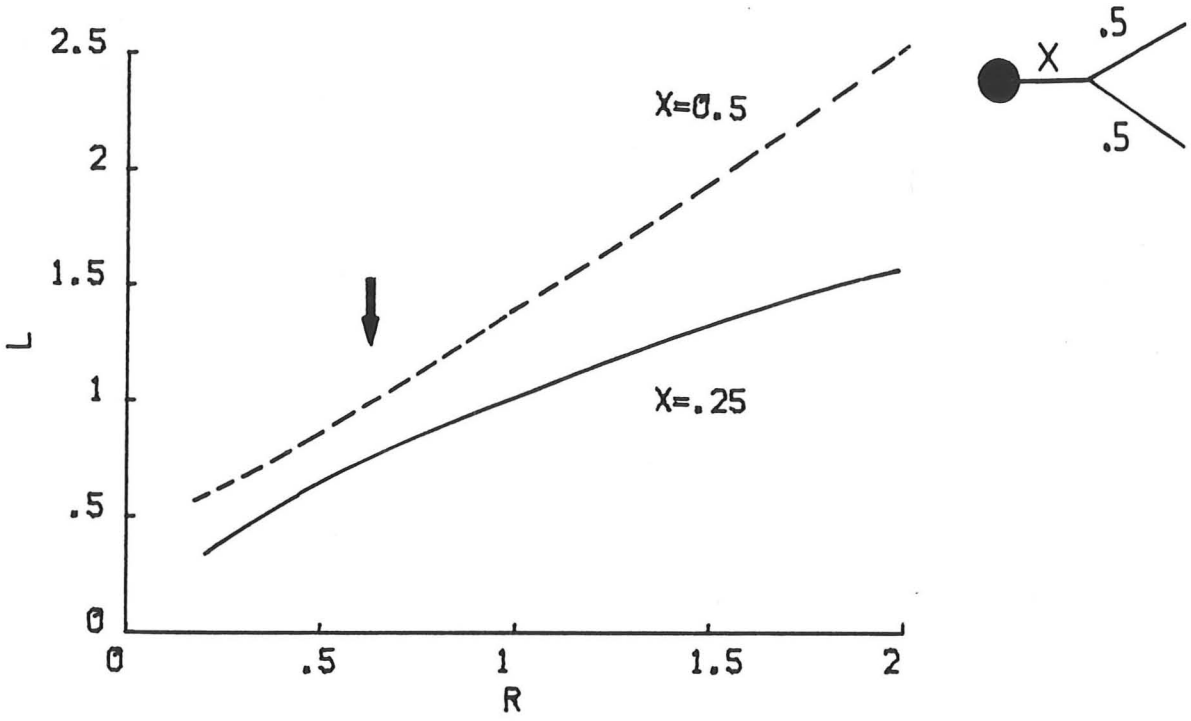

Figure 2.11. The estimated length (L) of a lumped soma with bifurcated cable, when an LSFC model is assumed, as a function of R (the ratio of the secondary to primary branch radius), at two different primary branch lengths.

At very short primary branch lengths the model behaves like a soma with two cables attached directly to it, which is indistinguishable from an LSFC model.

An impedance mismatch at the branch point leads to errors in the estimates of L and ρ_{∞}. The error in the length constant for a short neurone is illustrated in figure 10B.

The results of figures 10 and 11 can be extended to other electrotonic structures. For example if the secondary branches are replaced by a cluster of cables, all with the same electrotonic length, the input impedance will be unchanged if the diameters of the branches in the cluster are related to those of the original secondary branches by the 3/2 rule (equation 20).

CHAPTER 3

TIME DOMAIN ELECTROTONIC METHODS

3.1. INTRODUCTION

Electrotonic analysis has most often been performed in the time domain, estimating the electrotonic parameters of neurones from their transient response to a step or pulse of current. In this chapter the reliability of various time domain methods is investigated.

Four time domain techniques are evaluated, all of which are based on the assumption that the neurone can be represented by an LSFC model. In the first section a series solution for the time domain response of an LSFC model, derived by Rall (1977), is presented and used to illustrate the time domain techniques and their possible shortcomings. In section two the reliability of the time domain methods are evaluated by applying them to estimate the electrotonic parameters of LSFC models. These methods are then contrasted with the frequency domain technique described in the last chapter.

3.2. TIME DOMAIN METHODS IN THEORY

3.2.1. TIME DOMAIN RESPONSE OF LSFC MODEL

Both Jack and Redman (1971), and Rall (1977) have derived series solutions to the impulse response of an LSFC model, but only Rall's equation is considered here, as it mirrors more closely the form of the methods used for estimating electrotonic parameters.

The response of an arbitrary one-dimensional linear cable to a step current input, can be approximated by a sum of

exponentials (Rall, 1977):

$$v(t) = v_{\infty} - \sum_{n=0}^{\infty} c_n \exp\left(-t/\tau_n\right) \qquad (1)$$

where the longest time constant, τ_o, is the membrane time constant and the rest of the time constants, τ_i are termed the 'equalizing' time constants, as they reflect the decay of current within the cable rather than through the membrane. The terms c_i are constants that depend on the cable structure and boundary conditions, and v_{∞} is the steady-state voltage.

For a step of current, i(t), applied at a distance X from the soma of an LSFC model, the voltage response at the soma is (Rall,1977):

$$v(t) = v_{\infty} - \sum_{n=0}^{\infty} B_n \cos(\alpha_n (L-X)) \exp(-(1+\alpha_n^{\,2})t/\tau_o)) \qquad (2)$$

where; the steady state voltage, $v_{\infty} = i\, R_{inp} \cosh(L-X)/\cosh(L)$, and R_{inp} is the input resistance.

and α_n corresponds to the successive roots of the transcendental equation:

$$\alpha_n L \cot(\alpha_n L) = -\rho L \coth(L) = -k \qquad (3)$$

where $(n-1)\pi < \alpha_n L < n\pi$, $\rho = \rho_{\infty} \tanh(L)$ and,

The ratio of time constants is,

$$\tau_o / \tau_n = (1 + \alpha_n^{\,2}) \qquad (4)$$

$$B_o / i R_{inp} = \rho+1 / k+1 \qquad (5)$$

$$B_n \cos(\alpha_n L) = \frac{2B_o (\tau_n / \tau_o)}{(1+(\alpha_n L)^2)(k^2 + k)} \qquad (6)$$

As the system is linear the impulse response is simply the time derivative of the step response:

$$\frac{dv(t)}{dt} = \sum_{n=0}^{\infty} (1 + \alpha_n^2)(1/\tau_o)\ B_n \cos(\alpha_n(1-x))\exp[-(1+\alpha_n^2)(t/\tau_o)] \quad (7)$$

3.2.2. EXPONENTIAL PEELING

Most time domain methods rely on estimates of the first few time constants of equation 1 and of their corresponding intercept terms, c_n. The exponential components of a transient response are normally estimated by a process known as 'peeling' (Rall, 1969), which is performed by plotting the natural log of the decaying voltage transient against time. A straight line is fitted to the terminal portion of the plot; the reciprocal of the slope of this line corresponds to the membrane time constant, and the antilog of the intercept is equal to c_o. The expression, $c_o \exp(t/\tau_o)$ is subtracted from the observed transient and the peeling process is repeated until the resultant transient is reduced to zero. In practice it is seldom possible to strip more than three exponentials from a transient.

The components of a sum of exponentials cannot in practice be resolved for all values of the parameters τ_i and c_i. For example it is not possible to separate two exponential components with time constants that are of the same order of magnitude (Endrenyi, 1980). Even if the time constants are well separated, it may be difficult to measure a component if its magnitude is much smaller than the dominant component.

The magnitude of τ_i and c_i of an LSFC model are determined by the values of the electrotonic length of the cable and ρ_∞. Figure 1 shows the relative size of the first three equalizing

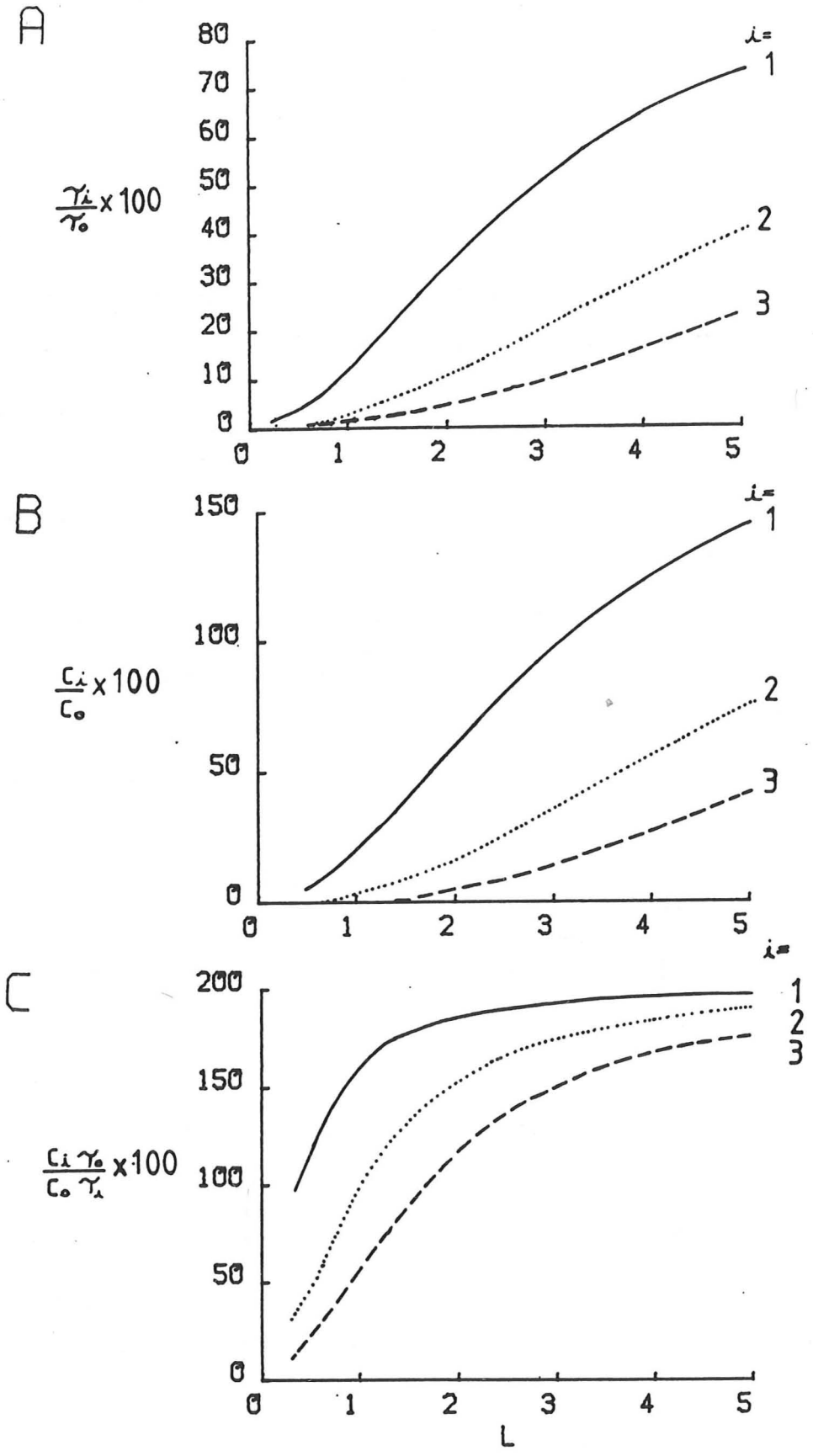

Figure 3.1. The size of the component exponentials of the response of an LSFC model, with ρ_0=5, as a function of L. (A) The size of the first three equalizing time constants relative to the membrane time constant. (B) The magnitude of the first three equalizing exponentials relative to that of the membrane time constant, of the step response. (C) The magnitude of the first three equalizing exponentials relative to that of the membrane time constant, of the impulse response.

time constants and c_i as a function of L. Note that the relative sizes of the equalizing components are greater in the impulse response than in the step response.

In some cases c_1 and c_2 may be too small relative to c_0, for the second and third exponential terms to be detectable. The relative sizes of these terms can be increased by differentiating the step response with respect to time. This procedure, first recommended by Rall (1969) has been used by numerous authors, however, since numerical differentiation amplifies any noise in the signal (Hamming, 1977), this procedure should be avoided. It is preferable to estimate the impulse response of the system, which corresponds to the derivative of the step response, but does not suffer from the artifacts associated with numerical differentiation. The response of a linear system to a pulse with duration $\leq$ 0.01 is a good approximation to the impulse response (Jack & Redman, 1971).

A further difficulty with the peeling method is that it is what mathematicians term an 'ill posed' problem. That is there are many indistinguishable ways of decomposing a transient into a sum of exponentials (Lanczos, 1956; Eisenberg & Mathias, 1980). For example, if data of limited precision is created using a sum of three exponentials it may be possible to find a sum of two exponentials that fits the data as well as the original equation. This should be contrasted with the Fourier analysis of a signal, where the resultant sum of sinusoids is unique. This difference arises from the fact that sinusoids form an orthogonal set while exponentials do not. The consequences of the theoretical flaws in the peeling method are illustrated in section 3.3.2.

3.2.3. ESTIMATING THE MEMBRANE TIME CONSTANT

The primary objective of electrotonic analysis is the accurate measurement of the membrane time constant, τ_m. For

neurones that can be identified with an LSFC model however, there are only two cases where the time constant can be reliably estimated from the transient response to a current input, without having to resort to parameter estimation. Firstly, if L is very short ($< 1\lambda$), a plot of the natural log of the voltage transient against time has a linear terminal portion, whose slope corresponds to the inverse of the membrane time constant. Secondly, if the cable is very long ($> 2\lambda$), and the transient response of the neurone to an impulse input (or to the time derivative of the step reponse) is plotted as $\log(v(t)^{1/2})$ against time, the terminal portion of this plot has a slope which is the inverse of the membrane time constant. This form of plot is referred to as an LRTV plot (log root time voltage; Rall, 1960).

For LSFC models with L in the intermediate range of 1 to 2 λ, the time constants estimated by either of the above procedures will not accurately reflect the membrane time constant. The log-time plot tends to underestimate the time constant, while the LRTV plot overestimates the time constant.

3.2.4 ESTIMATING L AND ρ_∞

Four methods are described in the following section for estimating L and ρ_∞ from the transient response of a neurone to a step or impulse response.

3.2.4.1. RALL'S METHOD

For the case of complete dendritic dominance (i.e. $\rho = \infty$) equation 4 implies that (Rall, 1960),

$$L = \pi / ((\tau_0 / \tau_1) - 1)^{1/2} \qquad (8)$$

This formula gives reliable estimates of L for $\rho > 5$.

3.2.4.2. BROWN'S METHOD

Brown et al. (1981) have derived an approximate method for estimating the parameters of an LSFC model from the transient voltage response to a step current input:

$$\rho = (\tau_o / v_\infty) \left[\sum_{i=1}^{\infty} (c_i / \tau_i) \right] - 1 \qquad (9)$$

As it is only possible to estimate at most three exponentials, ρ will here tend to be underestimated. The electrotonic length of the cable can be found from equation 3, using Newton's method (Gerald, 1978), and assigning L a starting value in the range $\pi/2 < \alpha_1 L < \pi$.

3.2.4.3. JOHNSTON'S METHOD

From Rall's equation (2), Johnston (1981) derived an exact equation for estimating L. The expression is:

$$\cot(\alpha_1 L)[\cot(\alpha_1 L) - 1/(\alpha_1 L)] = \frac{(c_1/\tau_1)}{(2(c_o/\tau_o) - (c_1/\tau_1))} \qquad (10)$$

The right-hand side can be estimated from an experimental transient, and knowing that L is in the range $\pi/2 < \alpha_1 L < \pi$,the equation can be solved for L using Newton's method.

The right hand side of equation 10 can range from 0 to $+\infty$. If it lies outside this range, either the exponentials have been peeled incorrectly, or the neurone does not correspond to an LSFC. Unlike Brown's method, equation 10 is exact and does not depend on the number of exponentials estimated. Once L has been found ρ can be calculated from equation 4.

3.2.4.4. JACK & REDMAN'S METHOD

The method of Jack and Redman (1971) is described in detail in the original paper and will only be outlined here. The

response of the neurone to an impulse of duration less than $.1\tau_m$ is measured and the time constant estimated from the final phase of a log(v) vs t plot. The values of ρ_∞ and L are then estimated from the measured voltage transient with the aid of the graphs given in Jack and Redman (1971), but in contrast to the other time domain methods, without the need to estimate the first equalizing time constant, which is particularly susceptible to error.

It is possible to determine the nature of the terminating resistance of an LSFC model using Jack & Redman's method, if $\rho_\infty > 5$ and $L < 1$. However, ρ_∞ is less than 5, in most invertebrate neurones and this particular aspect of the method cannot be exploited.

3.2.5. ALTERNATIVE ELECTROTONIC METHODS

3.2.5.1. THE INPUT RESISTANCE METHOD

An alternative method for measuring the membrane resistance (R_m) relies on the measurement of the neurone's detailed morphology and the neurone's input resistance (Barrett & Crill, 1974). The method assumes that linear cable theory is applicable, and that the membrane resistance is uniform, and that the cytoplasmic resistance is known. It is then possible to calculate the input resistance of the neurone from the morphology, at a range of membrane resistances, using either the B&C method or a method devised by Rall (1959). The membrane resistance is then the value of R_m that results in a calculated input resistance equal to that measured experimentally.

It is at present not possible to assess the distortions induced in a neurone's morphology by dye filling and fixation. Moreover, as the cell body and neurites of molluscan neurones are

extensively infolded, the morphology can only be accurately reconstructed from serial sections of the neurone. One is reluctant to embark on such a time-consuming procedure knowing that the final reconstruction may be a poor approximation of the true morphology. Furthermore, the method may in certain cases be very sensitive to errors in the measured morphology; for example an 5% error in the estimate of the radius of an LSFC may translate into an error of 20% in the unit membrane resistance (Kay, unpublished calculations).

3.2.5.2. THE GENERALIZED ADRIAN ALMERS METHOD

Following a suggestion by Eisenberg and Mathias (1980) a method is developed in appendix E for the estimation of the electrotonic parameters of an LSFC model; the method does not rely on exponential peeling. The derivation is omitted from the body of this text because of its complexity and the limited reliablity of the method in practice.

3.3. ELECTROTONIC PARAMETER ESTIMATION IN PRACTICE

In section 2.4. the effect of data noise and modelling errors on the accuracy of parameter estimation was assessed in the frequency domain. Since the impulse response and the input impedance are equivalent, the conclusions of that section also apply to time domain methods. However, the accuracy of the estimated parameters will also depend on the nature of the methods used for estimating the parameters. In the following section the time domain methods introduced above are evaluated, by applying them to steps and impulse responses of the LSFC model.

3.3.1. EXPONENTIAL PEELING

The step and impulse responses of an LSFC model were calculated using Rall's equations (2& 3), with 20 and 30 terms respectively in each approximation. In order to replicate the conditions of the experimental chapter, the transients were represented by an eight-bit number (i.e. with a precision of 1 in 256). For each transient the peeling method, as described below, was used to estimate the parameters of the first two exponentials. In all cases the peeling was repeated five times, using different initial conditions to start the peeling, and the solution was taken to be the sum of two exponentials that gave the lowest sum of squares.

The transients were analysed using an interactive BASIC program which first produces a plot of the log of the voltage against time on an X-Y plotter. The user is then requested to enter the initial and final points of a part of the transient which appears to be linear. The program performs a linear regression over the designated points. The antilog of the fitted line is subtracted from the data and the log of the resultant plotted against time. From this, a second exponential is peeled (see fig. 2). The goodness of fit of the estimated equations is assessed by the sum of squares.

Attempts to improve the initial fit with a Newton-Rhapson minimization method proved very time-consuming, and in no instance did this lead to fits that were significantly better than the first estimates.

To perform an LRTV plot on the voltage transient response to

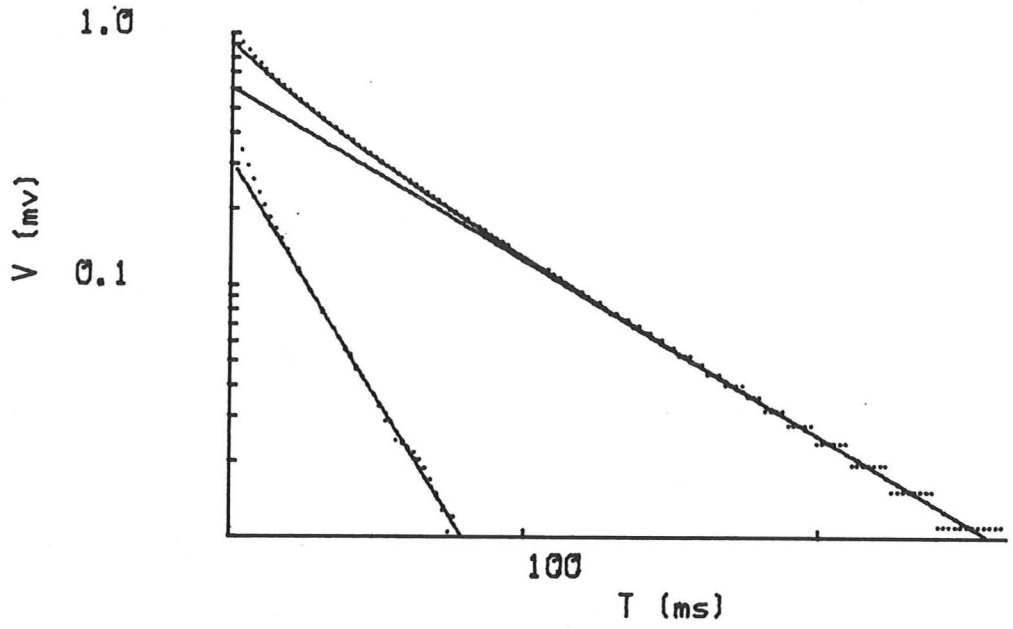

Figure 3.2. Peeling the first two exponential components of the step response of an LSFC model (τ_m = 75 ms, L=5.0, ρ_∞ = 5.0). Each dot represents a digitized point.

a step input, the transient was smoothed with a 5 point least squares quadratic (Hamming, 1977):

$$\bar{v}_n = (1/35)(-3v_{n-2}+12v_{n-1}+17v_n+12v_{n+1}-3v_{n+2}) \quad (11)$$

where $\bar{v}_n$ is the smoothed voltage at time n. The smoothed transients was then differentiated using the central difference formula (Gerald 1978):

$$\dot{v}_n = (1/12h)(-\bar{v}_{n+2}+8\bar{v}_{n+1}-8\bar{v}_{n-1}+\bar{v}_{n-2}) \quad (12)$$

where h is the sampling interval.

3.3.2. RESULTS OF PARAMETER ESTIMATION

The results of estimating the electrotonic parameters of LSFC models from theoretically generated step and impulse responses are illustrated in tables 1 and 2 respectively.

The error in a membrane time constant estimated from the slope of the terminal portion of a log(v) vs t plot, increases as the electrotonic length of the cable increases. This parallels the increase in the magnitude of the equalising time constants relative to the membrane time constant, which makes it progressively more difficult to resolve the exponential components as L is increased.

In all cases the membrane time constant estimated from the step response proved more accurate than that estimated from the impulse response. This is so because the size of the equalising time constants (c_i/τ_i) in the impulse response are elevated relative to those in the step response, making the resolution of the exponentials in the impulse response more difficult.

The results of tables 1 and 2 also illustrate the discrepancy between the estimated exponential components and their true values. This is a practical consequence of the ill posed nature of exponential peeling, mentioned in section 3.2.2.

TABLE 1

Comparison of the accuracy of three methods for estimating the electrotonic parameters of an LSFC model from its step response. The parameters τ_o, τ_1, c_o and c_1 (defined in equation 1), were estimated by exponential peeling and are expressed as ratios to render the quantities independent of the absolute value of the membrane time constant. $\%\tau_m$ and $\%\tau_{lrtv}$ are the time constants estimated from the log(v) vs t and LRTV plots respectively, as a percentage of the membrane time constant.

Actual values					Estimated values									
			$\frac{\tau_o}{\tau_1}$	$\frac{c_o}{c_1}$			$\frac{\tau_o}{\tau_1}$	$\frac{c_o}{c_i}$	Brown		Johnston		Rall
ρ	ρ_∞	L			$\%\tau_m$	$\%\tau_{lrtv}$			ρ	L	ρ	L	L
5	5.5	0.5	29.70	17.9	99.3	121.1	49.3	7.0	6.8	0.4	-	-	0.5
5	7.9	.75	14.07	8.3	99.2	124.0	15.2	4.8	2.7	0.7	-	-	0.8
5	6.6	1.0	8.57	4.9	98.0	114.5	10.7	3.8	2.1	0.7	-	-	1.0
5	5.5	1.5	4.52	2.5	95.0	120.0	6.4	2.4	1.6	0.9	-	-	1.3
5	5.2	2.0	3.06	1.6	91.6	110.1	4.1	1.7	1.1	1.3	-	-	1.8
5	5.0	5.0	1.36	0.7	81.6	101.3	3.1	2.1	0.5	1.4	2.1	1.4	2.1
2	4.3	0.5	22.50	20.2	99.6	134.5	40.0	11.6	3.4	0.4	-	-	0.5
2	3.1	.75	10.80	9.3	98.5	127.6	11.9	6.7	1.6	0.7	6.3	0.8	1.0
2	2.6	1.0	6.76	5.4	97.3	127.1	7.6	5.1	1.1	0.8	3.0	0.9	1.2
2	2.2	1.5	3.70	2.8	97.2	123.6	4.6	2.6	1.1	1.2	4.8	1.5	1.5
2	2.1	2.0	2.67	1.8	91.1	100.1	3.7	3.2	1.3	1.3	3.2	1.3	1.7
2	2.0	5.0	1.32	0.7	83.4	100.0	2.7	2.7	1.4	1.4	1.1	1.4	2.3

TABLE 2

Comparison of the accuracy of four methods for estimating the electrotonic parameters of an LSFC model from its impulse response. The parameters τ_o, τ_1, b_o and b_1 ($b_i = c_i / \tau_i$), were estimated by exponential peeling and are expressed as ratios to render the quantities independent of the absolute value of the membrane time constant. $\%\tau_m$ and $\%\tau_{lrtv}$ are the time constants estimated from the log(v) vs t and LRTV plots respectively, as a percentage of the membrane time constant.

Actual values					Estimated values										
									Brown		Johnston		Rall	Jack & Redman	
ρ	ρ_∞	L	$\frac{\tau_o}{\tau_1}$	$\frac{b_o}{b_1}$	$\%\tau_m$	$\%\tau_{lrtv}$	$\frac{\tau_o}{\tau_1}$	$\frac{b_o}{b_1}$	ρ	L	ρ	L	L	ρ_∞	L
5	5.5	0.5	29.70	0.60	99.7	132.0	20.7	0.9	0.9	0.5	1.7	0.5	0.7	4.0	0.6
5	7.9	.75	14.07	0.59	99.7	124.3	9.1	1.0	0.8	0.7	1.4	0.8	1.1	6.0	0.8
5	6.6	1.0	8.57	0.57	99.6	120.5	9.5	0.4	1.9	0.8	–	–	1.1	3.5	0.9
5	5.5	1.5	4.52	0.55	94.9	113.3	5.8	0.3	1.6	1.1	–	–	1.4	4.5	1.2
5	5.2	2.0	3.06	0.53	89.1	116.8	4.5	0.4	1.3	1.2	–	–	1.7	4.5	1.6
5	5.0	5.0	1.36	0.51	72.8	98.6	6.2	0.4	1.4	1.0	–	–	1.4	4.5	>2
2	4.3	0.5	22.50	0.89	99.8	125.7	24.8	0.7	1.4	0.4	3.4	0.5	0.6	3.5	<.5
2	3.1	.75	10.80	0.85	99.4	125.3	11.2	0.8	1.0	0.6	2.1	0.7	1.0	2.5	0.7
2	2.6	1.0	6.76	0.82	99.8	121.1	7.1	0.8	1.0	0.8	2.3	1.0	1.2	2.5	1.2
2	2.2	1.5	3.70	0.72	90.4	116.0	4.9	0.8	0.7	1.0	1.6	1.2	1.6	2.0	1.8
2	2.1	2.0	2.67	0.66	86.3	114.0	3.8	0.8	0.5	1.3	0.9	1.3	1.9	2.2	1.9
2	2.0	5.0	1.32	0.54	77.2	100.8	4.3	0.9	0.7	1.1	1.3	1.3	1.7	1.5	1.5

Errors in the estimates of the equalising time constants lead to inaccuracies in the estimates of ρ and L. In all cases Brown's method underestimates both L and ρ, the latter by as much 50%. Johnston's method is applicable in only a few instances as it is very sensitive to slight errors in exponential stripping. Of those methods based on exponential peeling, Rall's method proved to be the most reliable for estimating the electrotonic length, however, none of the three techniques could reliably detect the presence of an effectively infinite cable (i.e. L>2). (This last result has been noted by de Jongh and Kernell (1982) for Rall's method.)

Jack and Redman's method provided the most accurate estimates of ρ_∞ and L in the time domain, but it only reliably discloses the presence of an infinite cable if ρ_∞ is greater than or equal to 5.

The slope of the terminal portion of an LRTV plot, only gives an accurate estimate of the membrane time constant for neurones with cable lengths greater than 2λ. It is however difficult to estimate accurately the cables electrotonic length in the absence of reliable estimates of τ_m, and it is therefore hard to judge when the time constant estimated from the LRTV plot is appropriate.

In summary, the results of tables 1 and 2 suggest that the membrane time constant should be estimated from a log(v) vs t plot of the step response unless the appended cable can be shown to be greater than 2λ, in which case the time constant should be estimated from an LRTV plot of the impulse response.

3.3.3. FREQUENCY DOMAIN PARAMETER ESTIMATION IN PRACTICE

The input impedance of an LSFC model was generated with equation 2.11., with the same accuracy as the impulse response used in section 3.3.1. Thirty points of the impedance were calculated in the logarithmically spaced range of $.1/\tau_m$ to $100/\tau_m$ and a nonlinear least squares procedure (see section 4.2.7.) was used to estimate the electrotonic parameters τ_m, ρ_∞ and L. The results of parameter estimation are given in table 3. For all values of the parameters the frequency domain method proved more accurate than the time domain methods. Furthermore, the nonlinear least squares routine converged to the correct solution, even if the starting values of the parameters were in error by as much as fifty percent.

3.4. CONCLUSION

The results of this chapter demonstrate that time domain methods of electrotonic analysis may be very inaccurate leading to errors of as much as twenty percent in the estimate of the membrane time constant, even in the absence of modelling errors. In contrast, estimation of the parameters of an LSFC model in the frequency domain proves accurate irrespective of the actual values of the parameters.

TABLE 3

Parameter estimation in the frequency domain

True values τ_m = 100.0 ms			Estimated Values	
ρ_ω	L	τ_m	L	ρ_ω
1	0.5	107.14 ± 0.03	0.54 ± 0.14	0.89 ± 0.52
	1.0	103.35 ± 0.01	1.09 ± 0.04	0.96 ± 0.28
	1.5	106.01 ± 0.01	2.02 ± 0.09	0.95 ± 1.47
	2.0	104.54	5.46	0.98
	2.5	104.10	5.11	0.99
	3.0	104.28	8.26	0.99
5	0.5	102.05 ± 0.10	0.48 ± 0.05	5.16 ± 0.54
	1.0	103.61 ± 0.02	1.02 ± 0.05	5.12 ± 0.69
	1.5	101.79 ± 0.02	1.54 ± 0.05	5.02 ± 0.45
	2.0	102.39 ± 0.01	2.28 ± 0.07	5.02 ± 2.05
	2.5	102.12	3.10	5.03
	3.0	101.81	5.30	5.04
10	0.5	101.75 ± 0.14	0.48 ± 0.06	10.20 ± 1.26
	1.0	101.19 ± 0.09	1.01 ± 0.05	10.20 ± 0.52
	1.5	101.22 ± 0.03	1.57 ± 0.06	10.10 ± 0.95
	2.0	101.76 ± 0.01	2.11 ± 0.07	10.10 ± 1.50
	2.5	100.90 ± 0.01	2.59 ± 0.07	10.10 ± 2.54
	3.0	100.58	5.09	10.10

Value ± 99.5 % confidence interval.

In some cases the confidence interval could not be calculated.

CHAPTER 4

EXPERIMENTAL ELECTROTONIC ANALYSIS

4.1 INTRODUCTION

The B&C calculus allows the calculation of the attenuation of synaptic potentials between any two points on a neurone, if the electrotonic constants are known. Estimates of the unit membrane capacitance, of a great variety of cells, based on accurate measurements of the cell's area have generally arrived at values close to 1.0 μ F cm^{-2} (Cole, 1968), while the value of the intracellular resistivity, R_i, lies in the narrow range 50 to 100 (Foster et al., 1976) Ω cm. However, the unit membrane resistance, R_m may range between $1x10^3$ (squid giant axon) and $1x10^6$ Ω cm^2 (*Anisodoris nobilis*, Gorman & Mirolli, 1972). These observations suggest that while it is reasonable to assume values for R_i and C_m, it is not so for R_m. The objective of this chapter was to determine the unit membrane impedance of some identified neurones of the garden snail.

Frequency domain analysis has proved of value in understanding the complex electrical properties of skeletal muscle (Falk & Fatt, 1964; Valdiosera et al., 1974), yet the method has been applied to the analysis of nonspace-clamped neurones in only one instance, that of cat motoneurones (Nelson & Lux, 1970). In this chapter the input impedances of some identified snail neurones were measured and the minimization technique of chapter 2 was used to estimate the electrotonic properties. Inferences about the neurone's morphology derived from the input impedance were in some cases corroborated by filling the neurones with the dye Lucifer yellow.

Although parameter estimation is more accurate if performed in the frequency domain, the time domain responses of the neurones were measured because the step response is particularly sensitive to processess with very long time constants that might arise if the infoldings of the somatic membrane manifested as a resistance in series with the unit membrane resistance.

4.2. MATERIALS AND METHODS

4.2.1. PREPARATION

All experiments were performed on identified neurones of the suboesophogeal ganglion of the garden snail, *Helix aspersa*. The animals were collected locally and maintained in the laboratory at room temperature, on a diet of lettuce.

The brain was removed and mounted in a sylgard dish with the circulating saline maintained at a temperature of 19-20 ^{o} C. The experimental saline had the composition given by Kerkut and Meech (1966), with the addition of 10 mM glucose: NaCl 80 mM; KCl 4mM; $CaCl_2$ 7mM; $MgCl_2$ 5 mM; Tris HCl 5 mM; pH 7.8.

The connective tissue sheath was torn using a pair of jeweller's forceps. The ganglion was then exposed to a 1% (w/v) solution of protease (Sigma type VI) for 2 minutes, to soften the fine sheath overlying the cell bodies.

The neurones used are shown in figure 1. They were numbered according to Kerkut et al. (1975). Here the names of the ganglia are abbreviated to Lpr, Rpr and V, for the left parietal, right parietal and visceral.

4.2.2. RECORDING TECHNIQUES

Microelectrodes were filled with 3 M KCl and bevelled to a resistance of 15-20 MΩ using the the alumina slurry method of

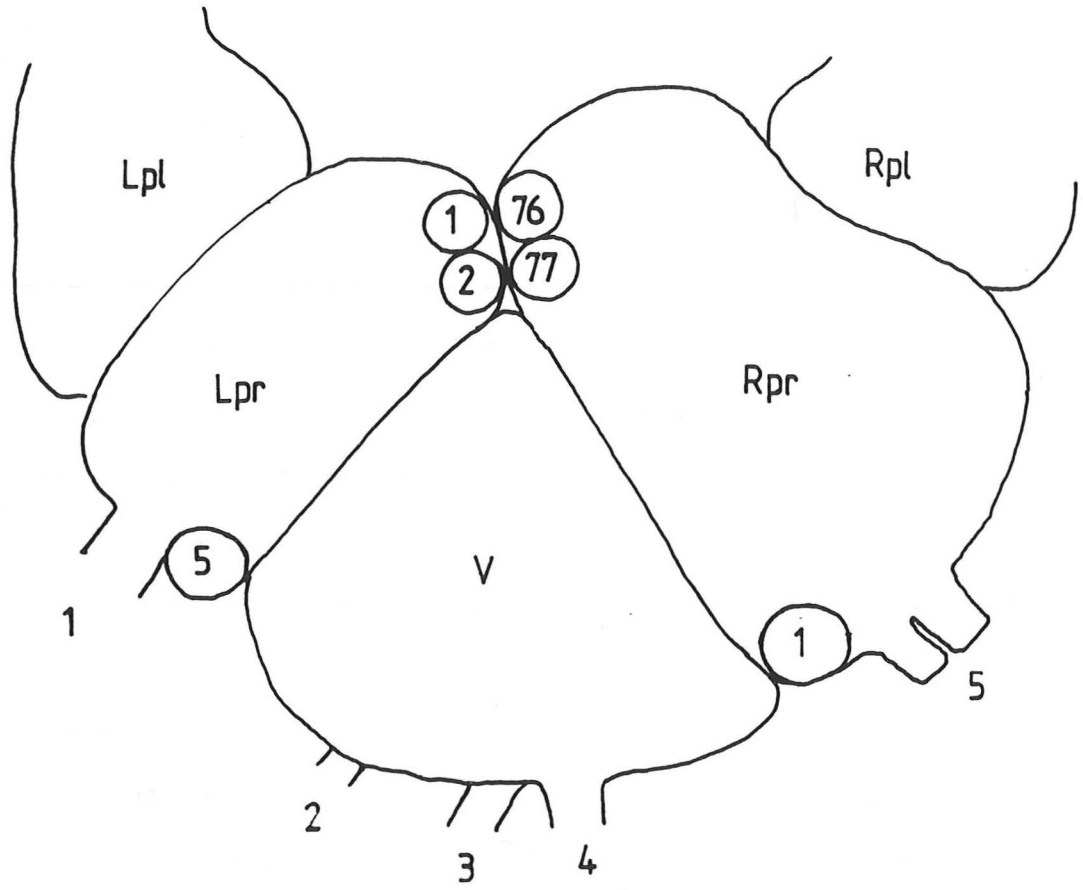

Figure 4.1. The location of identified neurones in the suboesophageal ganglion. The nerves are numbered; 1, left pallial; 2, cutaneous pallial ; 3, anal ; 4, intestinal ; 5, right pallial. (Lpl = left pleural ; Rpl = right pleural)

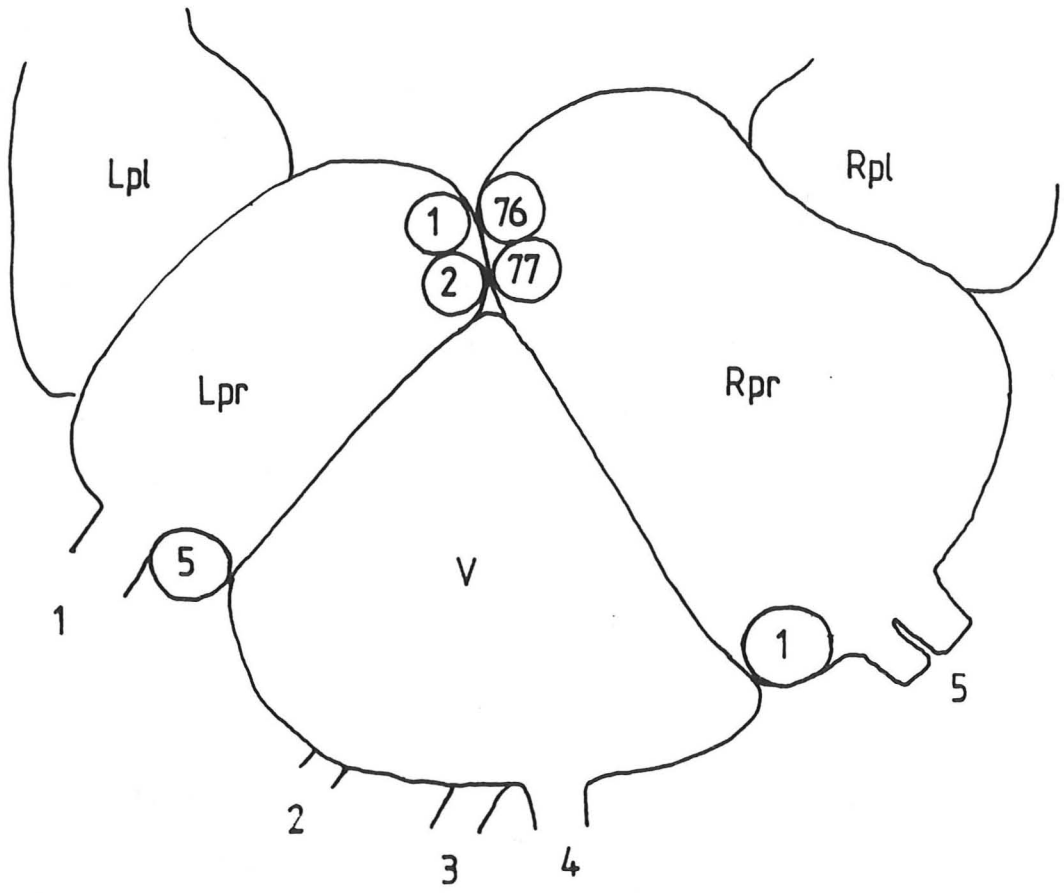

Figure 4.1. The location of identified neurones in the suboesophageal ganglion. The nerves are numbered; 1, left pallial; 2, cutaneous pallial ; 3, anal ; 4, intestinal ; 5, right pallial. (Lpl = left pleural ; Rpl = right pleural)

Lederer et al. (1979). In all experiments two independent microelectodes were used. The electrodes were held at an angle of approximately 60 ^{o} to one another, to minimize the artefact associated with the high access resistance of the current passing electrodes (Eisenberg & Engel, 1970).

Potentials recorded with this two electrode arrangement may be distorted by current flow in stray capacitances around and between electrodes. It is possible to estimate these capacitances and to correct the measured response (Falk & Fatt, 1964), however, the impedance of snail neurones is high and with precautions to minimize the stray capacitances, correction proves unnecessary.

The inter-electrode capacitance was reduced by interposing a grounded and insulated aluminium shield between the electrodes extending to within 0.5 mm of the tips of the electrodes. The microelectrode to bath capacitance was kept low, by ensuring that the saline only just covered the tips of the electrodes. A high input impedance, low input capacitance amplifier, without capacitance neutralization was used to record the voltage. (see appendix C for design). The input capacitance was minimized by driving the headstage lines and the FET case with a replica of the input voltage. The frequency response of the amplifier was flat up to 20 K Hz, this is well beyond the range over which the snail impedance was measured, ie .1 - 200 Hz. The inter-electrode coupling was measured by removing the current electrode from the neurone and measuring the coupling. In the frequency domain coupling up to 200 Hz. was insignificant.

Lederer et al. (1979). In all experiments two independent microelectodes were used. The electrodes were held at an angle of approximately 60 ^{o} to one another, to minimize the artefact associated with the high access resistance of the current passing electrodes (Eisenberg & Engel, 1970).

Potentials recorded with this two electrode arrangement may be distorted by current flow in stray capacitances around and between electrodes. It is possible to estimate these capacitances and to correct the measured response (Falk & Fatt, 1964), however, the impedance of snail neurones is high and with precautions to minimize the stray capacitances, correction proves unnecessary.

The inter-electrode capacitance was reduced by interposing a grounded and insulated aluminium shield between the electrodes extending to within 0.5 mm of the tips of the electrodes. The microelectrode to bath capacitance was kept low, by ensuring that the saline only just covered the tips of the electrodes. A high input impedance, low input capacitance amplifier, without capacitance neutralization was used to record the voltage. (see appendix C for design). The input capacitance was minimized by driving the headstage lines and the FET case with a replica of the input voltage. The frequency response of the amplifier was flat up to 20 K Hz, this is well beyond the range over which the snail impedance was measured, ie .1 - 200 Hz. The inter-electrode coupling was measured by removing the current electrode from the neurone and measuring the coupling. In the frequency domain coupling up to 200 Hz. was insignificant.

4.2.3. EXPERIMENTAL PROTOCOL

In all experiments a standard procedure was used to minimize the possibly deleterious effects of high current inputs. The order was : measure resting potential on entry ; note spontaneous spikes ; frequency domain impedance ; time domain reponse to small amplitude steps and impulses; current-voltage curve ; resting potential on exit ; repenetrate and fill cell with Lucifer yellow.

4.2.4. NEURONAL MORPHOLOGY

Microelectrodes for the iontophoretic injection of Lucifer yellow CH were prepared by filling the tips with a 5% solution of the dye and the barrels with 1M LiCl. The electrodes were bevelled to a resistance of 50-80 MΩ and the dye was injected using hyperpolarizing current pulses, 10-20 nA., of 500 ms. duration at a rate of 1 Hz. for one hour. The dye was allowed to diffuse for at least two hours and in some cases left overnight at 10^{o}C. To view neurones in a whole mount preparation, it was necessary to remove the pedal ganglion that underlies the visceral and parietal ganglia. The suboesophageal ganglion was fixed in 5% formaldehyde and then dehydrated in alcohol, and cleared in methyl salicylate.

The whole mounts were viewed with a Zeiss epifluorescence microscope. Drawings of the neurones were made with the aid of a 10 by 10 grid in the eyepiece. A program written for the North Star computer and digitizing tablet was used to rescale and where necessary mirror image the drawings. In addition, the program estimated the length and the area of all digitized branches.

4.2.5. DATA ACQUISITION SYSTEM

Most of the data capture and processing was performed on a North Star Horizon, an eight-bit microcomputer with 56K of RAM, a floating point board and two floppy disk drives. Analogue signals were digitized and output waveforms produced by a Cromenco eight-bit A/D. The data capture routines were written in Z80 machine code and the analysis of data was performed in North Star floating point BASIC.

4.2.5. TIME DOMAIN ELECTROTONIC METHODS

The input current and the transient voltage response were both digitized and stored on disk. The sampling rate was set such that there were at least 200 points sampled over the first two thirds of the transient. A minimum of ten transients were stored and subsequently averaged to improve the signal to noise ratio. The averaged response was stored on disk for further analysis. Transients were analysed as described in section 3.3.1.

The steady-state current-voltage (I-V) relationship of a neurone was measured in the following way. The neurone was stimulated with a triangular current wave-form with a period long enough to dissipate any capacitative effects. Both the input current and voltage output were stored on disk.

4.2.6. FREQUENCY DOMAIN ELECTROTONIC ANALYSIS

The input impedance in the frequency domain was measured by applying sinusoidal currents to the soma, and measuring the amplitude and phase of the voltage output as a function of input frequency. The amplitude and phase were determined using a single frequency Fourier transform, the Goertzel algorithm (see appendix D). An automatic procedure for measuring the impedance at a set of logarithmically spaced frequencies, was implemented

4.2.5. DATA ACQUISITION SYSTEM

Most of the data capture and processing was performed on a North Star Horizon, an eight-bit microcomputer with 56K of RAM, a floating point board and two floppy disk drives. Analogue signals were digitized and output waveforms produced by a Cromenco eight-bit A/D. The data capture routines were written in Z80 machine code and the analysis of data was performed in North Star floating point BASIC.

4.2.5. TIME DOMAIN ELECTROTONIC METHODS

The input current and the transient voltage response were both digitized and stored on disk. The sampling rate was set such that there were at least 200 points sampled over the first two thirds of the transient. A minimum of ten transients were stored and subsequently averaged to improve the signal to noise ratio. The averaged response was stored on disk for further analysis. Transients were analysed as described in section 3.3.1.

The steady-state current-voltage (I-V) relationship of a neurone was measured in the following way. The neurone was stimulated with a triangular current wave-form with a period long enough to dissipate any capacitative effects. Both the input current and voltage output were stored on disk.

4.2.6. FREQUENCY DOMAIN ELECTROTONIC ANALYSIS

The input impedance in the frequency domain was measured by applying sinusoidal currents to the soma, and measuring the amplitude and phase of the voltage output as a function of input frequency. The amplitude and phase were determined using a single frequency Fourier transform, the Goertzel algorithm (see appendix D). An automatic procedure for measuring the impedance at a set of logarithmically spaced frequencies, was implemented

on a North Star Horizon microcomputer.

The input wave-form was either a single sinusoid or a sum of two sine waves. For single sinusoid experiments the sine wave had a resolution of 32 points per period and the frequency could be set in the range .1 to 750 Hz. The output was sampled at the same rate as the input.

For each point on the impedance curve a minimum 16 periods were output and stored. Beginning at the 5th period, groups 4 periods long were averaged using a machine code routine. Up to 33, 4-period groups could be averaged. The first 4-period groups were omitted from the average to allow the system to come to a sinusoidal steady-state. The adequacy of this period was tested on a number of neurones, using different frequencies and varying the number of omitted periods. No significant difference was found between the phase and amplitude measured when more than two periods were omitted, for frequencies ranging from 1 to 500 hz.

The Goertzel algorithm was applied to the average wave-form stored in RAM. It is important to note that the algorithm was applied to a wave-form with 4 periods. This was done so as to reduce the broadness of the amplitude response of the Goertzel algorithm, the broadness being inversely proportional to the number of periods (Bracewell, 1965). The filter characteristics of the algorithm was measured by applying a constant frequency sine wave and sweeping the algorithm through a range of frequencies on either side of the input frequency (see fig. 2)

The eight-bit A/D used places an unavoidable limitation on the precision of time domain experiments. However, when single

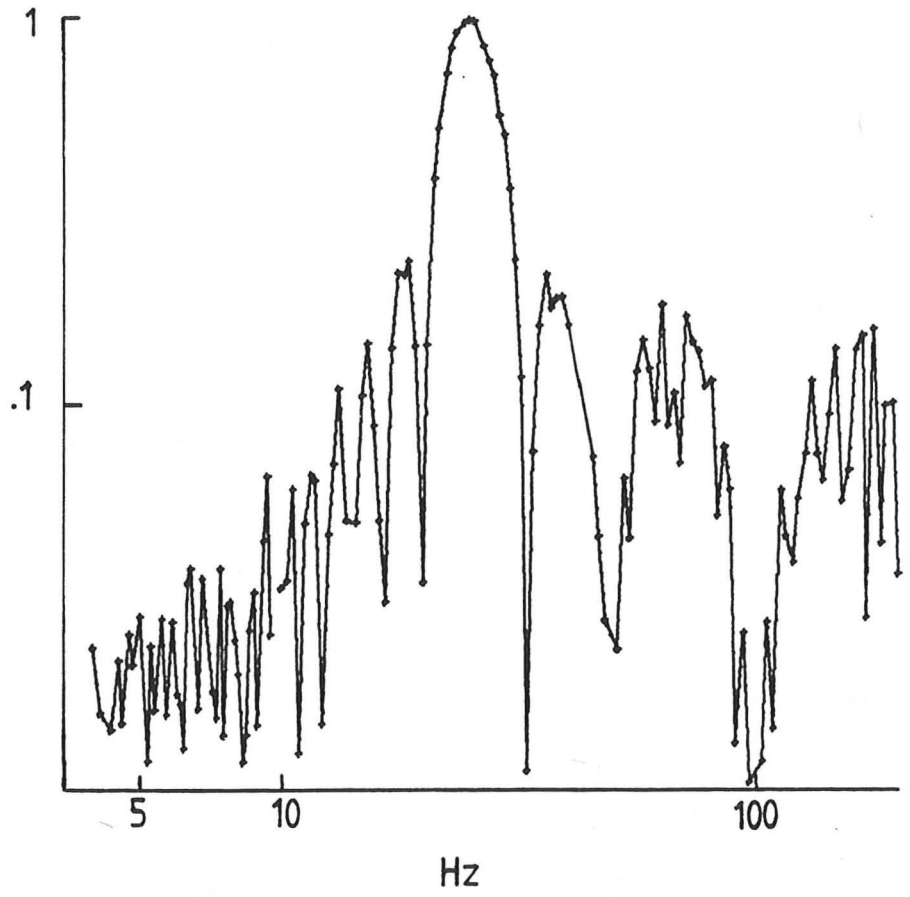

Figure 4.2. The filter characteristic of the Goertzel algorithm. The input was a 25 Hz sinusoidal signal. The ordinate of the figure represents the normalized amplitude of the input measured by the algorithm.

sinusoidal stimulation is used the precision can be extended by increasing the gain of the input amplifier as the amplitude of the output falls. In these experiments twenty frequencies in the range .5 to 10 Hz were sampled and stored, then the gain was increased and twenty frequencies in the range 10 to 200 Hz were sampled.

If a signal contains components with frequencies greater than half the sampling frequency, these high frequencies will be shifted to low frequencies in the sampled signal. This effect, termed aliasing, can be avoided by using a filter which eliminates all frequency components with frequencies half the sampling rate (Bracewell, 1965). However, in the experiments described in this chapter the system is driven with a sinusoidal signal, and the output has a greater amplitude than the aliased components. That aliasing was in fact insignificant, was demonstrated as follows. The Goertzel algorithm was used to measure the amplitude and phase of a sinusoidal signal, before and after filtering by an anti-aliasing filter. For signals with a signal-to-noise ratio as high as 5:1 there was no detectable difference between the filtered and unfiltered signal. As the signal-to-noise ratio in the experimental system was never greater than 5:1, the effects of aliasing should therefore be negligible and no anti-aliasing filter was used. Furthermore, the input and output signals were averaged in all experiments and this also has the effect of reducing aliasing.

4.2.7. PARAMETER ESTIMATION IN THE FREQUENCY DOMAIN

To estimate the neurone's electrotonic properties a homogeneous LSFC model was assumed and the error between the experimental and the theoretical impedance was minimized by

varying three parameters: the membrane time constant, τ_m ; the electrotonic length of the cable, L ; the dendritic to somatic conductance ratio for a cable with infinite length, ρ_∞

The input impedance of an LSFC model was derived section 2.2.5., and using the definition of ρ_∞, equation 2.10 can be rewritten as,

$$K_{ss}(j\omega) = \frac{R_{inp} \left(1 + \rho_\infty \tanh L \right)}{1 + j\omega\tau_m + \rho_\infty (1 + j\omega\tau_m)^{1/2} \tanh \left((1+j\omega\tau_m)^{1/2} L \right)} \qquad (1)$$

The impedance data was transfered to an IBM 3081 and the minimization affected with a modified Gauss-Newton algorithm (Numerical Algorithms Group E04FCF). The sum of squares to be minimized was given the form:

$$SOS = 1/N \sum_{i=1}^{N} \left[(A^e(i) - amp^t(i))^2 / (A^e(i))^2 + (\phi^e - \phi^t)^2 / F^2 \right] \qquad (2)$$

where, 'A' = amplitude, ϕ = phase, F the maximum modulus of the phase and 'e' and 't' denote the experimental and theoretical quantities respectively. This normalization is necessary to ensure that the amplitude and phase have equal weighting.

It is not possible to prove that the best fit obtained is a global minimum. The parameters obtained were considered satisfactory if the routine converged to the same solution when different starting values were used for the parameters. As an additional test of the fitted parameters their 99.5 % confidence intervals were calculated. If the confidence interval is an appreciable fraction of the parameter value itself the parameter is poorly determined by the available data.

4.3. RESULTS

4.3.1 NEURONAL MORPHOLOGY

The neurones used in the electrotonic experiments were Lpr1 and 2, and Rpr 76 and 77, which are located on the dorsal surface of the left and right parietal ganglia, as a symmetrical pair about the cleft separating the two ganglia (see fig. 1). The cell bodies are large, with diameters in the range 80-200 µm, and are clearly distinguishable from the neighbouring cells. In some preparations only two or three of the neurones were visible. In all cases where this was investigated the missing cells were found to be obscured by small overlying cells or were located deep within the cleft between the left and right parietal ganglia. The neurones showed little synaptic activity and few spontaneously generated action potentials. Nothing is known about the function of these neurones.

It was not possible to distinguish between LPr1 and Lpr2, or between Rpr 76 and Rpr 77 on the basis of cell position, neuronal activity or action potential shape. However, it was shown (see below) that one of the left-hand cells is coupled electrically to one of the right-hand cells. This coupling was only discovered towards the end of my period of research and was not used to identify neurones in the electrotonic experiments. As ipsilateral neurones were not distinguished in these experiments the left parietal neurones are referred to as Lpr 1/2 and the right parietal neurones as Rpr 76/77.

Lucifer yellow disclosed the presence of branches at distances of up to 1000 µm from the soma, and neurites having diameters less than 0.5 µm were revealed. In all Lpr 1/2 and Rpr 76/77 neurones where the finest branches were visible, there was

a marked difference between the diameters of the fine neurites and their parent branches. The fine neurites never exceeded a diameter of 1 µm, while the parent branches were seldom less than than 5µ in diameter (see fig. 3).

An attempt was made to distinguish between ipsilateral partners of Lpr1/2 and Rpr 76/77 on the basis of the shape of the neurones. To classify the neurones, only the major neuronal branches are considered. However, the branches running through to the pleural ganglia were often inadvertendly destroyed during the preparation of the ganglion, and as it is difficult to distinguish between a true termination and a broken branch these branches were not considered when classifying the neurones. Furthermore, it is difficult to distinguish between a true branch termination and an incompletely filled one, therefore only the presence or absence of a branch is taken into account in classifying the neurone, not whether or not the branch exits through a peripheral nerve.

4.3.1. Lpr 1/2

Of the eleven Lpr 1/2 neurones filled, nine were monopolar, with the primary neurite bifurcating 50 to 200 µm from the soma. Two neurones were bipolar.

In the eleven filled neurones there were four possible branches running in or towards the peripheral nerves. If the neurones were divided into classes on the basis of the number and type of branches, irrespective of where the branch terminated, there were three classes. There was no obvious way of dividing the filled neurones into two classes on topological grounds.

A composite diagram with the percentage occurrence of each

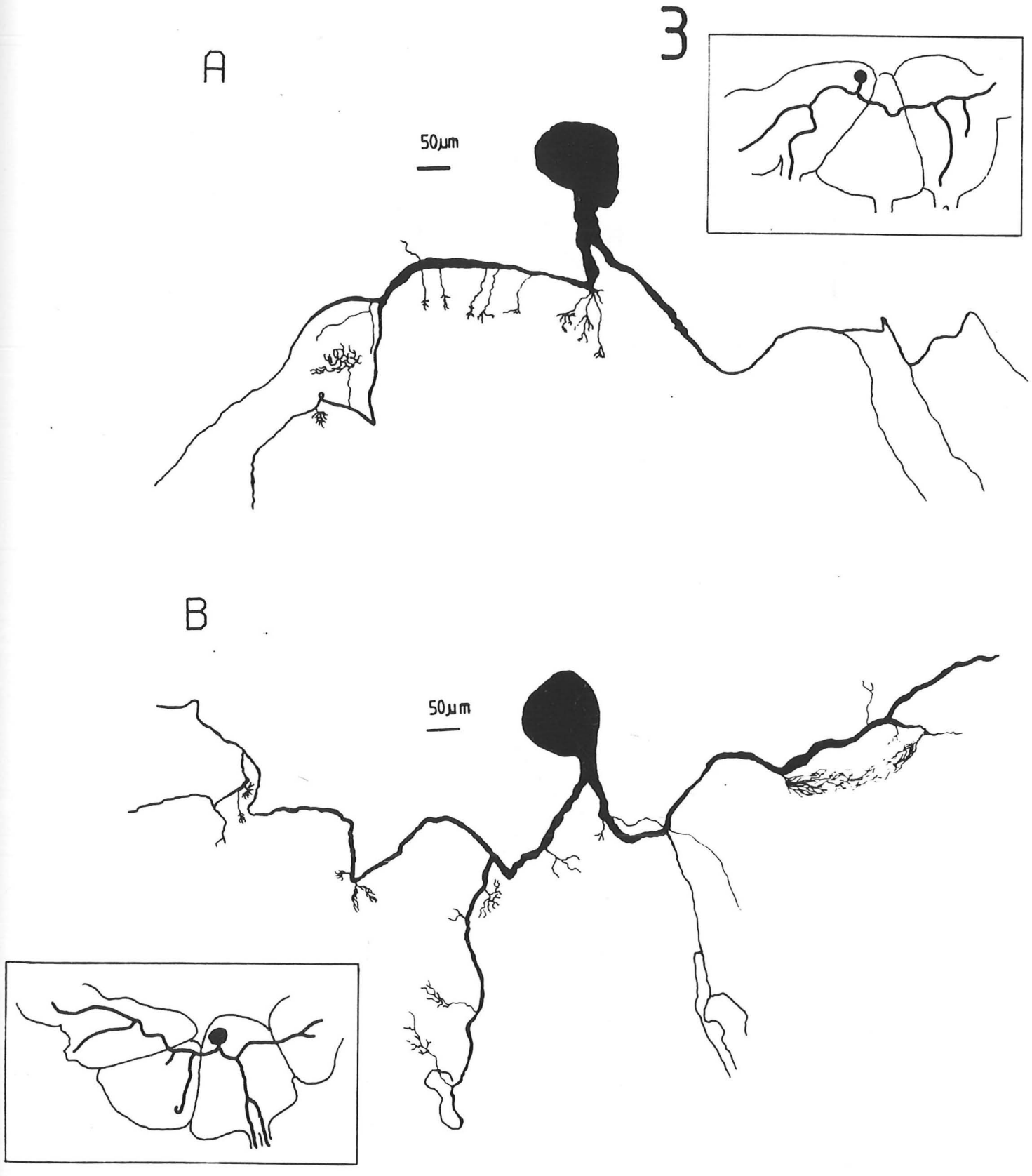

Figure 4.3 Drawings of Lucifer yellow fills of; (A) Lpr 1/2 (B) Rpr 76/77. The insets show the relationship of the neurone to the ganglion outlines.

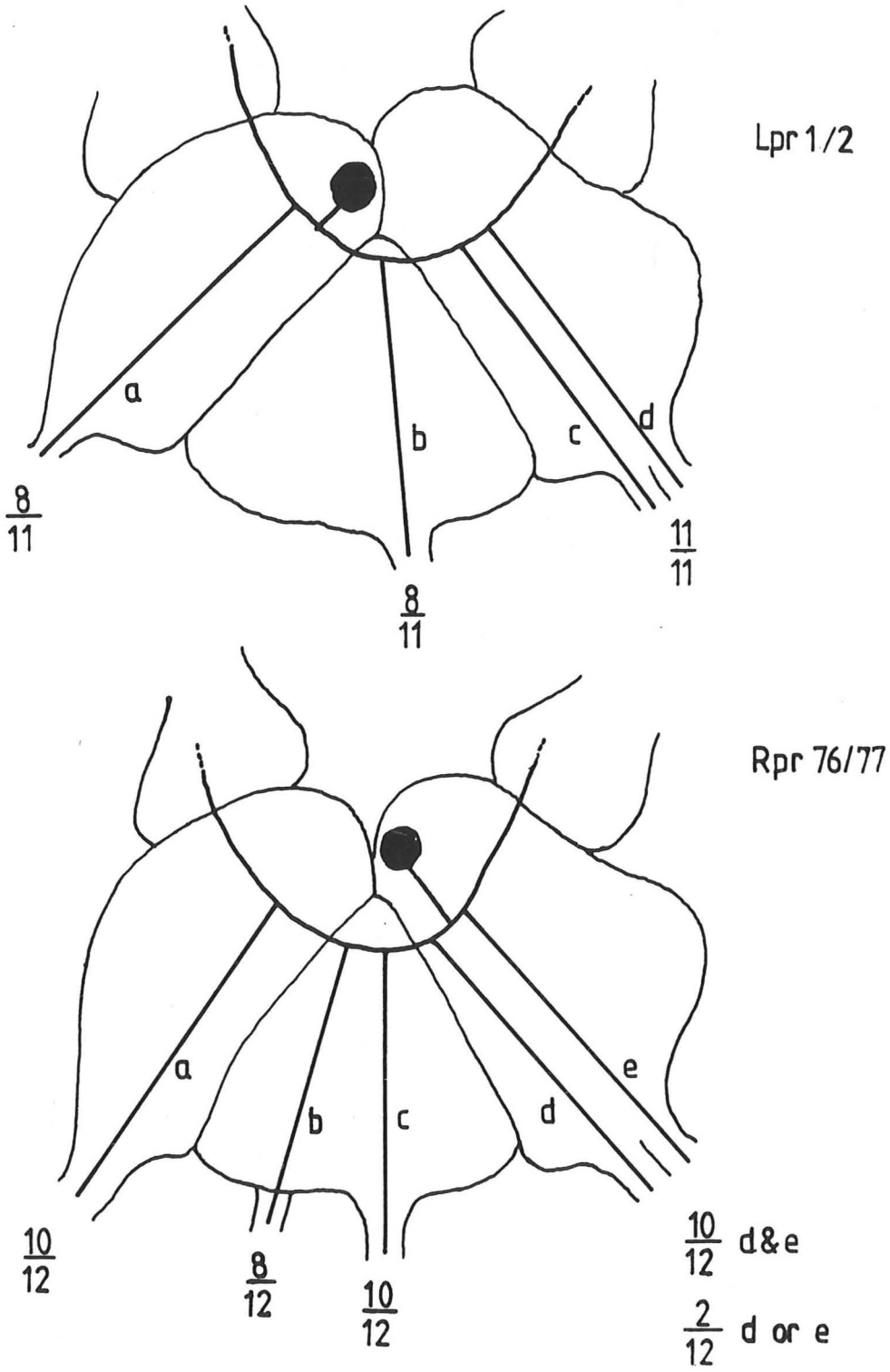

Figure 4.4 Diagram of the axonal projections of; (A) Lpr1/2 (B) Rpr 76/77. The fractions indicate the observed occurrence of the designated branch.

branch is given in figure 4A. The only invariant characteristic of the filled neurones was the possession of two tertiary branches in the right parietal ganglion (branches c&d).

4.3.2. Rpr 76/77

The primary and secondary branches were the mirror image of those of Lpr1/2. There were however now five possible branches running into or towards the peripheral nerves. Again creating classes on the basis of the number and type of branches, for the 12 filled neurones there were six classes. In contrast to Lpr1/2 the presence of two branches in the right parietal ganglion was not invariant, and there was always at least one branch in the visceral ganglion (see fig. 4B).

The inability to separate ipsilateral neurones on morphological grounds is consistent with the observed variability of identified molluscan neurones (Winlow & Kandel, 1976 ; Haydon & Winlow, 1981).

4.3.2. ELECTROTONIC COUPLING

Electrotonic analysis is to some extent dependent upon the revealed morphology corresponding to the electrotonic structure. If for example a neurone is coupled electrically to another neurone, and the coupling is not revealed by intracellular dye, the coupling will in effect behave like an invisible dendritic branch. This could severely distort the measured time constant if the coupling is strong and morphology is used to calculate the time constant.

Lucifer yellow fills of Lpr1/2 and Rpr 76/77 gave no evidence of dye coupling. However, in other invertebrate ganglia there are examples of electical coupling in the absence of Lucifer yellow coupling (Gibson, 1983). As a first approach to

the problem, coupling between members of the group Lpr1/2 and Rpr76/77 was tested electrophysiologically. In ganglia in which all four cells were clearly visible, all six possible coupling pairs were tested. In nine ganglia tested, one right parietal cell was coupled to one left parietal cell. The coupled pair was most often, though not invariably, the two most anteriorly located cells and the coupled pair were designated Lpr1 and Rpr 76. This method of identifying cells was discovered at the end of my period of research and was not used to identify cells in the electrotonic experiments.

The responses of the electrically linked neurones to hyperpolarizing and depolarizing steps are illustrated in figure 5A. The response to depolarizing current is broken periodically by hyperpolarizing bouts, which result from the electrotonic coupling of the after-potential of the action potential (see fig. 5B).

The transfer impedance between neurones Lpr1 and Rpr76 was measured by applying sinusoidal current signals to one neurone and measuring the amplitude and phase of the voltage in the other neurone. The voltage response was nonlinear (see fig. 6 A & B), however measurement of the fundamental content gives an estimate of the linear properties of the system (see ch. 5). A typical transfer function is illustrated in figure 6A. In all cases where the transfer function was measured, the phase decreased with frequency past -90^{o}. Should the neurones be linked at the soma, which is clearly impossible in this case, the phase could not be lower than -90^{o} (Di Caprio & French, 1975). The form of the transfer impedance curves demonstrates that the two somas are

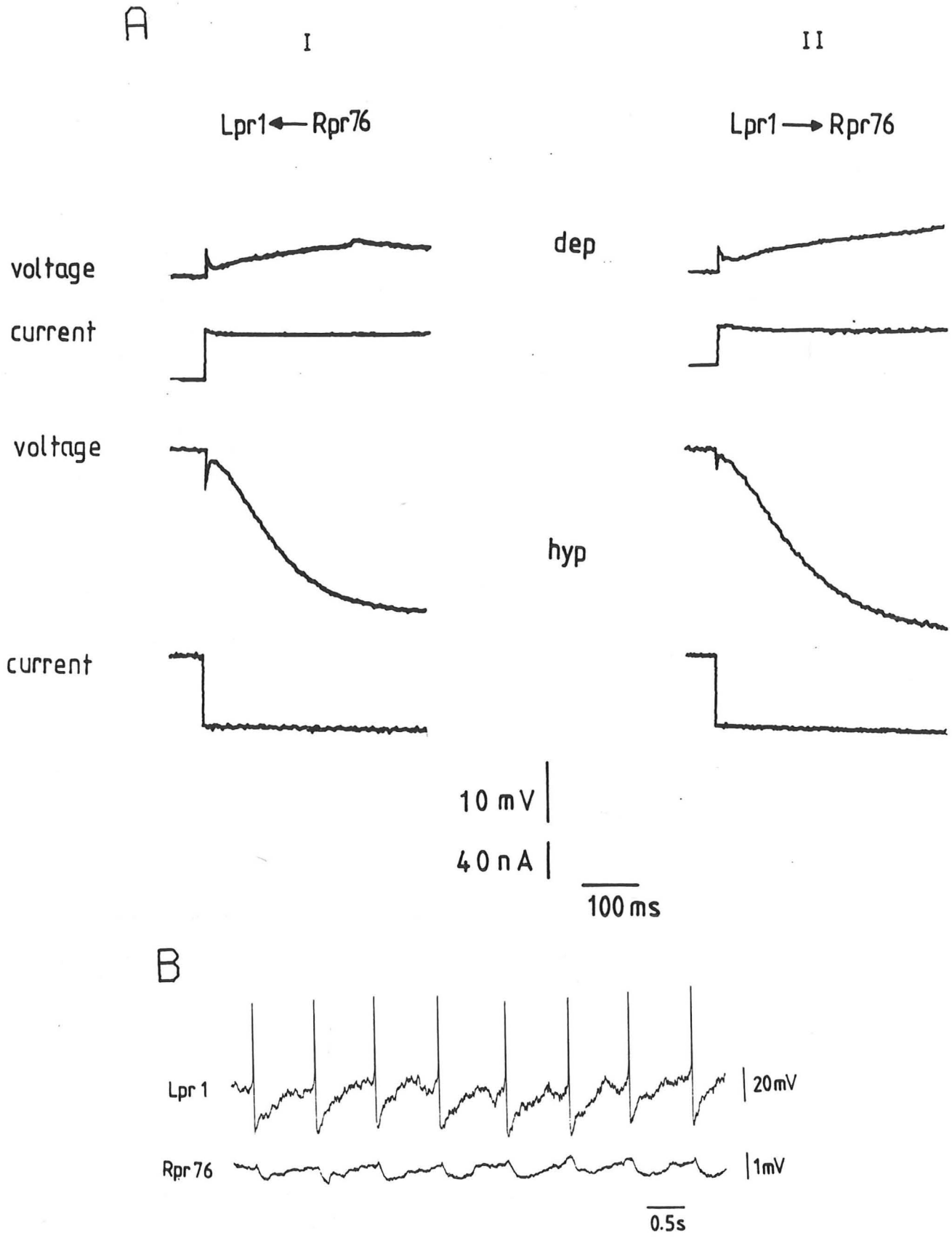

Figure 4.5. (A) The response of the coupled neurones, Lpr 1 and Rpr76 to hyperpolarizing (hyp) and depolarizing (dep) current steps. (I) Current input to Rpr 76 and voltage response of Lpr 1 (II) Current input to Lpr 1 and voltage response of Rpr 76. All voltage responses are the average of 25 transients. (B) Response of Lpr1 and Rpr76 to a step current input applied to Lpr1.

linked by a non-isopotential length of cable.

It might be argued that the phase change results from the nonlinearity of the neuronal membrane, however in chapter 5 it is shown that the phase change of the input impedance is in a direction opposite to that expected from an interposed cable.

If the electrotonic constants of both the linked neurones were known, and each neurone could be modelled as a simple electrotonic structure, the length of the connecting cable could be estimated from the transfer impedance by parameter estimation using the appropriate B&C equation.

To estimate the possible effects of electrotonic coupling on measurements of the electrotonic properties of the coupled neurones, they were modelled as two somas linked by a cable. The B&C formalism was used to derive a steady-state equation which allows the estimation of the diameter of the linking cable, if R_m, the soma radius and the length of the cable are known. Using the average value of the soma diameter (100 μm see section 4.3.4.2.), the average unit membrane resistance ($5x10^4$ Ω cm^2 see section 4.3.5) and the average coupling resistance (200 KΩ), the cable diameter at different cable lengths is; .5 λ, .06 μm ; 1 λ, .18 μm ; 2 λ, 0.39 μm. The effective diameter of the coupling branch is smaller than the major neuronal branches (diameters typically 5μm), and as the arguments of section 2.4.3.1. show the coupling should have no influence on the measured electrotonic properties.

4.3.3. MEMBRANE LINEARITY

The electrotonic methods described in chapters 2 and 3 are predicated upon the linearity of the system, and therefore, the accuracy of the methods will in part be determined by the adherence of the system to linear behaviour. Neurones, however, are intrinsically nonlinear, and linearity can only be ensured if the amplitude of the input is kept suitably small. Two methods

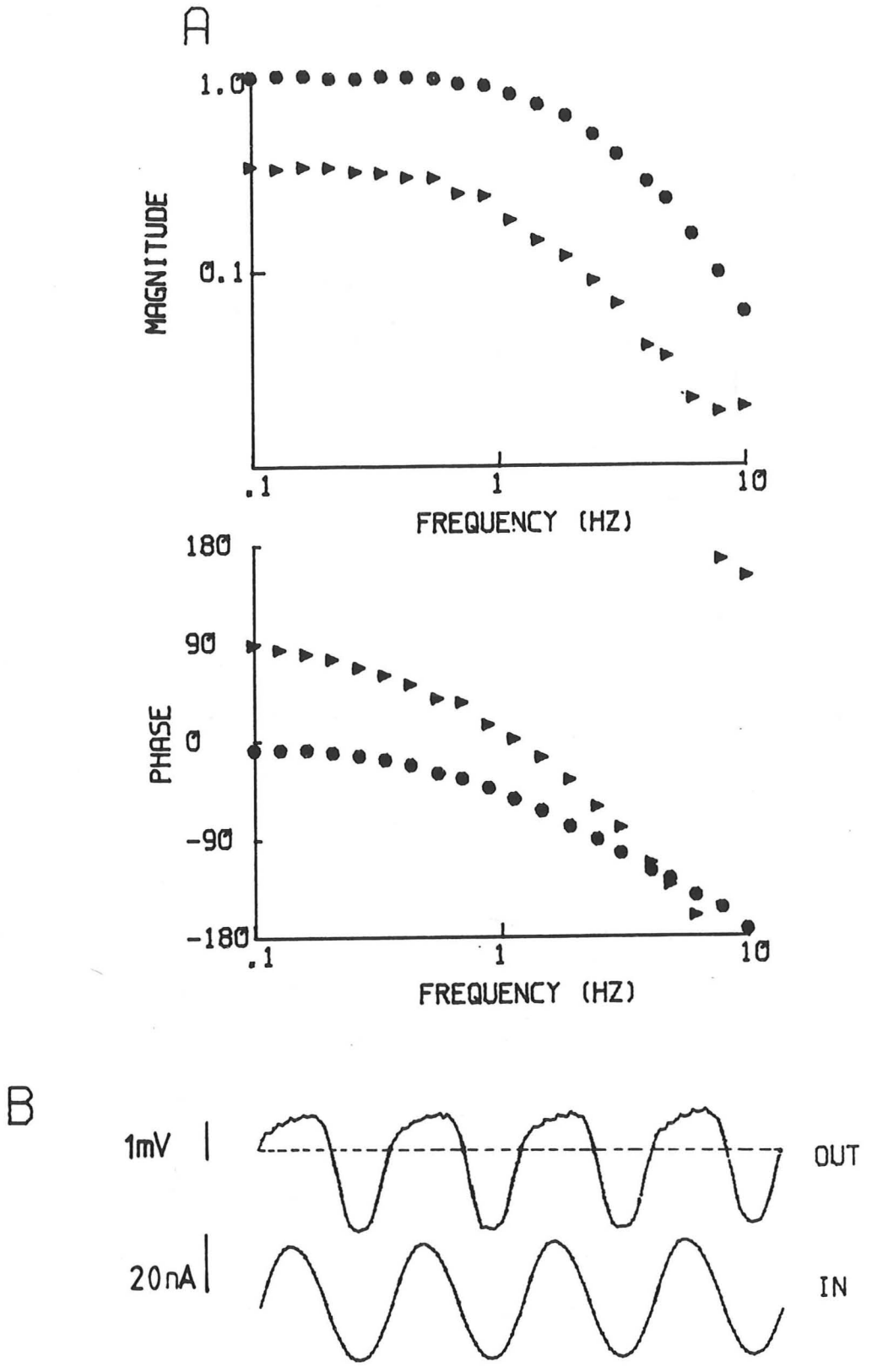

Figure 4.6. The transfer impedance from neurone Lpr1 to Rpr76, measured with an input of 40 namp. The magnitude has been normalized with the maximum amplitude of 3.5 mV of the fundamental component. (● - Fundamental component & ▶ - second harmonic) (B) Coupling of .1 Hz sinusoidal signal from Lpr1 to Rpr 76.

input current.

The steady-state I-V characteristics of a neurone were measured with a slowly rising current ramp (approximately 0.5 nA/s). In general, the curves were linear for 3 to 5 nA on the hyperpolarizing side of zero current and for 1 to 2 nA. on the depolarizing side (see fig. 7). For depolarizing and hyperpolarizing currents at high amplitudes, rectification was evident.

In the frequency domain linearity is simply defined: if the response of a system to a sine wave input contains no harmonic components, then the system is linear. In chapter 5 it is shown that if the response of Lpr1/2 or Rpr 76/77 is nonlinear, the second harmonic component is always the predominant harmonic component. Furthermore, the amplitude of the second harmonic decreases as the frequency of the input increases. To establish an appropriate amplitude for use in electrotonic analysis the following procedure was used; a 1 Hz sine wave was used to stimulate the neurone and the second harmonic content of the response was measured. The amplitude of the input was adjusted so that the nonlinear content of the response was negligibly small.

The frequency domain method proved more sensitive than the time domain method in detecting nonlinearities. Furthermore, the frequency domain method is simpler to perform on-line than the time domain method.

4.3.4. FREQUENCY DOMAIN ELECTROTONIC PROPERTIES

Two representative input impedance curves are displayed in figures 8 and 9 ; the first has a long cable (> 1λ) and the second has a short cable (< 1λ). In no case was the observed

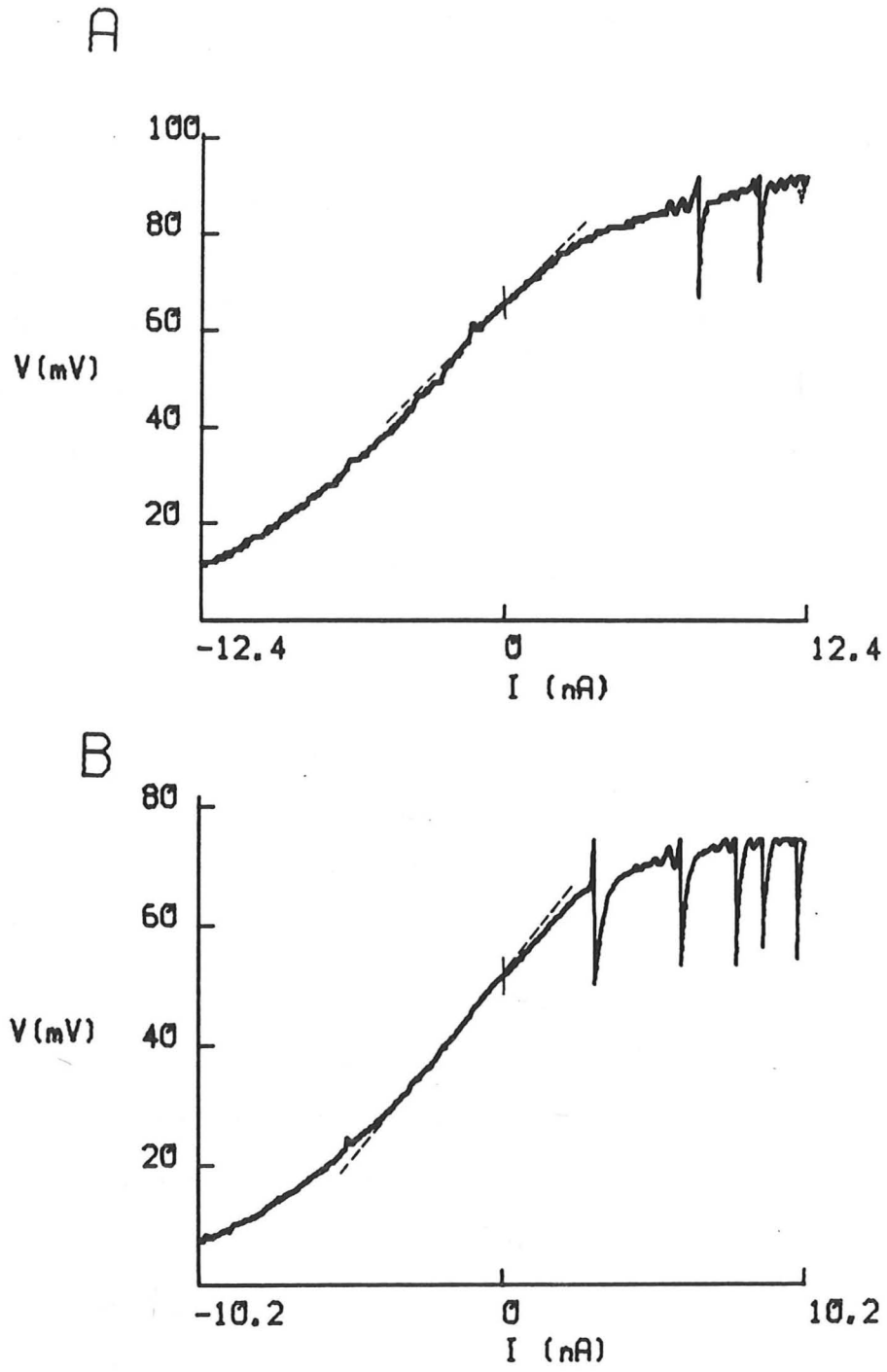

Figure. 4.7. Steady-state I-V curves of (A) Lpr1/2 (B) Rpr76/77. The frequency of the saw tooth input was 0.05Hz. No hysteresis was observed.

impedance compatible with the response of a parallel R-C circuit; the influence of a loading cable could always be detected. Parameter estimation indicated that the measured input impedance was consistent with a low ρ_∞ (< 5) and L in the range .7-3 λ. As mentioned in chapter 2, low values of ρ_∞ mask the influence of any appended cable, making it difficult to estimate reliably the length of the cable.

The parameters estimated from the measured input impedances are given in figures 8 & 9 together with the associated confidence levels. Both ρ_∞ and L had high confidence levels. In contrast the membrane time constant was in most cases well determined, the confidence level being no more than 2% of the absolute value. Two impedance curves were measured in most cases and they proved to be reproducible to within 3%.

In a number of cases attempts were made to fit the measured input impedance with an LSFC with a closed-termination (n = 8) and with an LSFC model with different somatic and dendritic unit resistances (n = 10). In no case did either of these models fit the data better than the LSFC model. Furthermore, the results of fitting an inhomogeneous LSFC model to the measured input impedance were in all cases consistent with a homogeneous unit membrane resistance. Neither of these models proved to be statistically better than the LSFC model. Furthermore, the results of fitting an inhomogeneous LSFC model to the measured input impedance were in all cases consistent with a homogeneous unit membrane resistance.

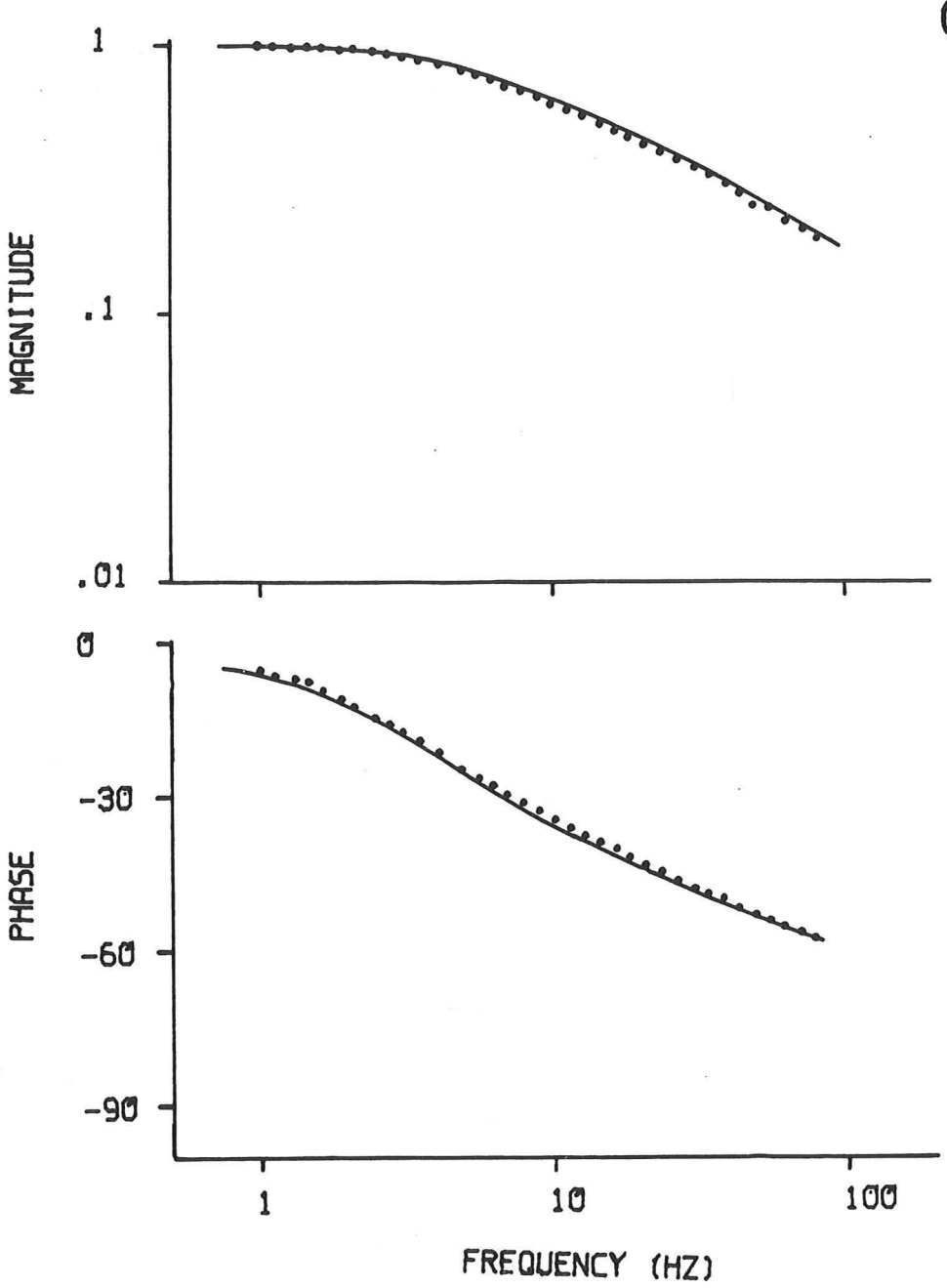

Figure. 4.8. Input impedance of Rpr 76/77 neurone. The input amplitude was 0.7 nA and the magnitude has been normalized by the maximum voltage of 3.2 mV. The continuous line represents the best fitting LSFC model with parameters; (estimated value ± 99.5 % confidence level) τ_m = 28.4 ± 0.3 ms ; L = 1.69 ± 0.9 ; ρ_∞ = 4.2 ± 2.4.

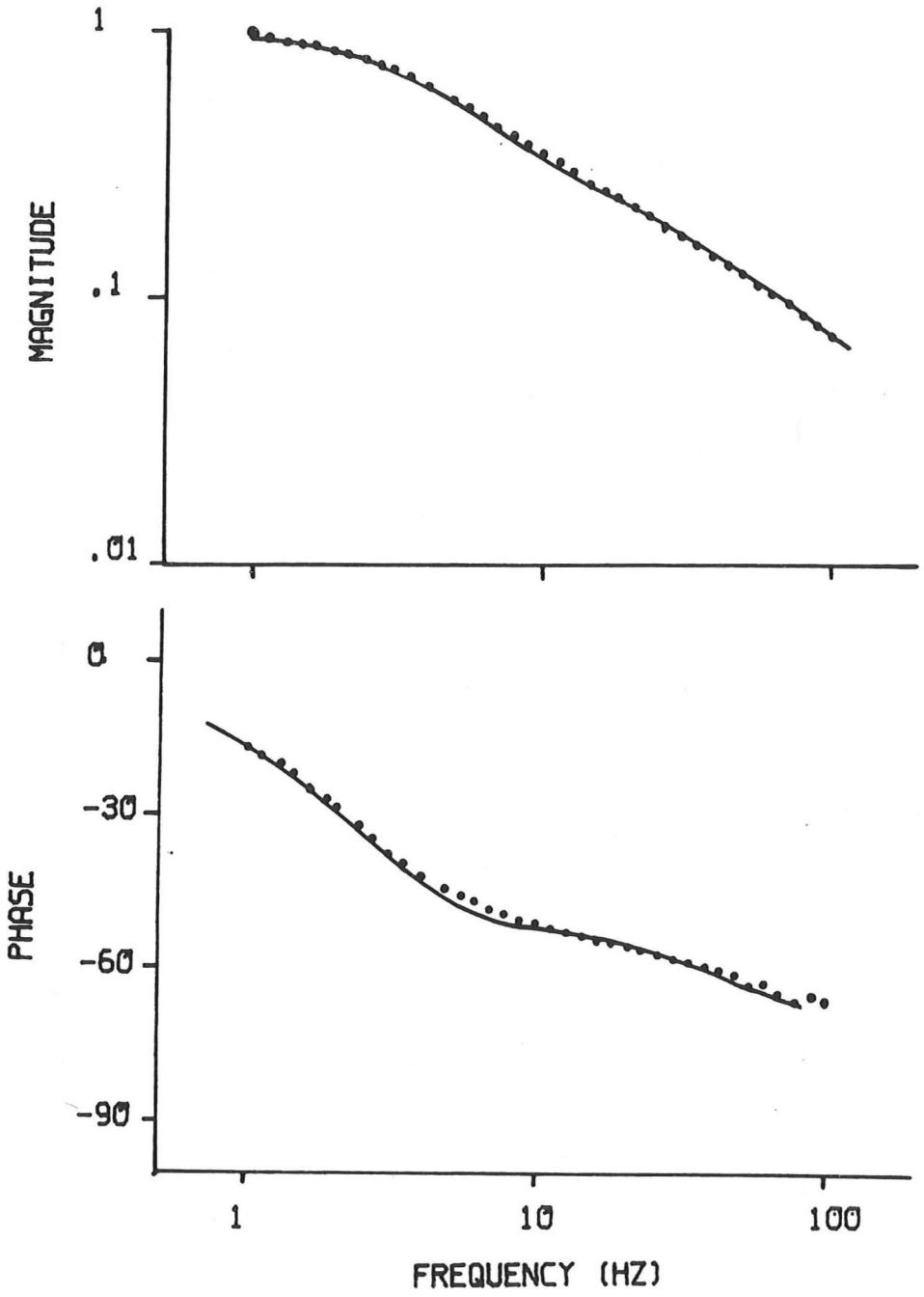

Figure. 4.9. Input impedance of a Rpr 76/77 neurone. The input amplitude was 0.8 nA and the magnitude has been normalized by the maximum voltage of 6.7 mV. The continuous line represents the best fitting LSFC model with parameters; (estimated value $\pm$ 99.5 % confidence level) τ_m = 56.7 $\pm$ 0.5 ms ; L = 0.87 $\pm$ 0.52 ; θ_∞ = 4.8 $\pm$ 1.4.

4.3.4.1 TWO-TIME CONSTANT RESPONSES

All neurones responded to a step input with a voltage transient that appeared to be a sum of exponentials. In 30.5% (n= 110) the transients the slowest time constant measured by exponential peeling was very slow, being in the range 100-200 ms. These values are compatible with membrane time constants reported in the literature (Gorman & Mirolli, 1972), however, comparison of the time and frequency domain responses demonstrates that this slow time constant cannot be identified with the membrane time constant.

The step response shown in figure 11b could be approximated by a sum of two exponentials with time constants of 179 and 50 ms. This suggest that the membrane time constant is 179ms, however, the time constant of the system estimated by fitting the frequency domain data to an LSFC model is 63 ms. The impedance was not sampled at a low enough frequency to detect the slow component. Nevertheless the slow component observed in the time domain cannot be equated with the membrane time constant because it would result in a half-maximal phase change at a frequency of about 1Hz whereas in practice it occurs at 3 Hz.

No attempt was made to define the origins of the slow component.

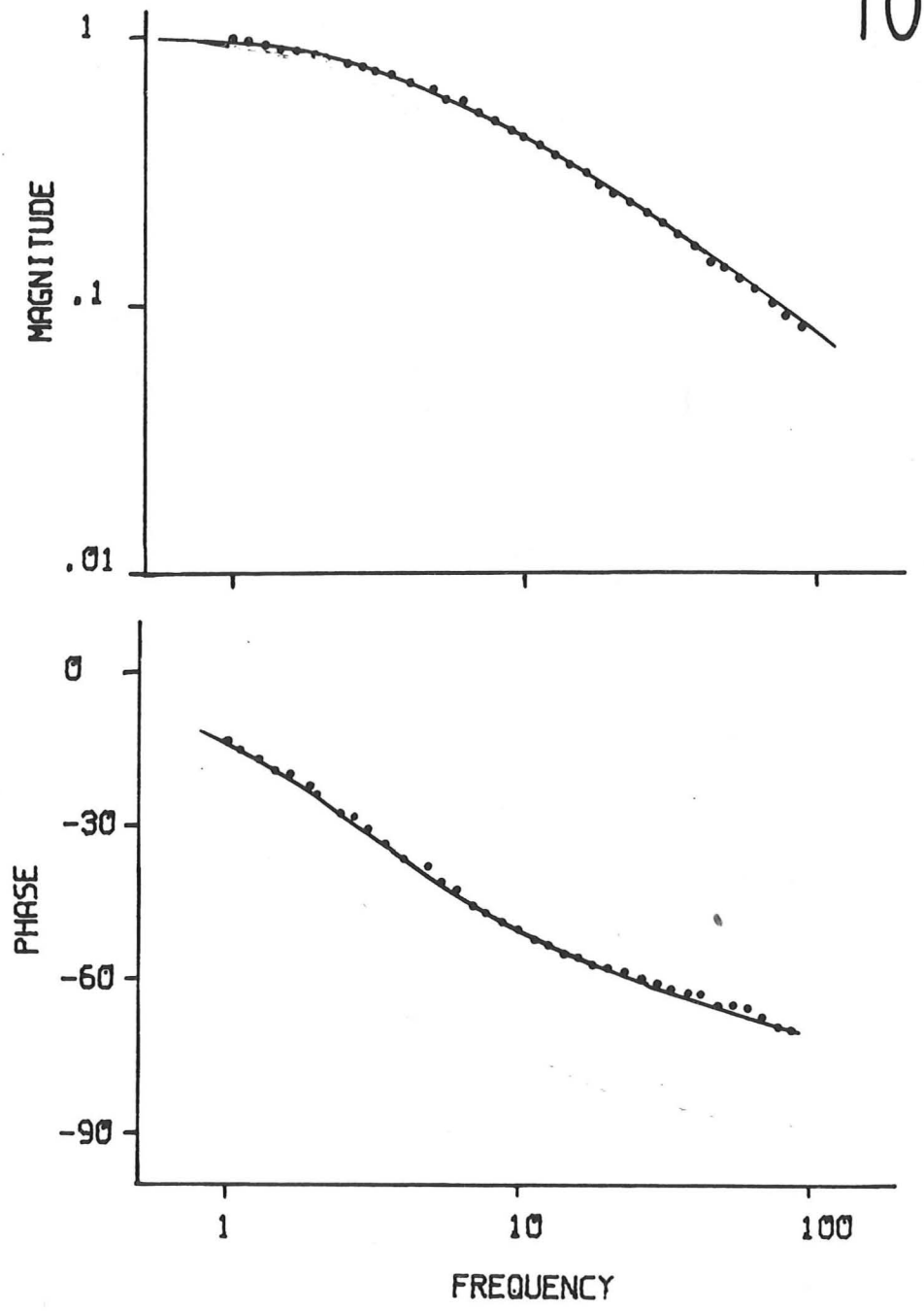

Figure. 4.10. Input impedance of a Rpr 76/77 neurone. The input amplitude was 0.4 nA and the magnitude has been normalized by the maximum voltage of 7.7 mV. The continuous line represents the best fitting LSFC model with parameters; (estimated value ± 99.5 % confidence level)

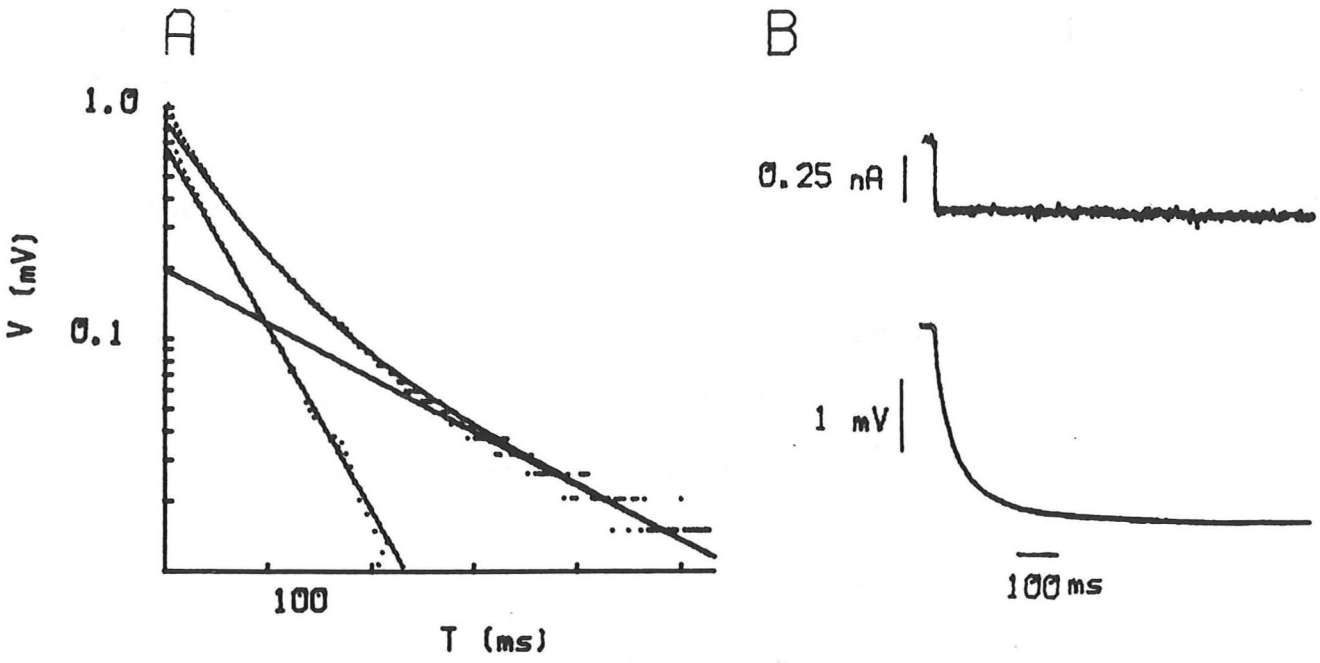

Figure 4.11. (A) log (V) vs t plot of the transient response of the Rpr 76/77 neurone of fig. 10, to a hyperpolarizing step current input. The transient was normalized by the maximum voltage of 3.8 mV. The average voltage transient (n=25) is represented in B.

4.3.4.2. MORPHOLOGY AND INPUT IMPEDANCE

In fifteen instances both the morphology and the input impedance of a neurone were measured. These are of interest because it is possible to attempt to relate the observed morphology to measured impedance. However, care should be exercised in the interpretation of the morphology as determined from whole mount preparations, as the membranes of molluscan neurones are known to have numerous infoldings (*Helix*; Akaike et al. (1983); Lane & Swales (1976)). In *Aplysia*, the observed diameter of a dendrite may underestimate the true diameter by a factor of ten (Graubard, 1975). The observed diameter in a whole mount preparation may therefore be much smaller than the true diameter and length constants estimated from the apparent diameter should be considered as lower bounds.

The input impedances of the neurones displayed in figure 3 A and B are shown in figures 13 and 14 respectively. In both cases the fit to an LSFC model is good and it is not possible to detect any obvious signs of an impedance mismatch from the input impedance.

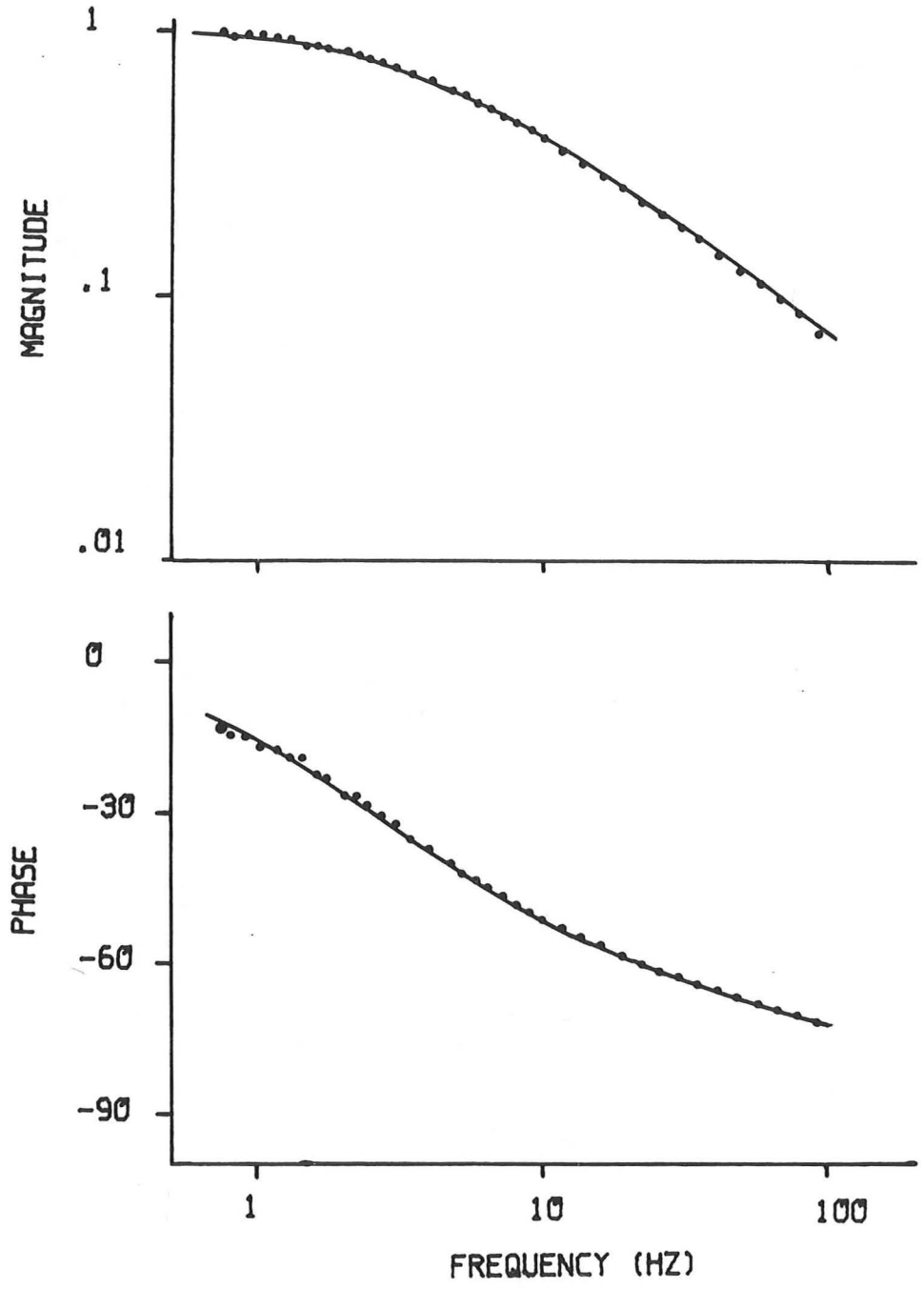

Figure 4.13. Input impedance of the Lpr 1/2 neurone represented in fig. 3A. The input amplitude was 1.3 nA and the magnitude has been normalized by the maximum voltage of 8.1 mV. The continuous line represents the best fitting LSFC model with parameters; (estimated value ± 99.5 % confidence level) τ_m = 45.7 ± 0.2 ms ; L = 0.97 ± 0.5 ; ρ_∞ = 3.21 ± 0.9.

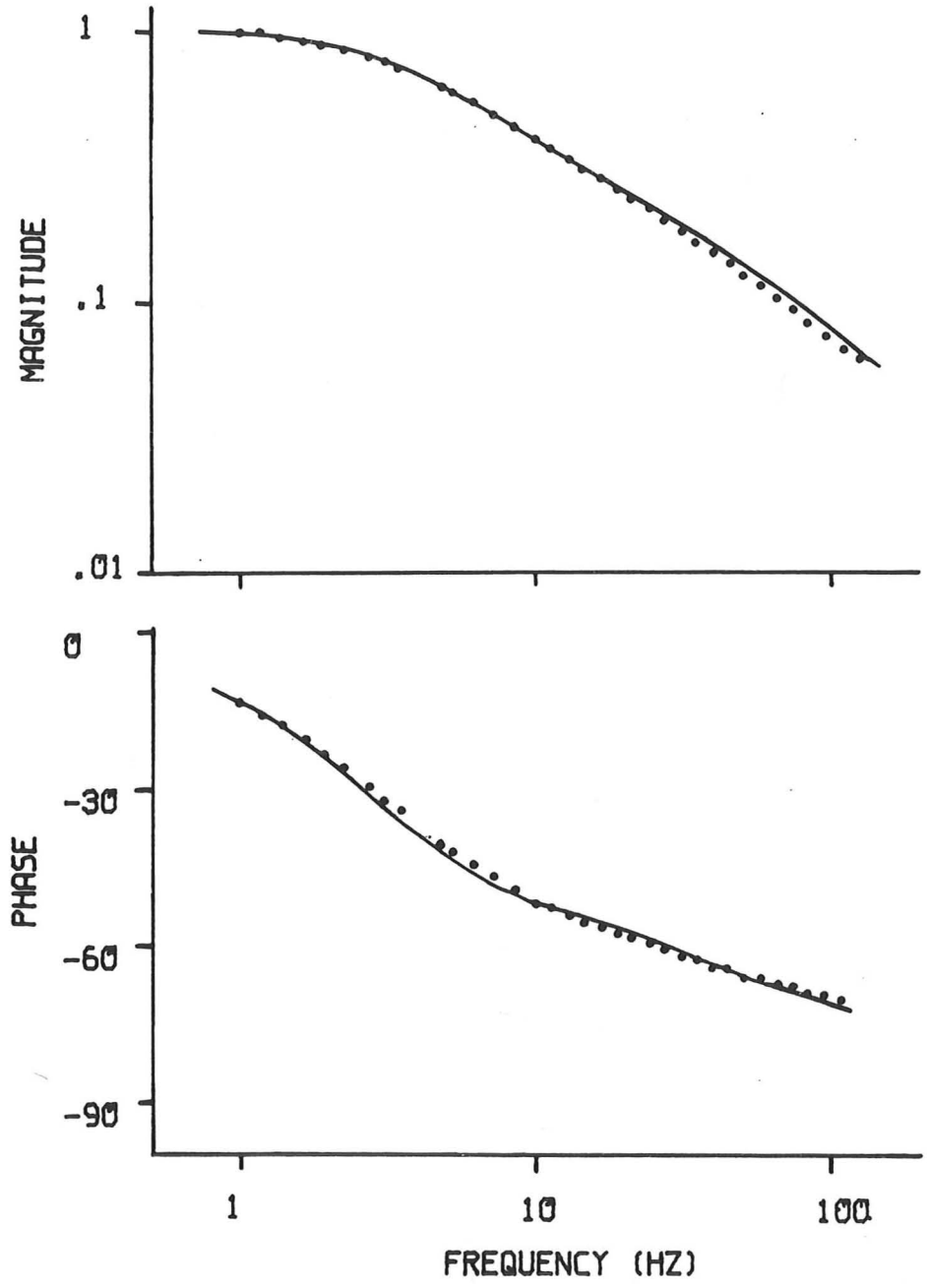

Figure 4.14. Input impedance of the Rpr 76/77 neurone represented in figure 3B. The input amplitude 0.8 nA and the magnitude has been normalized by the maximum voltage of 4.4 mV. The continuous line represents the best fitting LSFC model with parameters; (estimated value ± 99.5 % confidence level) τ_m = 45.7 ± 0.2 ms ; L = 1.0 ± 0.5 ; e_∞ = 3.2 ± 0.9.

The bifurcation of the primary neurite of the neurones depicted in figure 3 occurs very close to the cell body. If the measured time constants are used to estimate the electrotonic distance from the soma to the point of bifurcation, the distance for both neurones is approximately 0.01 λ. The shortness of the cable suggests that the soma and primary neurite may behave like an isopotential compartment (see section 2.4.3.2.). If the daughter branches had the same electrotonic length, but not necessarily the same diameter, the neurone would correspond exactly to an LSFC. The daughter branches do, however, show considerable variation in diameter throughout their course. This may give rise to some modelling error, but in the absence of a detailed reconstruction of the neurone it is difficult to estimate the magnitude of the expected errors.

The radius of a soma can be calculated from the estimated ρ_∞ and R_{inp} using the relationship derived from the definition of ρ_∞,

$$a = [\, R_m \,(\, 1 + \rho \,) \,/\, 4\pi R_{inp} \,]^{1/2} \qquad (8)$$

The area of the soma so estimated corresponds to that part of the neurone that behaves like an R-C circuit and need not necessarily be the same as the morphological soma.

Assuming that C_m is equal to 1×10^{-6} F cm^{-2}, the calculated radii of the neurones depicted in figures 13 & 14 are 440 and 470 μm respectively, which are approximately five times the radius of the morphological somas. This disparity could be explained by the inclusion of the primary neurite into the effective soma and by infolding of the somatic membrane.

The fine neurites attached to the primary and secondary branches of the neurone are some ten times smaller than their parent branches. These branches should, as the arguments in section 2.4.3.1. show, have little effect on the input impedance measured from the soma.

4.3.5. AVERAGE ELECTROTONIC CONSTANTS

The average electrotonic constants of Lpr1/2 and Rpr76/77, as estimated by the frequency domain method, are given in the following table;

Table 1

	τ_m (msec.)	L	ρ_∞	R_{inp} (MΩ)
Lpr1/2 (n=23)	41.2 ± 3.2 (21-76)	1.2 ± 0.2 (0.5-3)	3.3 ± 0.3 (0.8-4.4)	5.4 ± 0.5 (1.6-10.9)
Rpr76/77 (n=28)	46.1 ± 2.8 (24-73)	1.9 ± 0.2 (0.7-3)	2.6 ± 0.2 (.6-4.1)	5.3 + 0.5 (1.8-9.9)

Values are means ± SE. Values in parentheses are ranges.

The time constants should be compared with previous estimates ; all estimated by conventional time domain methods: 30 ms (*Helix pomatia* visceral neurones, Maiskii (1963)) 44 ms (*Helix pomatia* suboesophageal neurones, Meves (1968)); 96 and 68 ms (V13 and V16 respectively of *Helix aspersa*, Hayes and Kerkut, 1978).

4.4. DISCUSSION

In most cases the LSFC model provided a good approximation of the neurone's input impedance, in that it accounted for both the phase and the magnitude over the full range of frequencies. Since the observed structure of the neurones does not correspond to an LSFC and the dendritic branches displayed considerable variations of diameter along their length, some modelling error must occur, but it is not possible to estimate the exact extent of the error in the absence of a detailed reconstruction of the neurone's morphology.

Possible sources of error in the estimated membrane time constant were discussed in detail in section 2.4. and will not be reconsidered here. It is, however, worthwhile considering a further possible source of error. The insertion of a microelectrode into a neurone creates a leakage resistance and if this resistance is of the same order of magnitude as the somatic resistance the estimated time constant will be in error (Jack, 1979). In all cases where an attempt was made to distinguish between the unit membrane resistance of the soma and that of the dendrites, no difference was found. If the unit membrane resistance were uniform this would indicate that the microelectrode induced leak is insignificant. However, it is by

no means necessary that the unit membrane resistance be homogeneous. The question of the error induced by microelectrode penetration, and of the homogeneity of the membrane resistance can only be resolved if the microelectrode induced leakage can be measured by a method that does not rely on an assumption about the electrotonic structure of the neurone.

The very fine neurites attached to the primary and secondary branches of neurones Lpr 1/2 and Rpr 76/77 will, as the arguments of section 2.4.3.1. show, have little influence on the measured somatic input resistance. Therefore, even if the fine neurites had a different unit membrane resistance to the major branches it would not be possible to detect it from the soma. It may however, be possible to test the assumption of the homogeneity of the unit membrane resistance if both the transfer impedance between a neurite and the soma, and the somatic input impedance could be measured. Homogeneity would be indicated by a correspondence between the transfer impedance calculated from the somatic input impedance and the measured transfer impedance.

4.5. Conclusion

The measured input impedances of neurones Lpr1/2 and Rpr76/77 were consistent with an LSFC model. The average time constant, as determined in the frequency domain was 43 ms with a range of 23 to 76 ms.

Thirty percent of the neurones studied gave evidence of a slow time constant (ie. > 100 ms). It was shown that if a neurones exhibited this effect, time domain methods may give estimates of the membrane time constant that are severely in error. This emphasises the need for the measurement of both the time and frequency domain linear properties of neurones.

CHAPTER 5

NONLINEAR MEMBRANE PROPERTIES

5.1 INTRODUCTION

In chapter 3 the electrotonic parameters of a neurone were derived from its response to inputs that do not recruit nonlinearities. An electrotonic model based on these parameters may accurately predict the propagation and interaction of small synaptic potentials, however, large potential changes, such as needed to initiate action potentials, will be outside the range of linear cable theory.

In this chapter sinusoidal current inputs are used to probe the subthreshold nonlinear properties of molluscan neurones. The theoretical basis of this method, which can be considered as an extension of linear systems theory, is given in the first section of this chapter. The objective of this investigation is to explore the usefulness of this method in the phenomenological characterization of the nonlinear properties of neuronal membranes.

For the definition and measurement of nonlinearity, the frequency domain proves useful. Consider a system to which a sine wave of frequency f is applied. A linear system has an output which is a pure sine wave of the same frequency as the input. While a nonlinear system has an output which contains harmonics of the fundamental frequency, f (ie. 2f,3f,4f,...). The complexity of a nonlinear system can be measured by the number of significant harmonic terms in the response to a sine wave input. For example the simplest nonlinearity is that of a second-order system, in which the output only has terms of frequency f an 2f.

It is relatively simple in the time domain to determine whether or not a system is linear. If a step is applied to the system and the on and off-transients are exactly superimposable, then the system is linear. It is however difficult to quantify the nonlinearity in any useful way in the time domain.

5.2 THEORY

A linear system is completely characterized by its impulse response. For any input, the output of the system is the convolution of the input with the impulse response (see section 2.2.). Volterra generalized the notion of convolution to include nonlinear systems which are stationary and have a finite memory, through the following expression (Schetzen, 1980):

$$y(t) = g_o + \int_o^\infty g_1(\tau)x(t-\tau)d\tau$$

$$+\int_o^\infty \int_o^\infty g_2(\tau_1,\tau_2)x(t-\tau_1)x(t-\tau_2)d\tau_1 d\tau_2 + \ldots \qquad (1)$$

where $x(t)$ an $y(t)$ are the input and output respectively and $g_n(\tau_1 \ldots \tau_n)$ is the nth-order Volterra kernel of the system: g_1 corresponds to the impulse response of the system. The meaning of the second-order Volterra kernel, g_2 is illustrated operationally in what follows, in terms of its Fourier transform, $G_2\ (f_1,f_2)$.

A second-order system is completely defined by the first two terms in the Volterra series. To illustrate the meaning of the second-order Volterra kernel in the frequency domain, consider the following: if a signal composed of the sum of N sinusoids is applied to a second order system, the output contains components with the fundamental frequency, $f_1 \ldots f_N$. The output also contains components at the second harmonic

frequencies, $2f_1 \ldots 2f_N$, and at all possible sums of the N frequencies, $f_1+f_2, f_1+f_3 \ldots$ and at all possible difference frequencies, $f_1-f_2, f_1-f_3, \ldots$ (The latter two frequencies are collectively referred to as 'combination' terms.) The second-order Volterra kernel is a two dimensional complex function, and its amplitude is proportional to that of the second harmonic and combination terms of the output. To make this relationship more precise, the second-order *frequency* kernel, $K_2(f_j,f_k)$, is defined as the measured amplitude of the (f_j+f_k) component of the output, for an input which is the sum of two sinusoids of frequency f_j and f_k, with amplitudes a_j and a_k. The second-order Volterra kernel has a direct relationship to the frequency kernel (Victor & Shapley, 1980):

$$G_2(f_j,f_k) = K_2(f_j,f_k)/a_j a_k \text{ for } j \neq k$$
$$G_2(f_j,f_j) = 2K_2(f_j,f_j)/a_j a_j \qquad (2)$$

However, the zeroth-order frequency kernel of a second-order system, has contributions from the second order Volterra kernel (Victor & Shapley, 1980):

$$K_o = G_o + 1/2 \sum_{j=1}^{N} a_j^2 G_2(f_j,f_{-j}) \qquad (3)$$

(Note: For the second-order Volterra kernel to be completely specified measurements must be made at both sum and difference terms. Despite the claims of French (1976), the difference terms cannot be deduced from the sum terms. The frequency kernel is symmetrical about the line $f_i = f_j$ and $f_i = -f_j$ and the kernel is completely specified by one quadrant bounded by these lines (see fig.3))

The tendency for the frequency kernel to contain

contributions from higher-order Volterra kernels increases as the nonlinearity of the system increases. The simple relationship between the Volterra and frequency kernels that obtained for a second-order system, is lost. For example the first-order frequency kernel of a third-order system has contributions from both the first and third-order Volterra kernels (Victor & Shapley, 1980). For nonlinearities of order higher than two, it is in general impossible to measure the Volterra kernels unless the form of the system is known *a priori* (Aertsen & Johannesma, 1981). In chapter 6 an approach first suggested by Wiener (1958) is used to circumvent these problems. However in this series of experiments I have attempted to explore the region over which the system can be adequately modelled as a pure second-order system. This will be the case if the second-order frequency kernel is proportional to the product of the input amplitudes and if the contributions from higher order harmonics is negligible compared to the second-order terms.

5.3 MATERIALS AND METHODS

Experiments were performed on cells Lpr 1/2 and Rpr 76/77. Because of the relatively small size of the second and third harmonic components it was necessary to eliminate synaptic potentials. Initially attempts were made to ligate the cell bodies, however, this procedure always lead to leaky preparations (input resistance < 0.5 MΩ), with no restoration of the resistance even when the neurone was left to recover for up to three hours. The following procedure proved effective in producing isolated neurones with a high input resistance. The ganglion was desheathed and exposed to a 1% solution of protease

(Sigma type VI) for 2 minutes. Neurones surrounding the cluster of four cells, Rpr 76/77 and Lpr1/2, were destroyed with a fine pair of jeweller's forceps. The cell body was penetrated with two electrodes and the input impedance at 1 Hz was measured every minute. The input resistance in most cases increased and reached a stable limit within half an hour. Experiments were only performed on isolated neurones with a stable input resistance greater than 2 MΩ.

The input impedance of neurones was measured using the procedure described in section 4.2.6. In addition the second and third harmonic content of the voltage output was measured. In some cases the input was a sum of two sinusoids, which consisted of the standard sine wave of 32 points per period (designated f) to which a higher frequency term of the same amplitude had been added. The most frequently used sum of sinusoids, in this study was f+1.5f, which has the second harmonic terms 2f and 3f and the combination terms 2.5f and 0.5f. This input was used because it gave the largest nonlinear response. However, the third harmonic in this sum-of-sinusoids overlaps with the second harmonic of 1.5f, and was not measured. Plots of the harmonic content of the output as a function of the fundamental frequency are referred to as 'nonlinear transfer functions '.

In all experiments the sinusoidal purity of the input signal was estimated whenever a harmonic term was measured to check if the input was introducing any nonlinearity. If the second harmonic content of the input exceeded 1% of the fundamental, the experiment was terminated and the electrode replaced.

All nonlinear transfer functions were plotted as a function of the 1f component of the (1+1.5)f input. The amplitude of all components in any one nonlinear transfer function plot, were

normalized by the maximum value of the fundamental term (abbreviated as 'vmax'). All amplitudes quoted are peak-to-peak values.

5.4 RESULTS

5.4.1 INPUT IMPEDANCE, ISOPOTENTIALITY AND STATIONARITY OF ISOLATED NEURONES

The input impedance of all isolated neurones used in this study was determined with an input of less than 0.5 nA. An input impedance curve of an isolated neurone is illustrated in figure 1. The average electrotonic parameters of isolated Lpr1/2 (n=6) and Rpr 76/77 (n=5) neurones, determined by the methods of section 4.2.7, were ; τ_m = 52.7 $\pm$ 6.6 ms, ρ_∞ = 2.0 $\pm$ 0.4 , L = 1.5 $\pm$ 0.4. (Mean $\pm$ S.E.)

The presence of a dendrite will reduce the nonlinearity of the membrane current-voltage relationship as measured at the soma (Jack, Noble & Tsien, 1975). This effect of dendritic loading will to some extent be compensated by the low value of ρ_∞. Nevertheless, in the absence of methods for correcting the effect of a loading cable, the measured nonlinearity should be considered as a lower limit of the true membrane nonlinearity.

In no cases did the neurones give evidence of non-isopotentiality. In some cases the electrodes were placed at opposite ends of the soma to accentuate any possible non-isopotentiality. This inhomogeneity of voltage across the soma would manifest in the frequency domain as an upward convex amplitude plot, and at high frequencies a phase shift less than -90^o (see section 2.3.10). So for the frequency range covered in these experiments ,.1-100 Hz, the soma behaves like a

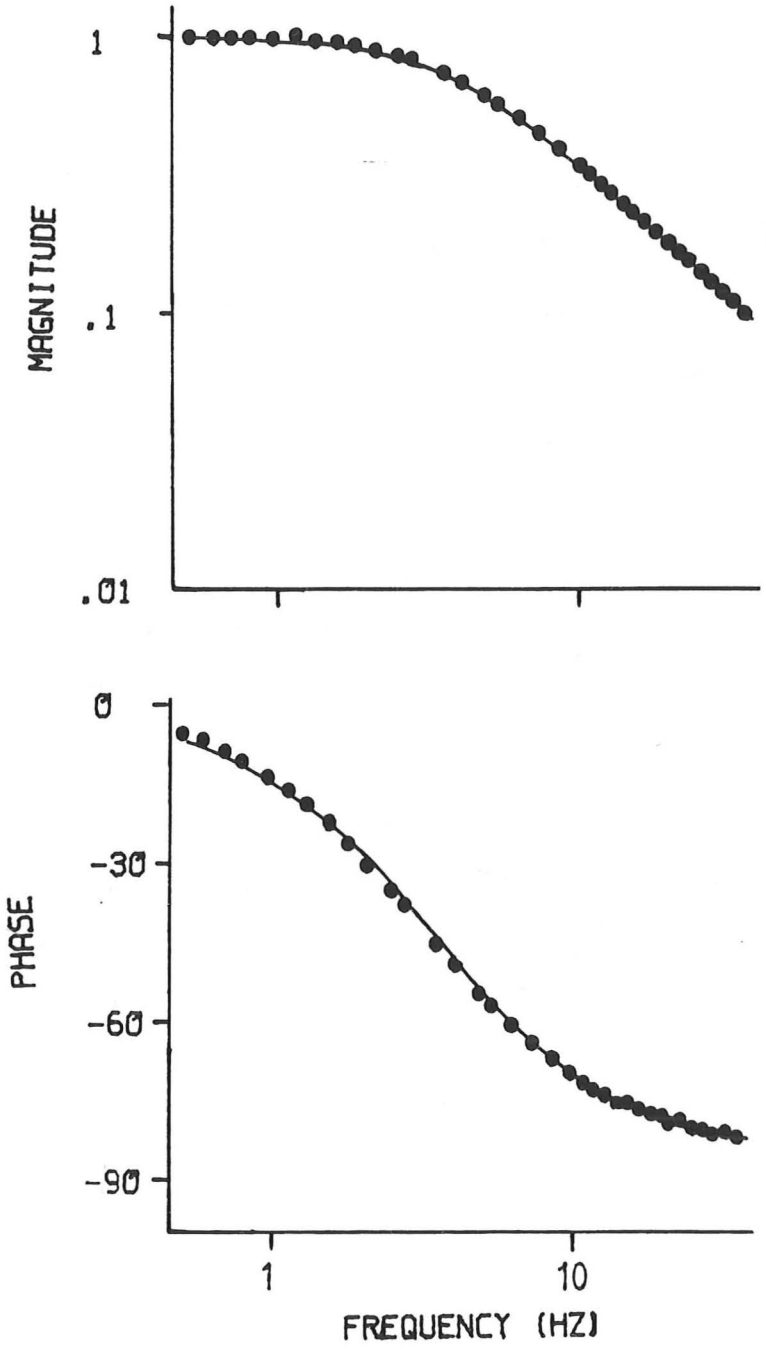

Figure 5.1. Impedance of an isolated Rpr 76/77 neurone measured with an input of .5 nA. The amplitude was normalized with the maximum amplitude of 7.9 mV. The solid curve represents the best fitting LSFC curve with parameters: τ_m = 44.7 ms , L= 0.27 and ρ_∞ = 1.0

isopotential compartment.

For the Volterra representation to be applicable to the isolated neurone preparation, it is necessary that the fundamental and harmonic content of the ouput reach and maintain a steady-state and be independent of the previous stimulus history. This stationarity of the output was tested in detail in a number of isolated neurones with an input sine wave of 1 Hz and an amplitude of 2-3 nA. The fundamental and second harmonic amplitudes were measured at intervals of three seconds for one minute. In no case was the standard deviation of the fundamental or second harmonic more than 2 % or 5% of their mean values respectively. Neither did the fundamental or harmonic component display any systematic increase with time.

A typical response of an isolated neurone to a sum of sinusoids input is illustrated in figure 2, together with the Fourier synthesis and decomposition of the response.

5.4.2 NONLINEAR TRANSFER FUNCTIONS

Nonlinear transfer functions of an isolated neurone are displayed in fig 3A. Each nonlinear transfer function, represents a diagonal 'slice' through the second-order frequency kernel. This relationship is illustrated in figure 3B. (If the second-order transfer function is to equal to the second-order frequency kernel, the second harmonic amplitude should be multiplied by two.)

Although there were differences in detail between the frequency kernels from different cells there were a number of constant features. For the f+1.5f frequency set, measuring the output at 2f,2.5f and 0.5f the following held true:

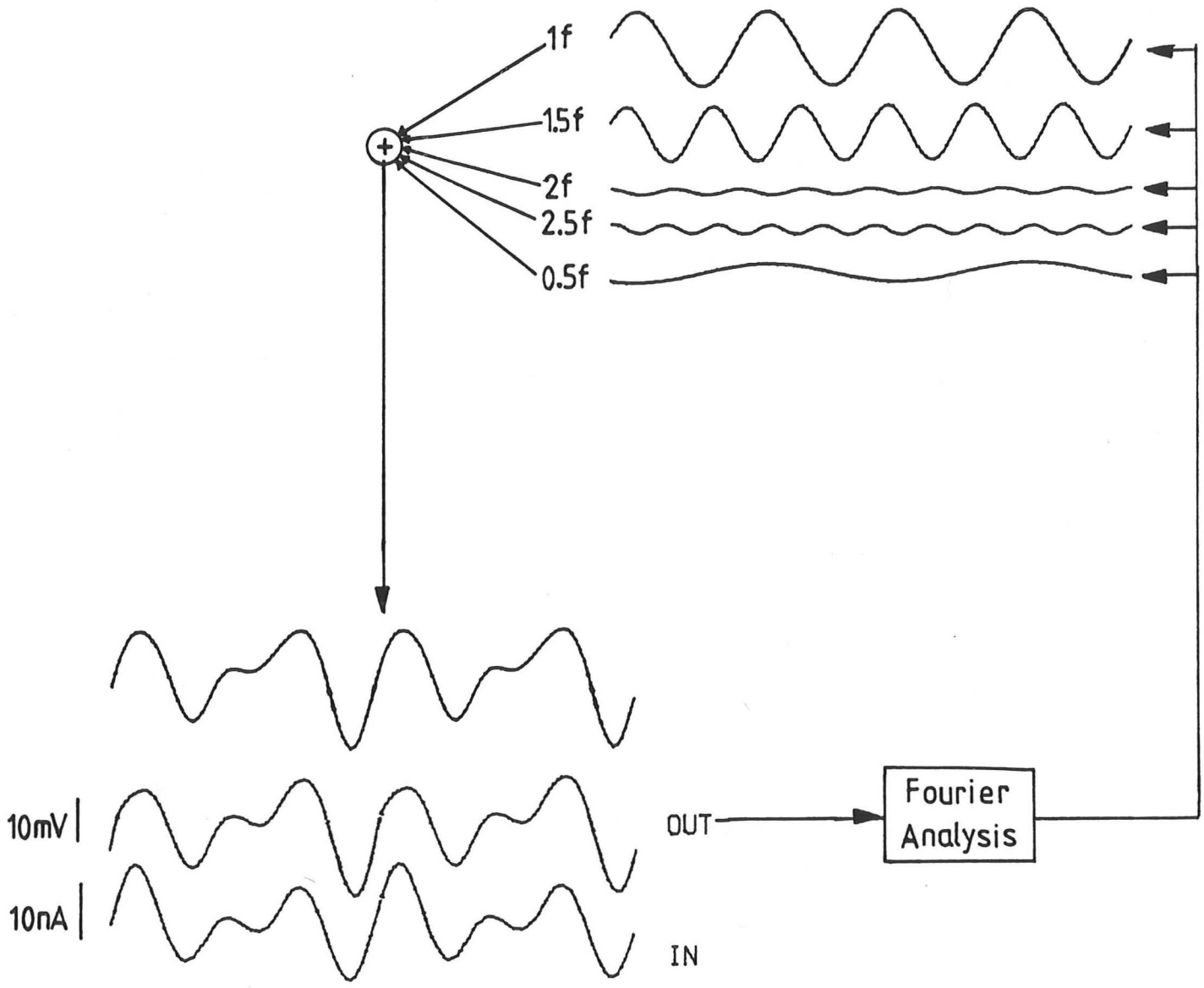

Figure 5.2. Input and output of an isolated Lpr1/2 neurone to a sum-of-sinusoids (1 + 1.5 Hz). The output was analysed into its Fourier components with the Goertzel algorithm. Fourier synthesis was achieved by adding the components.

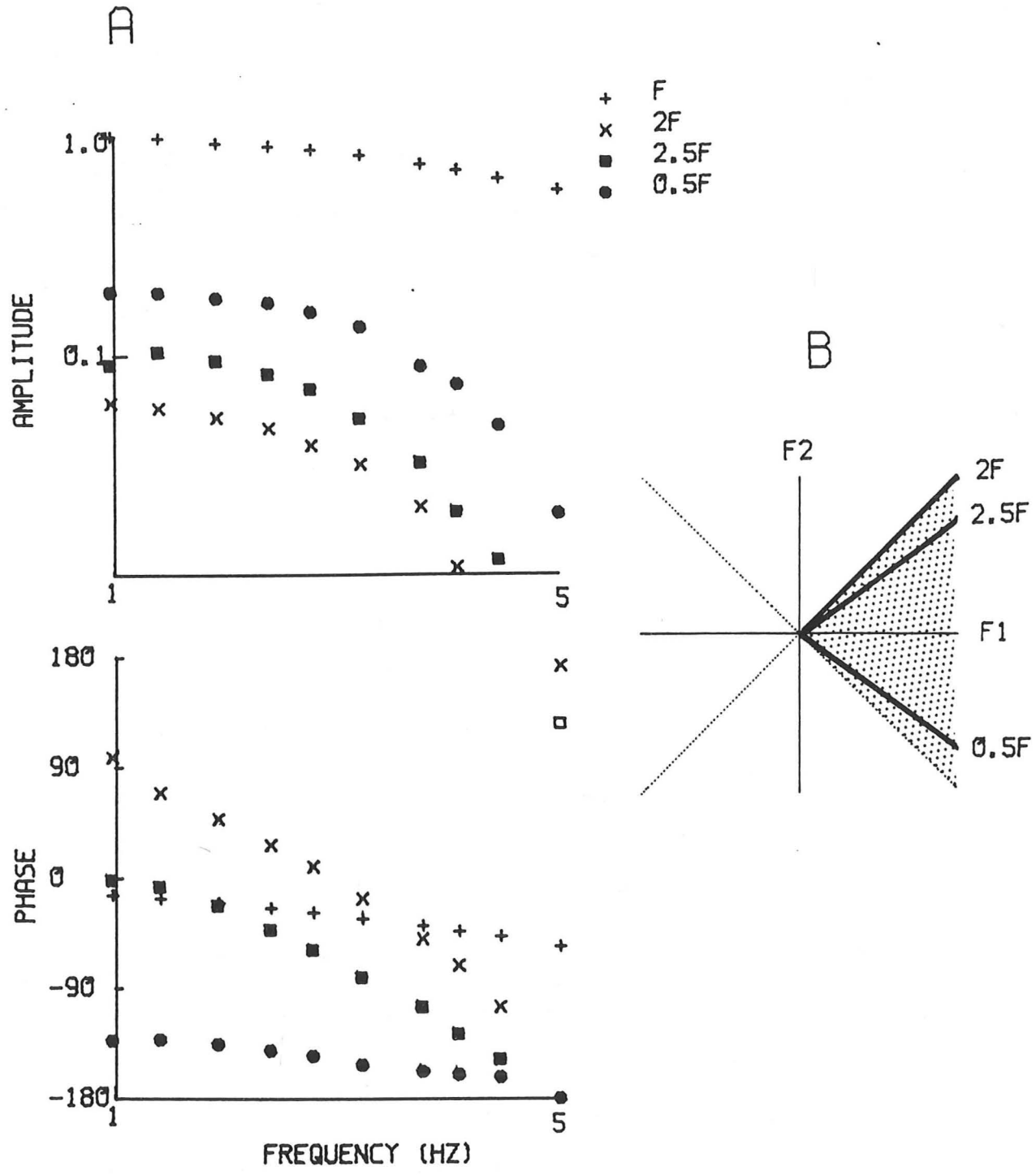

Figure 5.3. (A) Nonlinear transfer function of an isolated Rpr 76/77 neurone measured with an input of f+1.5f, with an amplitude of 3 nA and vmax = 36 mV.
(B) projection of the second-order frequency kernel, $K_2(f_1,f_2)$ illustrating the symmetry and the position of the 'slices' measured in the nonlinear transfer functions. The dotted lines are two fold symmetry axes. The shaded portion is the segment needed to completely specify the whole kernel.

(a)The dominant nonlinearity was the 0.5f term and the order of the second order nonlinearity amplitudes was 0.5f>2.5>2f.

(b) The amplitude of all three terms began to decrease at about 2 Hz and became undetectable below 10 Hz.

(c) In a given frequency kernel the amplitude as a function of frequency, was approximately the same shape for all three nonlinear terms.

(d) The relative position of the phase of the three nonlinear components at 1 Hz was similar from cell to cell : 0.5f, $130^{o} \pm 4^{o}$; 2.5f, $35^{o} \pm 5^{o}$ and 2f, $91^{o} \pm 6^{o}$ (n=11, mean $\pm$ standard error).

The shape of the nonlinear transfer function was sensitive to the imposed DC bias. This is illustrated in figure 4 where the frequency kernel was determined at three different bias currents. In contrast,at a fixed bias current, increasing the input amplitude did not cause a marked change of the shape of the nonlinear transfer function (see fig. 5).

5.4.3 DEPENDENCE OF NONLINEARITY ON CURRENT AMPLITUDE

Figure 6 illustrates the dependence of the first two harmonic components and fundamental on the amplitude of input current, at a frequency of 1 Hz. The fundamental component initially varies linearly with the current amplitude, however rectification becomes evident at high input current amplitudes. The second harmonic component first becomes detectable at a current amplitude of about 0.5 nA. The initial rise of this component is approximately proportional to the second power of the input current amplitude (fig. 6). In some cases this dependence broke down at higher input amplitudes to give way to a

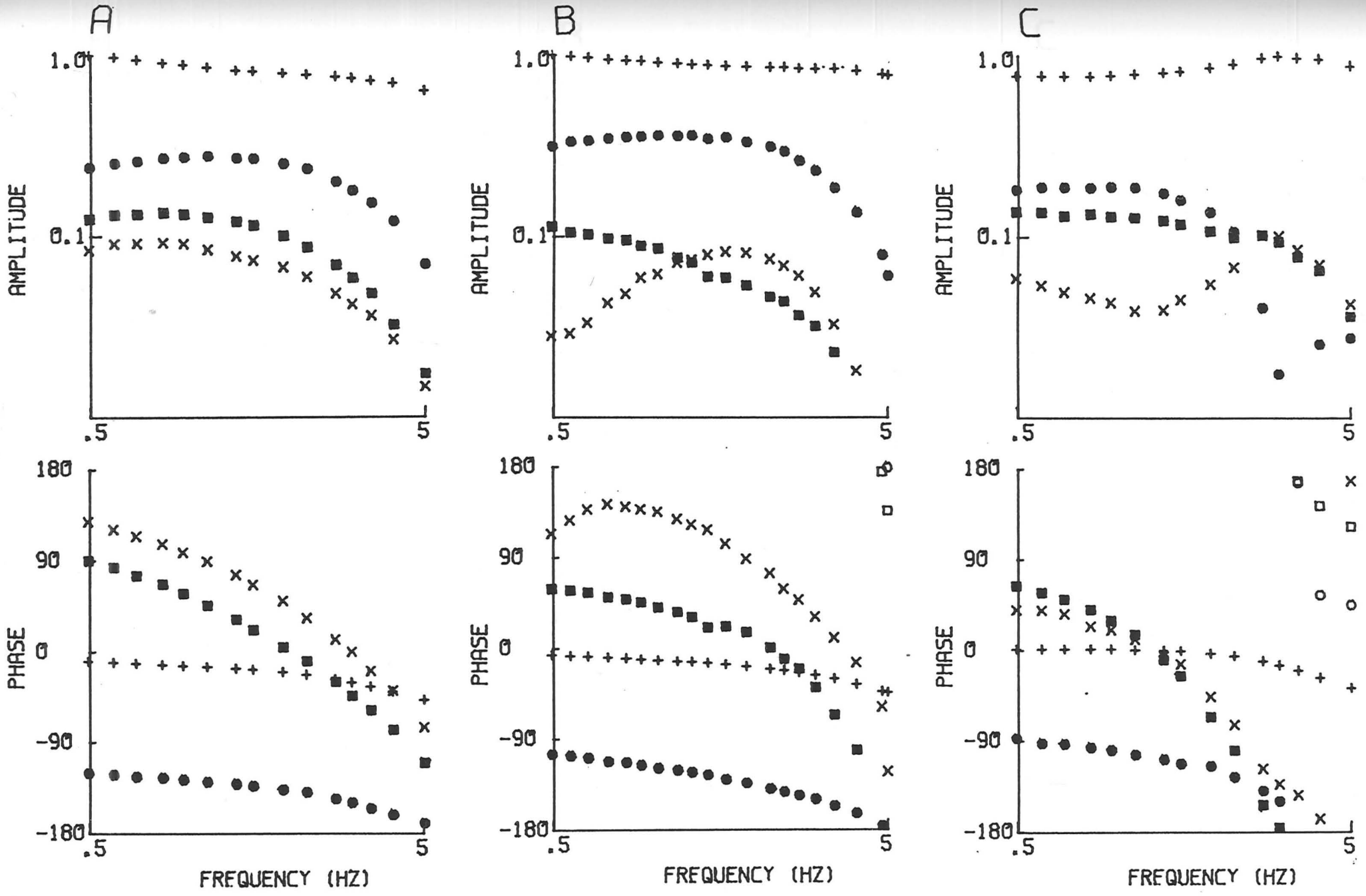

Figure 5.4. Nonlinear transfer functions of an isolated Rpr 76/77 neurone, at three different bias currents. The input was f+1.5f with a magnitude of 1.7 nA. (a) DC=0, vmax= 18.9 mV (b) DC=-1 nA, vmax = 16.6 mV (c) DC=0.5 nA, vmax = 11.5 mV. (+ = f, x = 2f, ■ = 3.5f, ● = 0.5f)

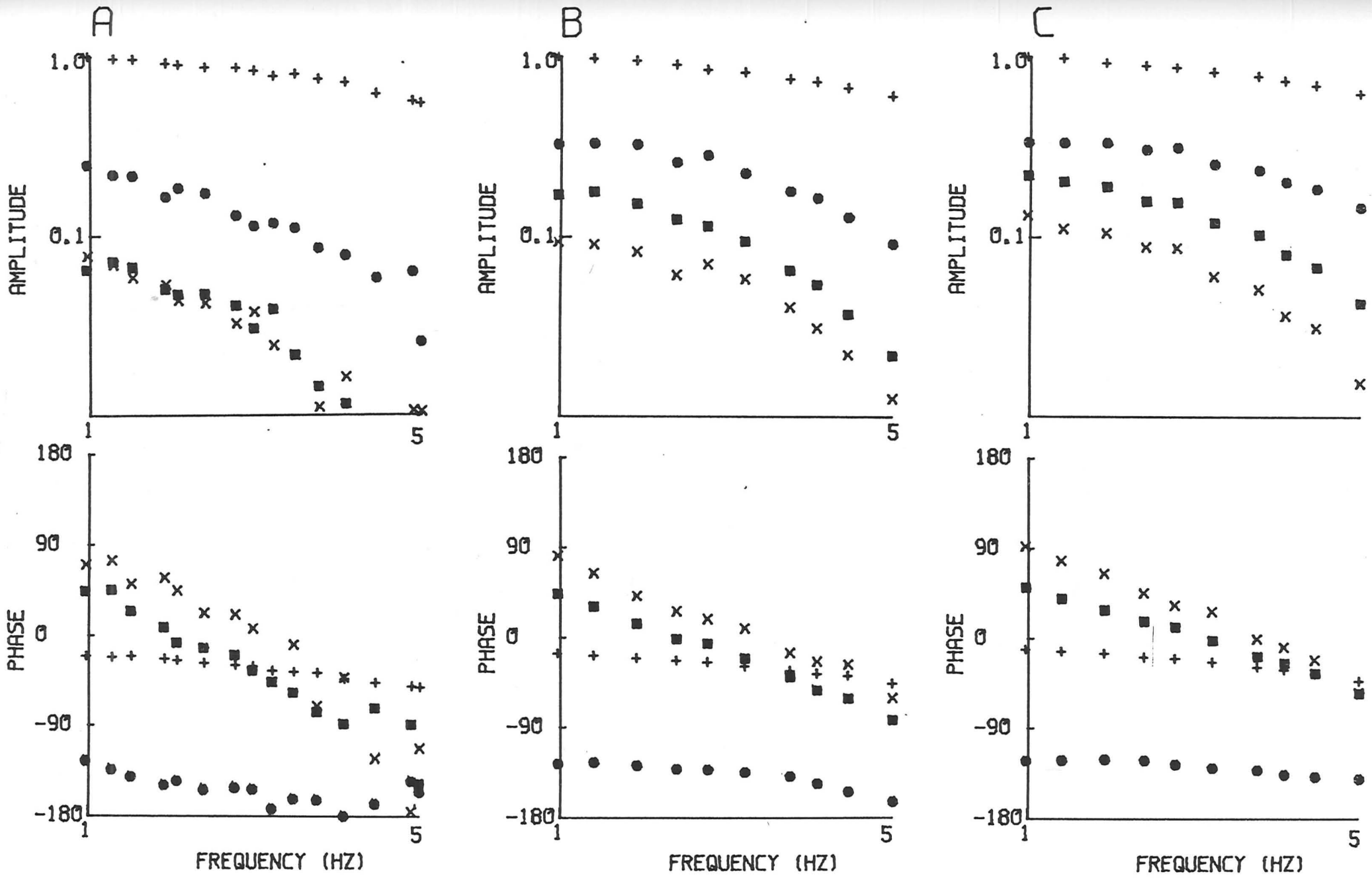

Figure 5.5. Nonlinear transfer functions an isolated Rpr 76/77 neurone, measured with a f+1.5f signal, at three different amplitudes; (A) 0.9 nA (vmax = 8.0 mV) (B) 2.5 nA (vmax = 18.8 mV) (C) 5.2 nA (vmax = 33.8mV). (+ = f; x = 2f; ■ = 2.5f; o = 0.5f).

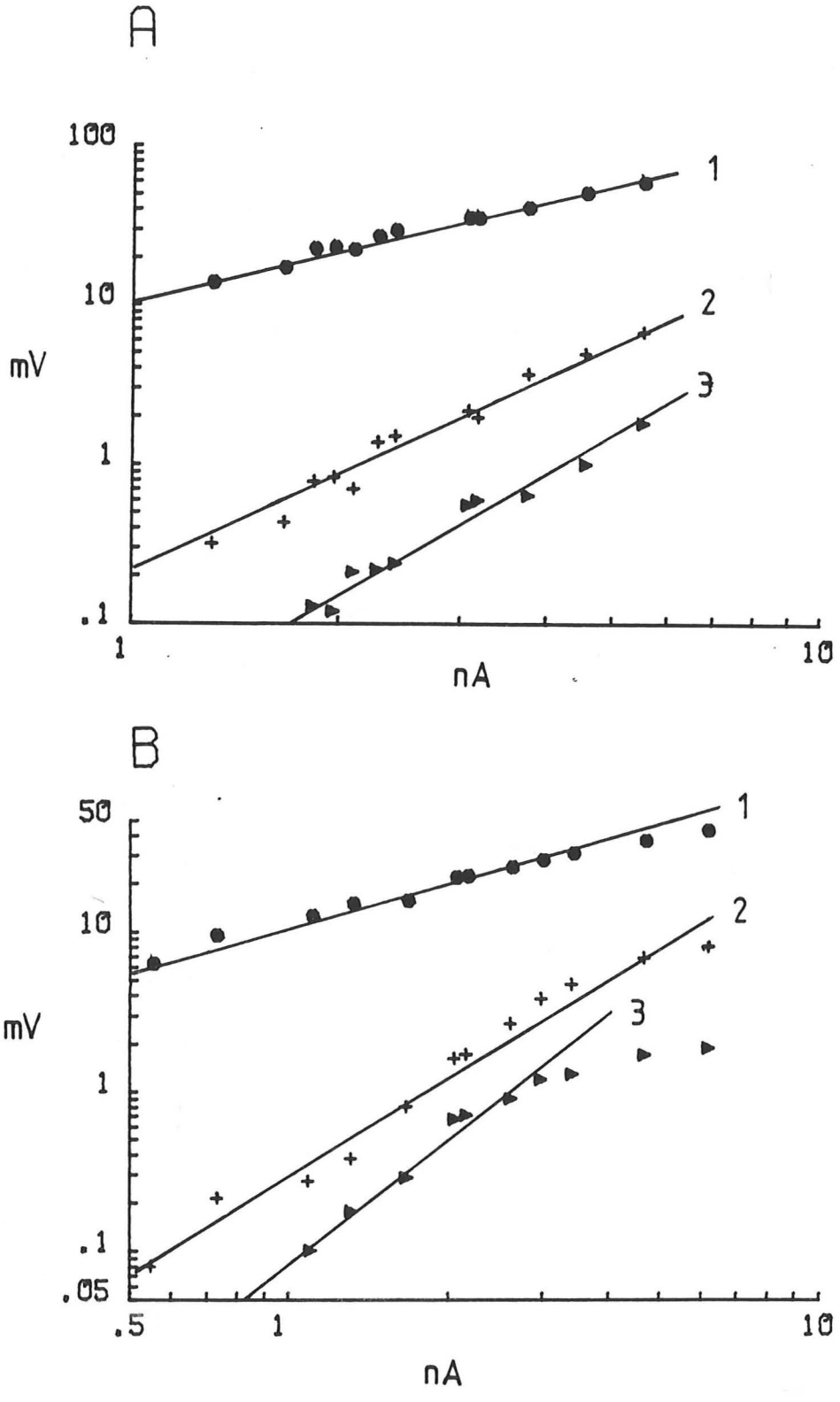

Figure 5.6. First (●), second (+) and third (▶) harmonic components of the voltage response, as a function of the input current amplitude of a 1 Hz sinusoidal signal, for two different Rpr 76/77 neurones. Lines of slope 1, 2 and 3 have been drawn through the data by eye.

form of rectification. The third harmonic component generally emerged from the background noise at higher input current strengths than the second harmonic (1-2 nA).

The nonlinear I-V curves as plotted in figure 6 provide a graphic illustration of the regions over which different models need to be deployed. Consider figure 6B. Up to .5 nA the system can be adequately described by a linear input impedance. From .5 to 1 nA the system is to a good approximation a second-order system. Over this region the simple one-to-one relationship between the frequency and Volterra kernels holds , as expressed in equation 2. With the emergence of the third harmonic term it not possible to extract the Volterra kernel.

5.4.4 EFFECT OF DC BIAS ON NONLINEARITY

In figure 4, the form of the nonlinear impedance curves were shown to be very sensitive to the imposed DC bias. Figure 7 shows the dependence of both fundamental and second harmonic components on the bias current. The relationship was complex and showed variations from cell to cell. In all cases where this relationship was examined the only consistent feature was the tendency of a hyperpolarizing bias to reduce the nonlinearity.

5.5 DISCUSSION

The isolated neurones of Lpr 1/2 and Rpr 76/77 respond linearly to current inputs with a peak-to-peak amplitude of less than .5 nA. Increasing the amplitude of the current, progressively recruits nonlinearities of higher order. For inputs up to an amplitude of 1-2 nA, the response is consistent with that of a second-order system.

form of rectification. The third harmonic component generally emerged from the background noise at higher input current strengths than the second harmonic (1-2 nA).

The nonlinear I-V curves as plotted in figure 6 provide a graphic illustration of the regions over which different models need to be deployed. Consider figure 6B. Up to .5 nA the system can be adequately described by a linear input impedance. From .5 to 1 nA the system is to a good approximation a second-order system. Over this region the simple one-to-one relationship between the frequency and Volterra kernels holds , as expressed in equation 2. With the emergence of the third harmonic term it not possible to extract the Volterra kernel.

5.4.4 EFFECT OF DC BIAS ON NONLINEARITY

In figure 4, the form of the nonlinear impedance curves were shown to be very sensitive to the imposed DC bias. Figure 7 shows the dependence of both fundamental and second harmonic components on the bias current. The relationship was complex and showed variations from cell to cell. In all cases where this relationship was examined the only consistent feature was the tendency of a hyperpolarizing bias to reduce the nonlinearity.

5.5 DISCUSSION

The isolated neurones of Lpr 1/2 and Rpr 76/77 respond linearly to current inputs with a peak-to-peak amplitude of less than .5 nA. Increasing the amplitude of the current, progressively recruits nonlinearities of higher order. For inputs up to an amplitude of 1-2 nA, the response is consistent with that of a second-order system.

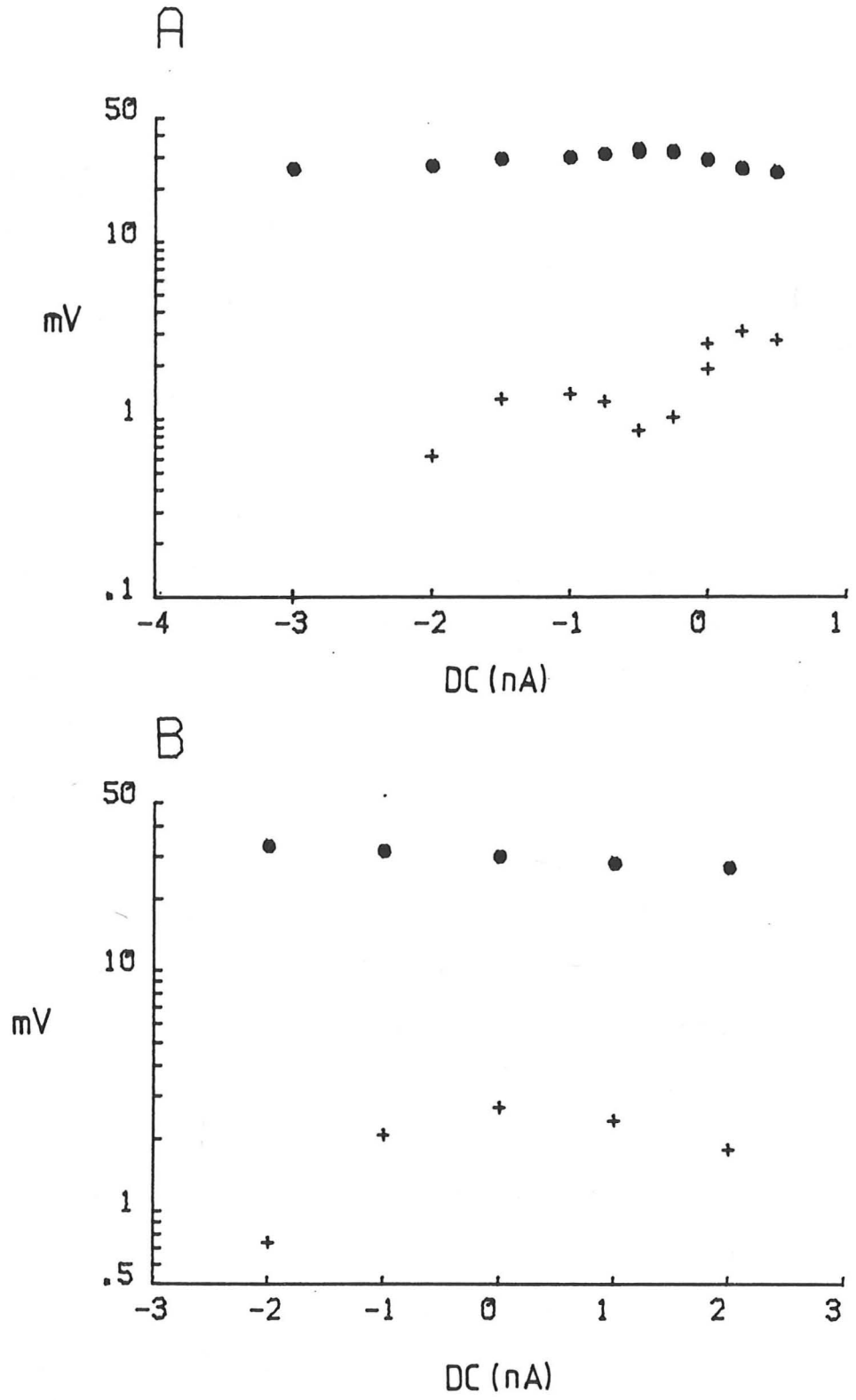

Figure 5.7. Fundamental (●) and second harmonic (+) components as a function of the bias current. The input was a sine wave of frequency 1 Hz. Input amplitude; (A) 2.0 nA (B) 3.4 nA. A and B were different neurones.

The nonlinear impedance curves measured in this study are only a part of the full second-order frequency kernel. If we assume that the kernel can be adequately represented by ten points in the range 1 to 10 Hz, and that the nonlinearity above 10 Hz is negligible, then it would require the measurement of 100 complex numbers (amplitude and phase) to specify the second order frequency kernel. But the frequency kernel changes with the imposed bias current. If ten frequency kernels measured at different bias currents are sufficient to accurately represent the system, then it would take 1000 complex numbers to fully characterize the second-order properties of the system. This model would be very cumbersome. It may be possible to find analytic representations of the second-order frequency kernels as was done for the linear impedance in chapter 4, and this would greatly facilitate the calculation of the Volterra series (Schetzen, 1980).

The measured second-order nonlinear transfer function is a well defined function of frequency and is consistent in overall form for all the neurones studied. The shape of the frequency kernel is ultimately determined by the kinetics of the ion channels in the neuronal membrane (FitzHugh, 1981). FitzHugh (1983) has derived analytic expressions for the harmonic components of the Hodgkin-Huxley equation, subjected to a sinusoidal voltage clamp. The relationship between the parameters of the Hodgkin-Huxley equations and the second harmonic amplitude are very complex: this makes it unlikely that the kinetics of an unknown system can be deduced from the dependence of the second harmonic on frequency. However, for a system with known kinetics the measurement of the frequency

The nonlinear impedance curves measured in this study are only a part of the full second-order frequency kernel. If we assume that the kernel can be adequately represented by ten points in the range 1 to 10 Hz, and that the nonlinearity above 10 Hz is negligible, then it would require the measurement of 100 complex numbers (amplitude and phase) to specify the second order frequency kernel. But the frequency kernel changes with the imposed bias current. If ten frequency kernels measured at different bias currents are sufficient to accurately represent the system, then it would take 1000 complex numbers to fully characterize the second-order properties of the system. This model would be very cumbersome. It may be possible to find analytic representations of the second-order frequency kernels as was done for the linear impedance in chapter 4, and this would greatly facilitate the calculation of the Volterra series (Schetzen, 1980).

The measured second-order nonlinear transfer function is a well defined function of frequency and is consistent in overall form for all the neurones studied. The shape of the frequency kernel is ultimately determined by the kinetics of the ion channels in the neuronal membrane (FitzHugh, 1981). FitzHugh (1983) has derived analytic expressions for the harmonic components of the Hodgkin-Huxley equation, subjected to a sinusoidal voltage clamp. The relationship between the parameters of the Hodgkin-Huxley equations and the second harmonic amplitude are very complex: this makes it unlikely that the kinetics of an unknown system can be deduced from the dependence of the second harmonic on frequency. However, for a system with known kinetics the measurement of the frequency

dependence of the second harmonic component may provide a sensitive test of the kinetic model (De Felice et al., 1981). This approach may be of particular value in studying gating currents (Carius, 1979).

CHAPTER 6

SPIKE INITIATION

6.1. INTRODUCTION

Most neurones convert inputs, in the form of synaptic current, into a train of action potentials. The dependence of this process on the time course of the input shapes the input-output properties of the neurone, and will in part determine the operation of neuronal networks. This chapter describes how both stochastic and deterministic signals were used to estimate the dynamics of spike initiation in some identified neurones of the snail.

In this study a method formulated by Wiener (1958) is used to build up a nonparametric model of spike initiation. The method involves estimating a series approximation to the system from its response to a defined input. A number of different inputs are valid in the framework of Wiener's theory (Schetzen, 1980), but in this series of experiments Gaussian white-noise (GWN) is used (Marmarelis & Marmarelis, 1978).

The series approximation is built up in a stepwise fashion, starting with the best first-order estimate of the system's response. The process is often terminated after the estimation of the second-order approximation, because the computation of higher order terms is prohibitively time-consuming.

To probe the dynamics of spike initiation, electrodes should ideally be located at the impulse initiation zone. This was not possible in *Helix* neurones. The experiments described here were

performed by injecting current into the soma, and detecting action potentials with an independent electrode, also in the soma. In molluscan neurones, spikes are first initiated at the spike initiation zone and only after this in the soma (Tauc, 1962). So in the experiments performed here the process estimated is that of the transfer of current to the initiation zone , axonal and then somatic spike initiation. This path of spike initiation is not normally observed, as there are no synapses on the soma: it is however often the only route open to the experimental neurobiologist.

As a tentative hypothesis, it is assumed that the process of spike initiation can be represented as in fig. 1. The current injected into the soma is transformed into a smooth *internal variate*, u(t), at the impulse initiation zone. Whenever u(t) exceeds a threshold u^*, an action potential is initiated and the threshold element then remains refractory for some time (termed the 'dead time'). The internal variate is left unspecified, but it should be emphasized that it does not necessarily correspond to the voltage at the impulse initiation zone. It could, as is the case for a homogeneous Hodgkin-Huxley axon, correspond to the spatial integral of the membrane current.(Noble & Stein, 1966).

In this study white noise analysis was used to model spike initiation in some identified snail neurones and to test the adequacy of the model of spike initiation in figure 1. Furthermore, the white noise method was used to explore the constancy of the dynamics of spike initiation in a given identified neurone from individual to individual.

Step current inputs have been used extensively to study spike initiation in both invertebrate and vertebrate neurones

performed by injecting current into the soma, and detecting action potentials with an independent electrode, also in the soma. In molluscan neurones, spikes are first initiated at the spike initiation zone and only after this in the soma (Tauc, 1962). So in the experiments performed here the process estimated is that of the transfer of current to the initiation zone , axonal and then somatic spike initiation. This path of spike initiation is not normally observed, as there are no synapses on the soma: it is however often the only route open to the experimental neurobiologist.

As a tentative hypothesis, it is assumed that the process of spike initiation can be represented as in fig. 1. The current injected into the soma is transformed into a smooth *internal variate*, u(t), at the impulse initiation zone. Whenever u(t) exceeds a threshold u^*, an action potential is initiated and the threshold element then remains refractory for some time (termed the 'dead time'). The internal variate is left unspecified, but it should be emphasized that it does not necessarily correspond to the voltage at the impulse initiation zone. It could, as is the case for a homogeneous Hodgkin-Huxley axon, correspond to the spatial integral of the membrane current.(Noble & Stein, 1966).

In this study white noise analysis was used to model spike initiation in some identified snail neurones and to test the adequacy of the model of spike initiation in figure 1. Furthermore, the white noise method was used to explore the constancy of the dynamics of spike initiation in a given identified neurone from individual to individual.

Step current inputs have been used extensively to study spike initiation in both invertebrate and vertebrate neurones

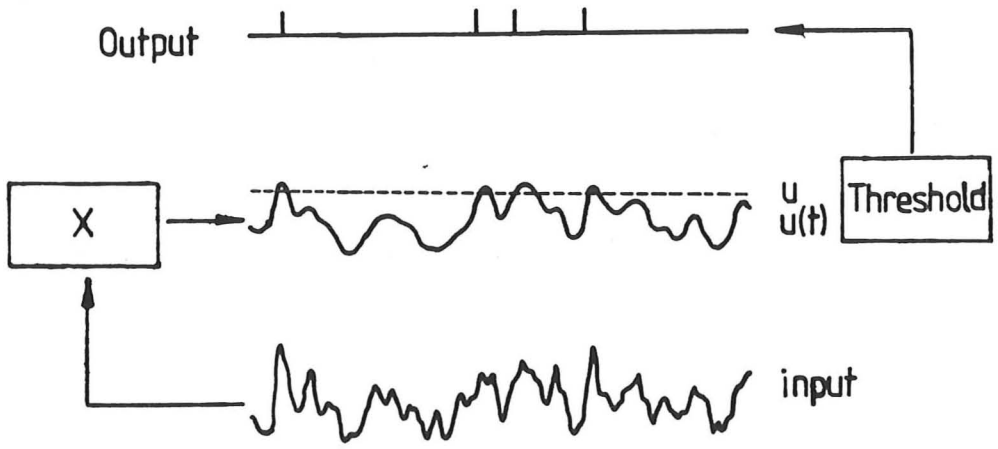

Figure 6.1. Model of spike initiation. The element 'X' represents a system that transforms the input current into the internal variate, u(t) at the spike initiation zone.

(reviewed by Calvin 1975, 1978). In this study the dynamics of spiking evoked by step current inputs was contrasted with that elicited by GWN signals to explore the possible dependence of the dynamics upon the form of the input used (Aertsen & Johannesma, 1981)

6.2. THEORY

In chapter 5 the representation of a nonlinear system by a generalized convolution integral, the Volterra series, was introduced. This series converges very poorly, and for complex systems it is not possible to measure the kernels. Wiener (1958) however, found a way of bypassing these problems. As with the Volterra series, he represented the output of the system as a sum of functionals, but he chose a set of functionals which are mutually orthogonal. (Operationally, orthogonality means that the time average of the product of any two functionals, is zero). This has the following practical implications (Marmarelis & Marmarelis, 1978).

(1) Each kernel can be measured independently.

(2) The Wiener functional expansion, truncated at the nth-order term, will be, statistically the best possible nth-order approximation to the system.

Wieners orthogonal functional expansion , the so called G-Functional expansion is given by:

$$y(t) = \sum_{m=0}^{\infty} G_m [h_m (\tau_1,\ldots,\tau_m); x(t)] \quad (1)$$

where:

$$G_o [h_o; x(t)] = h_o \quad (2)$$

$$G_1 [h_1; x(t)] = \int_0^{\infty} h_1 (\tau) x(t-\tau) d\tau \quad (3)$$

$$G_2 [h_2; x(t)] = \int_o^{\infty}\int_o^{\infty} h_2(\tau_1,\tau_2)x(t-\tau_1)x(t-\tau_2)d\tau_1 d\tau_2 - P \int_o^{\infty} h_2(\tau_1,\tau_1)d\tau_1 \quad (4)$$

where G_i is the ith-order orthogonal functional, $x(t)$ is the GWN input, h_i is the ith-order Wiener kernel, and P is the power density of the input signal.

The first-order Wiener kernel corresponds to the impulse response introduced in chapter 2. By convolving h_1 with any input a linear approximation of the output is obtained.

The second-order Wiener kernel, $h_2(\tau_1,\tau_2)$ is a two dimensional surface which is symmetrical about the line $\tau_1=\tau_2$. The height of the second-order kernel is proportional to the difference between the response of the system to the simultaneous application of two impulses and the response predicted from the separate application of the two impulses, when only second order interactions occur. The variables τ_1 and τ_2 correspond to the time after the application of the first and second impulses respectively.

To estimate the Wiener kernels the crosscorrelation method of Lee and Schetzen (1966) was used. Their formulae for the

Wieners orthogonal functional expansion , the so called G-Functional expansion is given by:

$$y(t) = \sum_{m=0}^{\infty} G_m [h_m (\tau_1,\ldots,\tau_m); x(t)] \quad (1)$$

where:

$$G_o [h_o; x(t)] = h_o \quad (2)$$

$$G_1 [h_1; x(t)] = \int_0^{\infty} h_1 (\tau) x(t-\tau) d\tau \quad (3)$$

$$G_2 [h_2; x(t)] = \int_0^{\infty}\int_0^{\infty} h_2(\tau_1,\tau_2)x(t-\tau_1)x(t-\tau_2)d\tau_1 d\tau_2 - P \int_0^{\infty} h_2(\tau_1,\tau_1)d\tau_1 \quad (4)$$

where G_i is the ith-order orthogonal functional, $x(t)$ is the GWN input, h_i is the ith-order Wiener kernel, and P is the power density of the input signal.

The first-order Wiener kernel corresponds to the impulse response introduced in chapter 2. By convolving h_1 with any input a linear approximation of the output is obtained.

The second-order Wiener kernel, $h_2(\tau_1,\tau_2)$ is a two dimensional surface which is symmetrical about the line $\tau_1=\tau_2$. The height of the second-order kernel is proportional to the difference between the response of the system to the simultaneous application of two impulses and the response predicted from the separate application of the two impulses, when only second order interactions occur. The variables τ_1 and τ_2 correspond to the time after the application of the first and second impulses respectively.

To estimate the Wiener kernels the crosscorrelation method of Lee and Schetzen (1966) was used. Their formulae for the

estimation of the first three kernels are:

$$h_o = 1/T \int_o^T y(t)\, d\tau \tag{5}$$

$$h_1(\tau) = 1/PT \int_o^T y(t)\, x(t-\tau)\, dt \tag{6}$$

$$h_2(\tau_1,\tau_2) = 1/2P^2T \int_o^T (y(t)-h_o)\, x(t-\tau_1)\, x(t-\tau_2)\, dt \tag{7}$$

where T is the duration of the input.

The process to be estimated in this study is the transformation of input current into action potentials. If the duration of the action potential is considered unimportant, the output can be represented as a sequence of delta functions. If N spikes occur at times t_i (i=1...N), then the output can be written as:

$$y(t) = \sum_{i=1}^{N} \delta\,(t-t_i) \tag{8}$$

$$\delta(t-t_i) = \begin{cases} 1 \text{ if } t=t_i \\ 0 \text{ if } t\neq t_i \end{cases}$$

It is possible to transform the discontinuous spike train output into a smooth function of time. However, all such transformations are noncausal, and the form of the kernel may depend simply on the form of the transformation chosen (Baker & Hartline, 1978). Such arbitrary transformations were first shown to be unnecessary by de Boer (1967). Equation 8 can be substituted into the Lee-Schetzen equations (5-7) , and after

some simplification the following equations result:

$$h_o = N/T \tag{9}$$

$$h_1(\tau) = h_o/PN \sum_{i=1}^{T} x(t_i-\tau) \tag{10}$$

$$h_2(\tau_1,\tau_2) = h_o/2P^2 \left[1/N\left(\sum_{i=1}^{N} x(t_i-\tau_1)x(t_i-\tau_2)\right) - (1/T\int_o^{\tau} x(t-\tau_1)x(t-\tau_2)dt)\right] \tag{11}$$

It is worthwhile at this stage introducing a useful mathematical result; for the class of systems that can be represented by a cascade of linear elements and static nonlinear elements , the so-called *sandwich* systems, the first-order kernel Wiener corresponds exactly to the cascade of linear elements (deBoer, 1976) (a static system is one in which the output depends only on the instantaneous value of the input).

There are two possible interpretations of the output of the functional model, equation 1, when the kernels are represented by equations 9-11. Firstly, the output may be regarded as the probability of firing. Secondly, if the neurone can be represented by a sandwich system, composed of an input current-to-internal variate system in cascade with a threshold device, then the output of the estimated first-order system, corresponds to the internal variate at the impulse initiation zone (deBoer & de Jongh, 1978).

6.3. MATERIALS AND METHODS

The experimental procedure and electronics were the same as those described in chapter 3. All experiments were performed with two separate microelectrodes inserted into the cell body. The neurones used in these experiments were Lpr1/2, Rpr76/77, Rpr1

and Lpr5.

6.3.1. Generating Gaussian White Noise

The 'distribution' method of Eckhorn and Popel (1979) was used to create band-limited Gaussian white-noise (GWN). A section of the computer's RAM, 3096 bytes long, was filled with integers in the range -127 to 127, following a Gaussian density distribution centered on zero. The distribution was truncated at $\pm$ 2.54 standard deviations from the mean. Two independent uniform random numbers were generated, and used to select two locations in the RAM, and the numbers so designated were exchanged. This shuffling procedure was carried out 30960 times before the RAM's contents were written to a disk. The process was repeated until a pre-selected number of files were completed.

6.3.2 Data Acquisition

The GWN experiments were performed on-line. The neurone was stimulated with GWN delivered by the computer at a pre-selected frequency, while the neurone's voltage was monitored for action potentials.

For each step of the noise record, a single measurement of the current monitor was stored in the RAM. The voltage channel was checked every 1 msec for a threshold crossing, and when this occurred the time elapsed since the last spike was stored. At the end of the noise signal, the contents of the RAM, containing the measured input signal and the interspike intervals, were written to a data disk.

6.3.4. Output Stationarity

The stationarity of the output spike train was assessed using the 'run' test described by Marmarelis and Marmarelis

(1978). Only data that was stationary at a significance level of 0.05 was used in the estimation of the Wiener kernels.

In order to avoid fruitless accumulation of data, a simple preliminary test of stationarity was established. A segment of GWN with 512 steps was repeatedly applied to the system. If the number of spikes per record changed by less than 15%, over four sequential applications of the noise, the GWN experiment was allowed to proceed. This criterion was in most cases consistent with the run test, however only data satisfying the run test was used to calculate the Wiener kernels.

6.3.5. Average Current Trajectory (ACT)

The first-order Wiener kernel, as defined in equation 10, is the average of all current trajectories that lead to spike initiation. To facilitate the statistical evaluation of the kernel, the average current trajectory (ACT), s_τ, was measured (Bryant & Segundo, 1976),

$$s_\tau = 1/N \sum_{i=1}^{N} x(t_i - \tau) \qquad (12)$$

where τ is the time before action potential initiation and N the number of action potentials. This function differs from the first-order Wiener kernel by a constant multiplicative factor (h_o/P).

If action potentials occur at random, the ACT will tend to zero. Assuming a confidence level of 96%, a point on the ACT is significantly different from zero if it lies outside a band two standard errors on either side of the mean current (Bryant & Segundo, 1976) (where one standard error = σ_x / $(N)^{1/2}$, and where σ_x is the standard deviation of the input)

In order to reveal the full dynamics of a neurone, the

highest frequency of the input noise should be greater than the highest frequency to which the system is responsive. If this condition is not met the ACT will be broadened. However the cut-off frequency of the noise should not extend too much over the systems band-width as this would lead to an increase in the variance of the kernel estimates (Marmarelis & Marmarelis, 1978). It would also lead to an increase in the amount of data, and may render the computation too time-consuming to be practical.

The high frequency cut-off of the neurone was established by sinusoidal stimulation, in the following way. The frequency of the input signal was increased, starting at a frequency of 2 Hz., until the neurone failed to respond in the steady-state. The cut-off frequency of the input GWN, was taken to be twice the cut-off frequency of the neurone. The adequacy of this procedure was checked in a number of cases, by measuring the ACT with GWN signals having twice and four times the cut-off frequency of the neurone. In all cases increasing the frequency of the GWN signal did not result in a change of the ACT, demonstrating that the lower input frequency does cover the system band-width.

The resolution of the ACT is determined by the frequency at which the input is sampled. The timing of action potentials was determined with greater accuracy (1000Hz.) than the input (5-10Hz.), and this extra resolution was used to interpolate values of the ACT. This simply provides a greater density of points in the ACT, but does not increase the frequency resolution that is set by the input sampling rate.

An estimate of the dispersion of the ACT was obtained by

measuring the standard deviation of the current as a function of time ($\sigma(\tau)$). The 96% confidence limits for $\sigma(\tau)$ are (Bryant & Segundo, 1976):

$$\alpha\,\sigma_x < \sigma(\tau) < \beta\,\sigma_x \qquad (13)$$

$$\alpha = (1 - 2/9N - 2.326\,(\,2/9N\,)^{1/2}\,)^{3/2}$$

$$\beta = (1 - 2/9N + 2.326\,(\,2/9N\,)^{1/2}\,)^{3/2}$$

6.3.6. Threshold

The internal variate u_t was computed from the convolution of the sampled version of the ACT, s_t and the input x_t:

$$u_t = \sum_{i=0}^{n} s_i\, x_{t-i} \qquad (14)$$

where $t=0,1,2...$ and n corresponds to the time when the ACT reaches zero. The internal variate is assumed to be fed through a threshold device , and whenever u_t crosses a threshold u^*, a spike is produced.

To locate the threshold, a histogram of u_t was measured, with 100 bins over the full range of the variable. Concurrently, the number of spikes occurring at each value of u_t was measured. The ratio of the two represents the empirical firing probability (Brillinger & Segundo, 1980) and the threshold is defined as the value of u_t at which the probability of firing is 0.5.

6.3.7 Leaky Integrator

The leaky integrator is perhaps the simplest plausible model of spike initiation (Holden, 1976). The leaky integrator can be represented by a parallel R-C circuit, in cascade with a threshold element. For a subthreshold impulse of current the voltage response decays exponentially with a time constant τ (= RC). If the voltage exceeds the threshold, a spike is generated

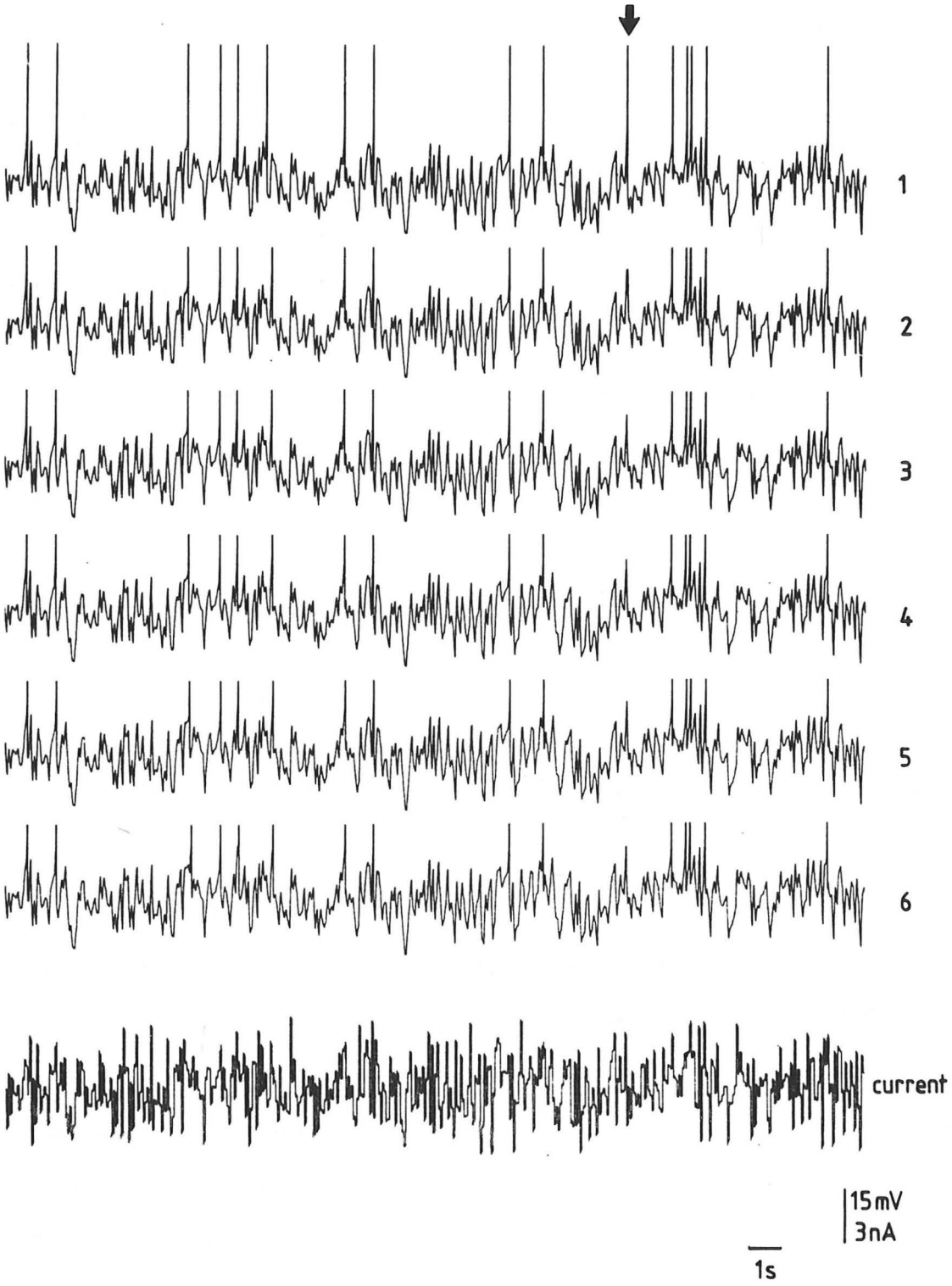

Figure 6.2. The response of a Lpr 5 neurone to the repeated application of a GWN signal, applied at intervals of 2 secs. The arrow indicates the position of the spike that occurs as a somatic spike in trace 1, and as an axonal spike in all other traces. The numbering of the records corresponds to the order in which they were recorded.

and the integrator is reset to zero volts. An analogue model of the leaky integrator was constructed in order to test the GWN analysis programs, and to estimate the kernels and firing probability function of this canonic model.

6.3.8 Adaptation

The response of neurones to step current inputs was measured with a modification of the program used for the GWN experiments. The interspike intervals were determined with a precision of 0.5 ms and, together with the input current amplitude, were stored on disk for subsequent analysis.

6.4. RESULTS

6.4.1. NEURONAL TIME-INVARIANCE

Wiener's method is applicable only to time-invariant systems, but time-invariance is by no means a necessary attribute of neurones. Indeed, many neurones in this study proved to be nonstationary; particularly neurones of the groups Lpr1/2 and Rpr76/77, which often responded to the repeated application of a segment of GWN with continuously declining numbers of spikes. Furthermore, it was not possible to sustain a time-invariant response at a firing rate of greater than approximately 0.7 spikes per second for more than 2 minutes, with any of the neurones used in this study.

A typical response of a neurone to repeated applications of a segment of GWN is illustrated in figure 2. The timing of spikes and subthreshold responses are virtually identical. The only notable difference is that the action potential, marked with an arrow in trace 1, is a somatic spike, while in the other records

and the integrator is reset to zero volts. An analogue model of the leaky integrator was constructed in order to test the GWN analysis programs, and to estimate the kernels and firing probability function of this canonic model.

6.3.8 Adaptation

The response of neurones to step current inputs was measured with a modification of the program used for the GWN experiments. The interspike intervals were determined with a precision of 0.5 ms and, together with the input current amplitude, were stored on disk for subsequent analysis.

6.4. RESULTS

6.4.1. NEURONAL TIME-INVARIANCE

Wiener's method is applicable only to time-invariant systems, but time-invariance is by no means a necessary attribute of neurones. Indeed, many neurones in this study proved to be nonstationary; particularly neurones of the groups Lpr1/2 and Rpr76/77, which often responded to the repeated application of a segment of GWN with continuously declining numbers of spikes. Furthermore, it was not possible to sustain a time-invariant response at a firing rate of greater than approximately 0.7 spikes per second for more than 2 minutes, with any of the neurones used in this study.

A typical response of a neurone to repeated applications of a segment of GWN is illustrated in figure 2. The timing of spikes and subthreshold responses are virtually identical. The only notable difference is that the action potential, marked with an arrow in trace 1, is a somatic spike, while in the other records

it is an axonal spike. The persistence of axonal spikes in the absence of somatic spikes was often observed in neurone Lpr5. In all experiments the threshold was set so that only somatic spikes were detected, and in consequence, the models measured represent the conversion of somatic current to somatic spikes.

6.4.2. AVERAGE CURRENT TRAJECTORY

The ACT is the average of all current waveforms that successfully lead to spike initiation. Four ACTs of different neurones are plotted in figures 3 & 4. It is important to note that the time axis represents the time *before* action potential initiation, the action potential being initiated at time zero. The ordinate represents the average current: positive values correspond to depolarizing current and negative to hyperpolarizing current.

In all cases the ACTs were at least twice as broad as the autocorrelation function of the input (100-200 ms). If the neurone fired an action potential whenever the input current exceeded some threshold, the ACT would be a sharp pulse of approximately the same length as the input autocorrelation function. The relatively great duration of the ACT implies that the decision to fire an action potential does not depend simply on the instantaneous value of the current, but also on the history of the input up to that time. The length of time for which a stimulus has an effect on the firing probability will be termed the neurone's 'memory', and it corresponds to the time before spike initiation, at which the ACT *first* emerges from the confidence bands (Bryant & Segundo, 1976).

In most instances the ACT was roughly biphasic and to facilitate discusion of its qualitative shape, the ACT is divided

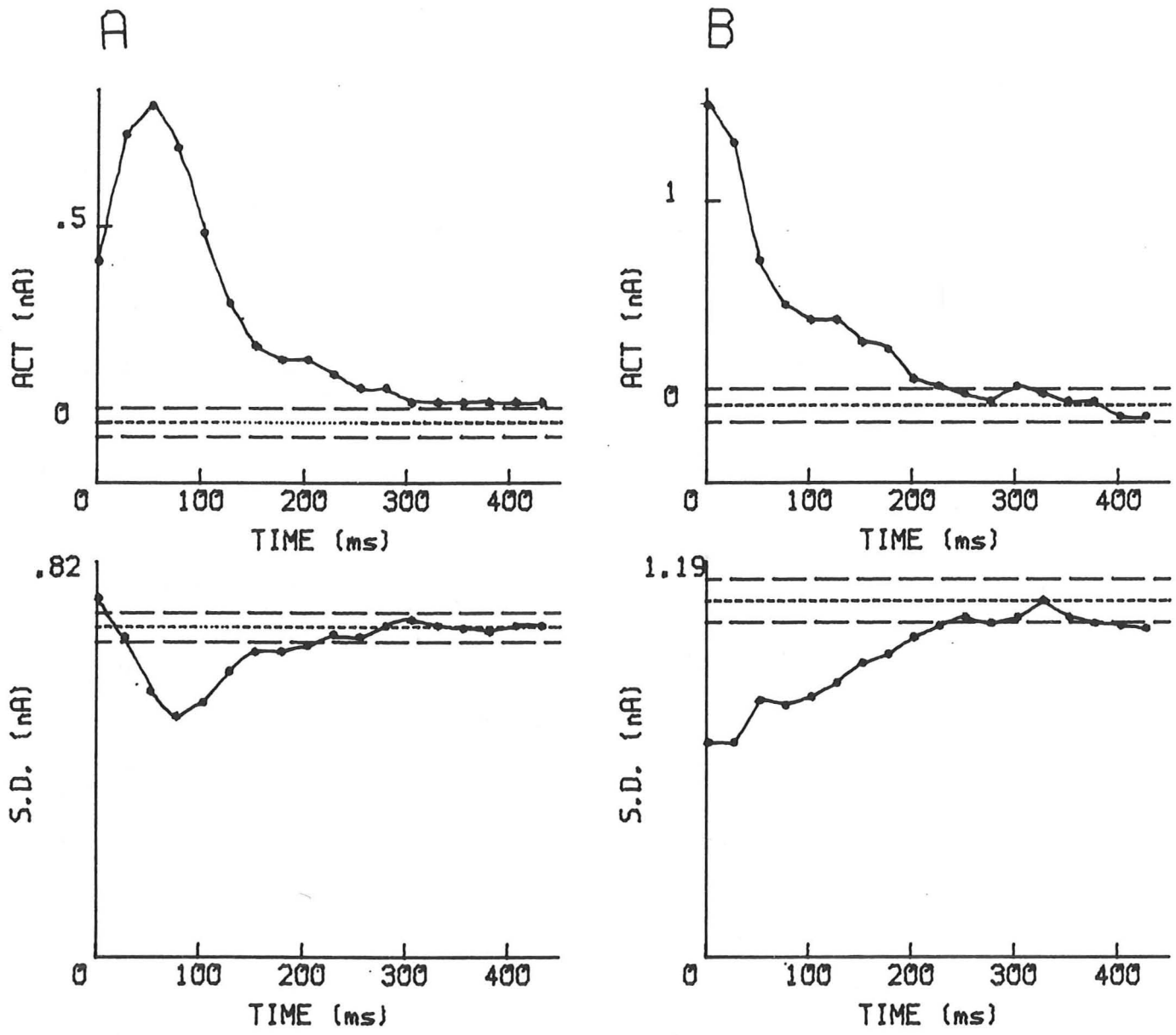

Figure 6.3. The ACT and its associated standard deviation, of two identified neurones. The confidence limits are denoted by dashed lines.

(A) Rpr1 (σ_x = 0.7 nA ; band pass = 10 Hz).

(B) Lpr5 (σ_x = 1.1 nA ; band pass = 10 Hz).

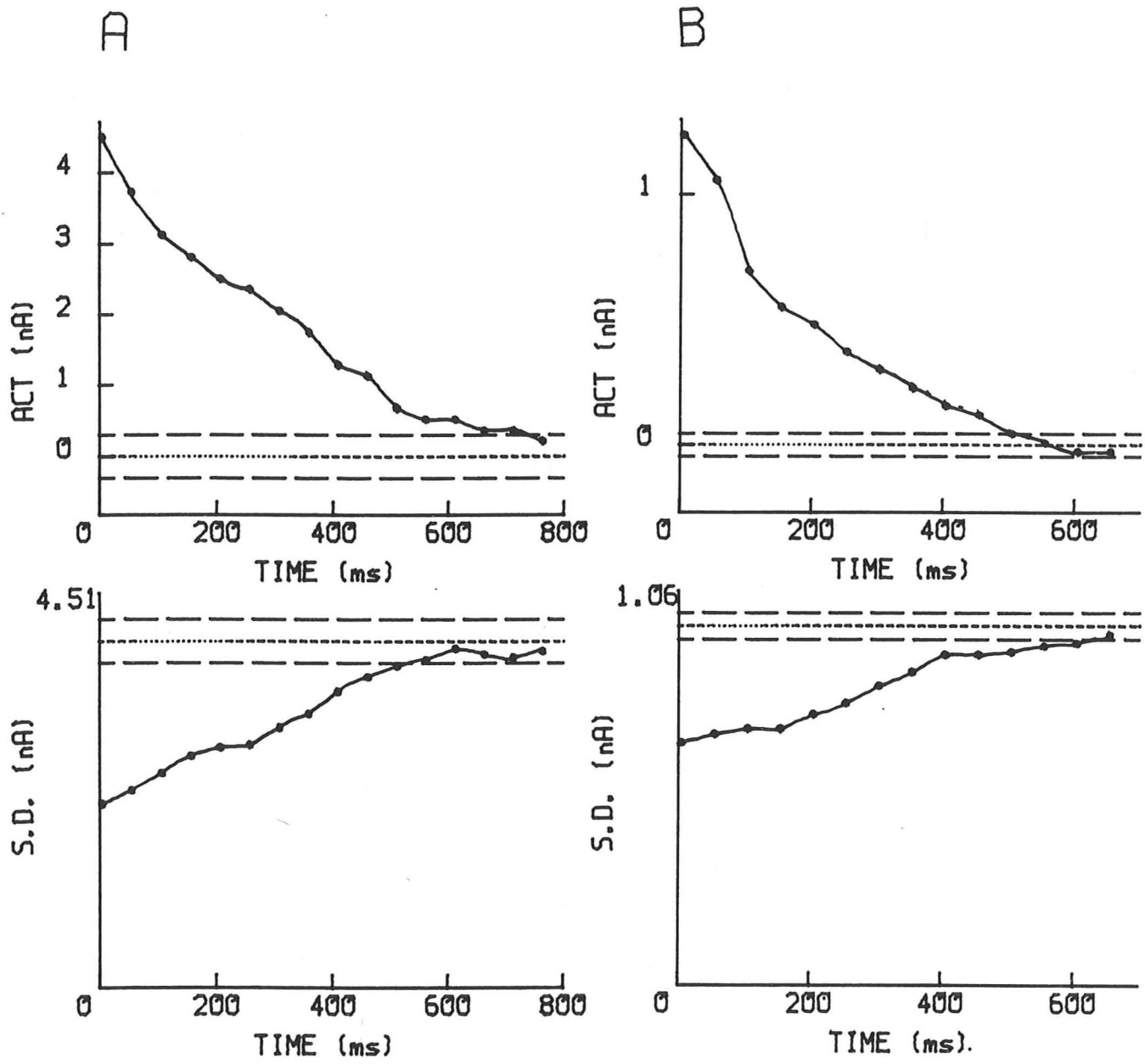

Figure 6.4. The ACT and its associated standard deviation, of two identified neurones.
(A) Rpr 76/77 (σ_x = 4.0 nA ; band pass = 5 Hz).
(B) Lpr 1/2 (σ_x = 1.0 nA ; band pass = 5 Hz).

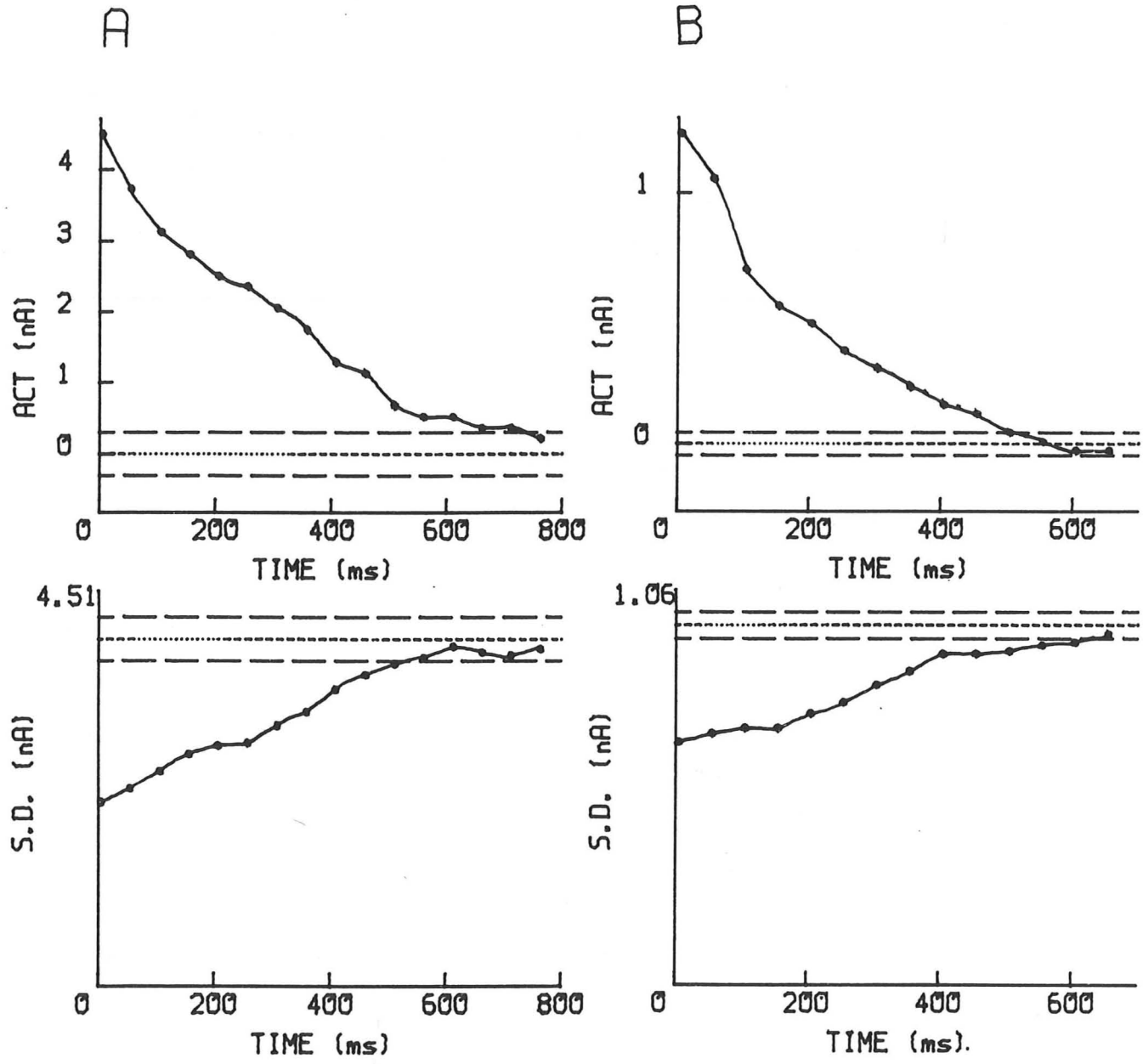

Figure 6.4. The ACT and its associated standard deviation, of two identified neurones.

(A) Rpr 76/77 (σ_x = 4.0 nA ; band pass = 5 Hz).

(B) Lpr 1/2 (σ_x = 1.0 nA ; band pass = 5 Hz).

into two phases: a late phase, corresponding to the peak just before action potential initiation, and an early phase which begins as the ACT emerges from the confidence bands.

If action potentials were initiated by a few stereotyped inputs, the standard deviation of the ACT would be close to zero. Figures 3 and 4 show that this is not the case. The standard deviation emerges from the confidence band at approximately the same time as the average current. It decreases with a roughly biphasic time course to a minimum that occurs on the rising phase of the ACT. That the ACT is the average of a multiplicity of different current trajectories can be seen more clearly from plots of the current distribution. The current distributions at 50 and 200 ms before action potential initiation, are plotted in figure 5. The distributions are clearly narrower than the input distribution and the mean is shifted towards depolarizing current values.

6.4.2.1. EFFECT OF BIAS CURRENT AND POWER ON THE ACT

The imposition of a DC bias on the input GWN, without changing the frequency or the standard deviation, results in a transformation of the shape of the ACT. Some examples are shown in figure 6. In the six cases where the effect of bias current was studied there was little change in the late phase of the ACT. However, the early phase changed in a systematic way: in all cases a hyperpolarizing bias made the early phase more depolarizing, while for depolarizing biases the converse held true. This generalization is identical to that found by Bryant and Segundo (1976) for *Aplysia* neurones.

Increasing the standard deviation, and hence the power of

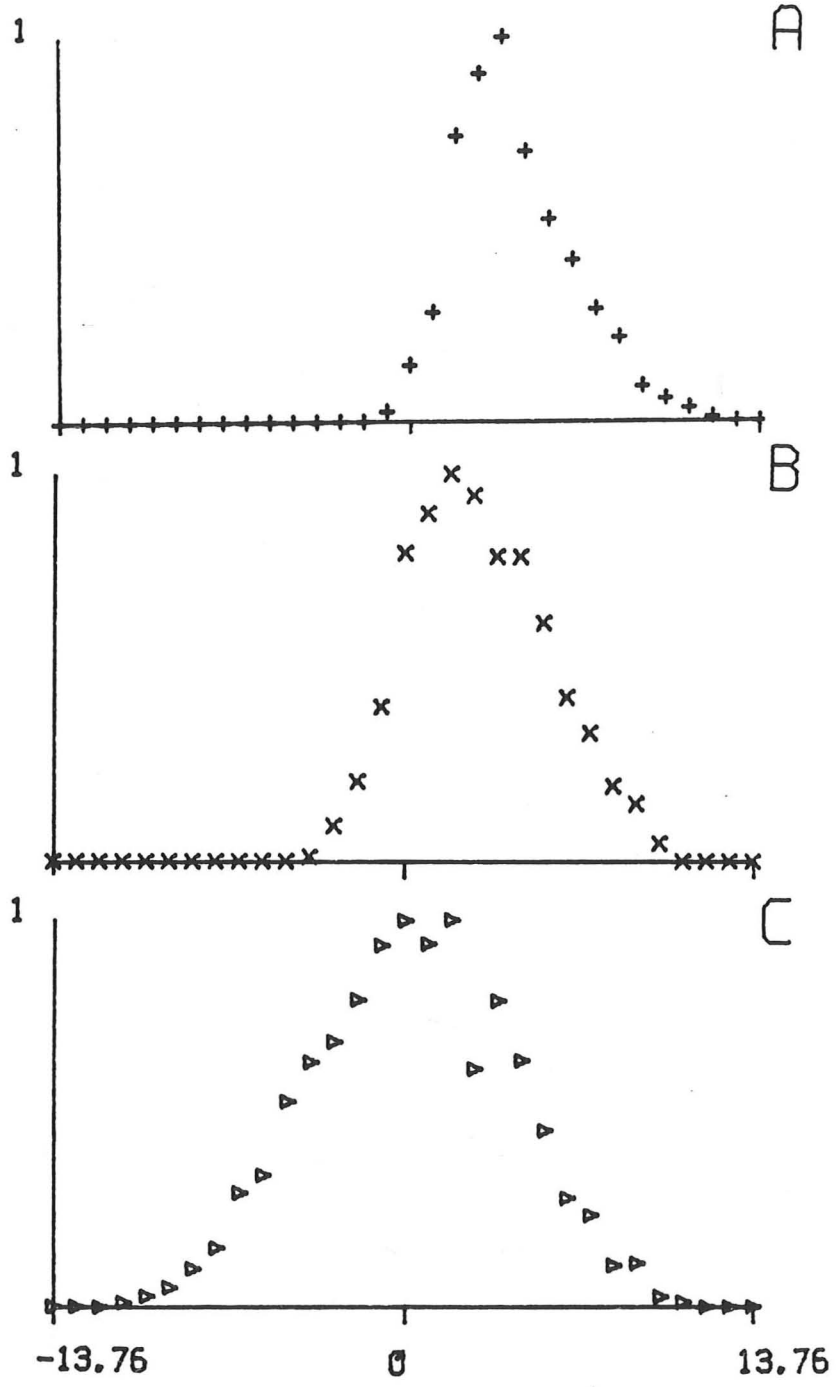

Figure 6.5. The normalized distribution of current values at time lags of; (A) 50 ms and (B) 200 ms before spike initiation for a Rpr 76/77 neurone. The ACT of this neurone is shown in figure 6.4A. (C) Normalized distribution of the current values in the input signal.

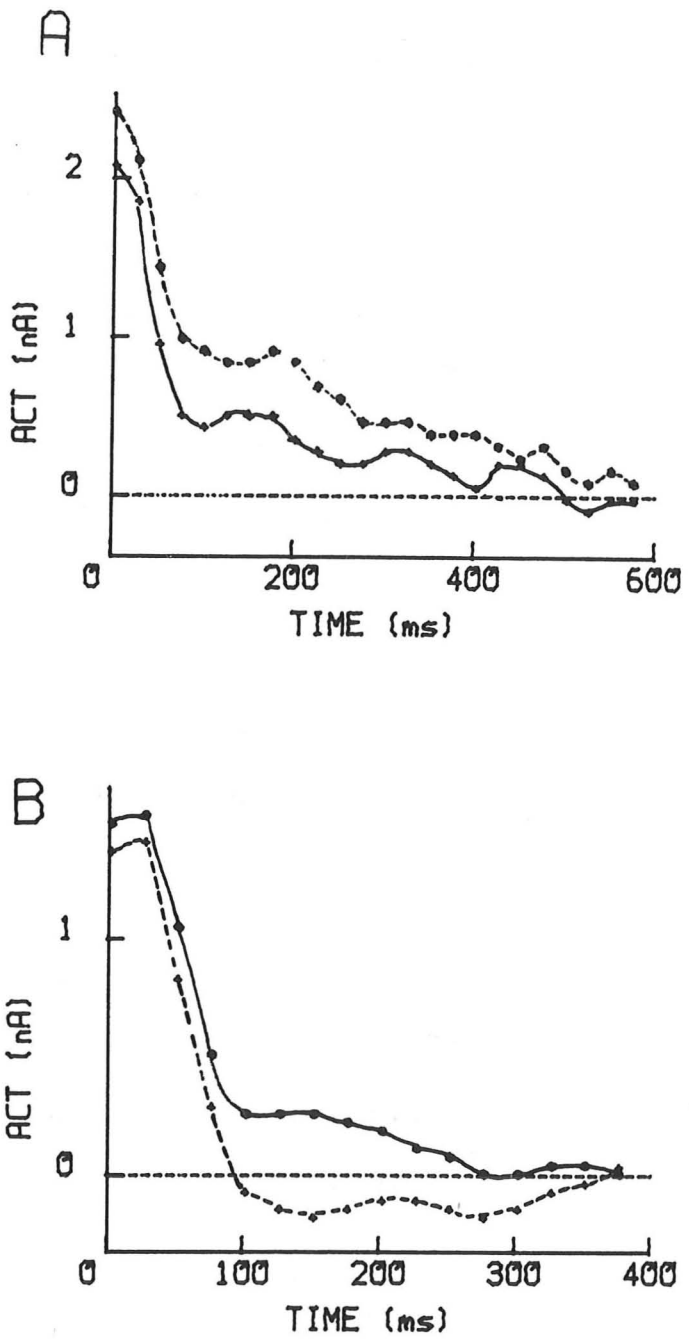

Figure 6.6. The effect of bias current on the shape of the ACT of a neurone.
(A) Lpr5 (——) DC = 0, (-----) DC = -.5 nA (σ_x = 1.6 nA, band pass = 10 Hz)
(B) Lpr5 (——) DC = 0, (----) DC = 1.0 nA (σ_x = 1.0 nA, band pass = 10 Hz)

the input noise, but without changing the DC bias current or the frequency, changes the shape of the ACT. Three examples of the sort of changes induced by increasing the power of the input are shown in figure 7. The most commonly observed change was that, as the power increased, the early phase of the ACT showed a tendency to increase in amplitude relative to the late phase. This change was observed for 63% of the neurones studied (n =8). However, in no case did the integral of the ACT remain constant when the power of the input was changed; a phenomenon that held true for Aplysia neurones (Bryant & Segundo; 1976).

This dependence of the shape of the ACT on the input power illustrates that the Wiener functional series, measured at a particular power level, does not necessarily predict the response of the system to a noise signal with a different power level. It is likely that the functional model is a good approximation of the system for a continuous range of powers, however it would be difficult to measure this range because it is only rarely possible to measure more than two ACTs before the system becomes nonstationary.

The failure of the ACTs to preserve their shape when the input power was changed also demonstrates that the input current-to-spike transformation cannot be modelled as a sandwich system. This does not, however, exclude the possibility that for a given power level the system can be represented by a sandwich system.

6.4.2.1. ACT AND IDENTIFIED NEURONES

The homologous neurones Rpr1 and Lpr5, have quite different behaviours in the isolated ganglion. Neurone Rpr1 exhibited bursting or continuous firing, while Lpr5 showed occasional and irregular firing. The form of their ACTs was also clearly

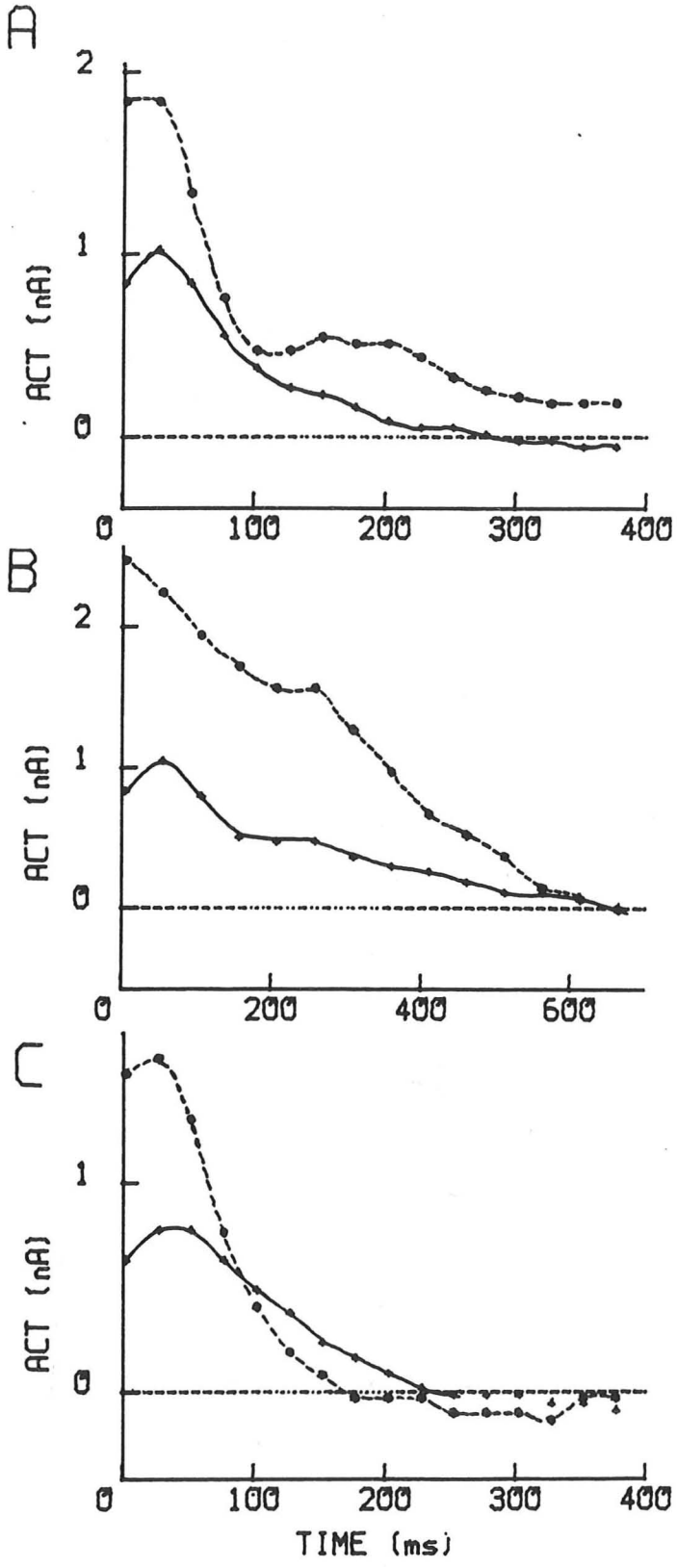

Figure 6.7. The influence of the standard deviation of the input GWN on the form of the ACT.

(A) Lpr5 (——) σ_x = 0.6 nA, (----) σ_x = 1.0 nA, (band pass = 10 Hz)

(B) Lpr 1/2 (——) σ_x = 0.7 nA, (-----) σ_x = 1.9 nA, (band pass = 5 Hz).

(C) Rpr1 (——) σ_x = 0.6 nA,(----) σ_x = 1.2 nA, (band pass = 10Hz).

distinguishable. In figure 8, the ACTs, normalized by their maximum values, have been plotted for a number of different preparations. All the experiments on Lpr5 and RPr1 were performed with a GWN signal having a standard deviation in the range .9 to 1.1 nA, and a cut-off frequency of 10 Hz. The ACT of Rpr1 is half maximal at time zero and rises to a peak at 50 ms. It then declines monotonically to zero within 150 to 200 ms. In contrast, the ACT of Lpr5 at time zero is approximately 90% of its maximum value. It peaks at 50 ms but then decreases more rapidly than Rpr1. The decline ceases when the ACT reaches 20-40% of the maximum and remains approximately constant for about 150 ms before declining to zero. The ACTs of Lpr5 have longer memories (334±24 ms., n = 15) than that of RPr1 (213±12 ms., n = 17).

The ACTs of neurones Rpr76/77 and Lpr1/2 were measured with a GWN signal with a standard deviation in the range 1-3 nA and a bandwidth of 5 Hz. There is an overall consistency in the shape of the ACTs of all four cells, and it is not possible to distinguish between the curves from contra-lateral cells. The normalized ACTs of this group of neurones is plotted in figure 8C. The form of the ACT is quite distinct from that of Lpr5 and Rpr1, and it is especially distinguished from these by the length of the neurone's memory (505 ± 22 ms, n = 17).

6.4.3. THRESHOLD

If a neurone has a discrete threshold, and the threshold variate is correctly identified, then the firing probability function (defined in section 6.3.6.) will exhibit a step from zero to one at the threshold value of the internal variate

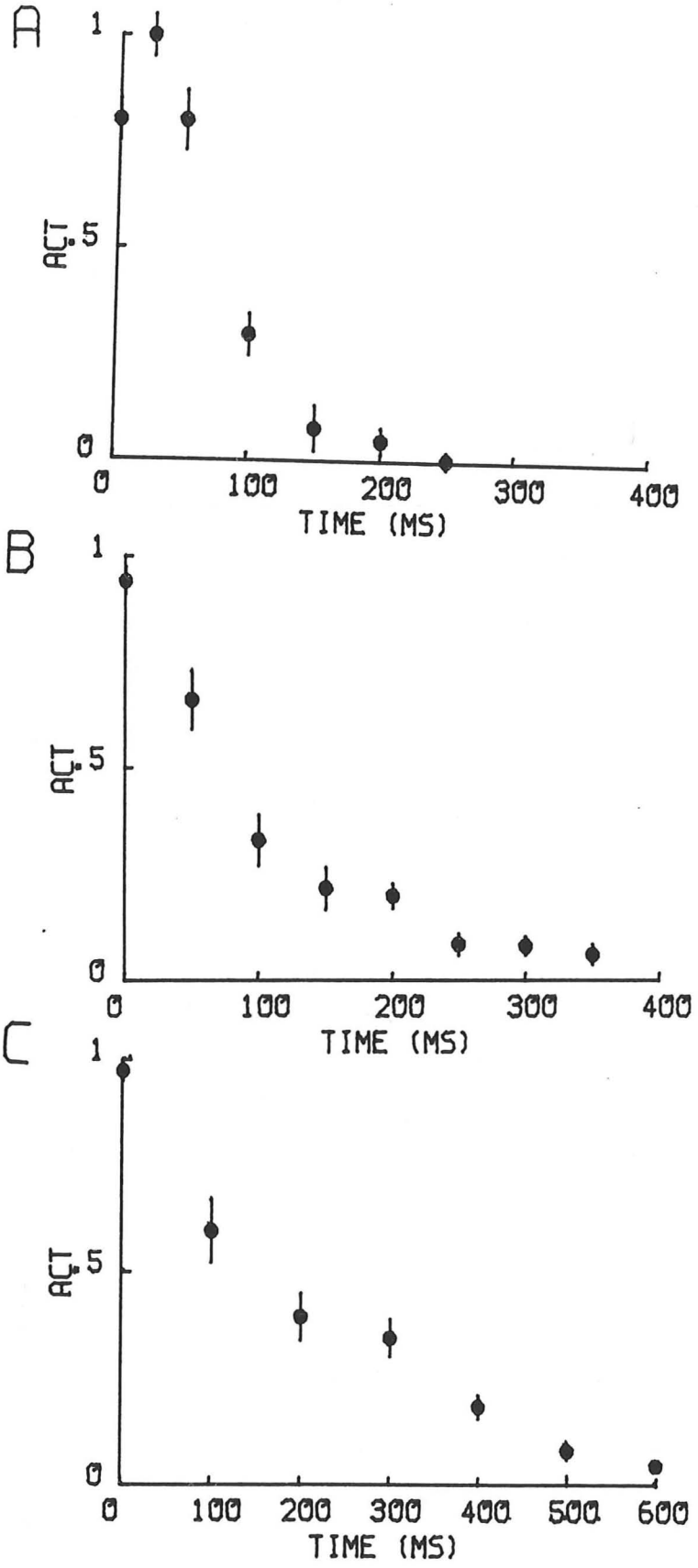

Figure 6.8. Normalized average of ACTs of; (A) Rpr1 (n=8) (B) Lpr 5 (n=7) (C) Rpr 76/77 & Lpr 1/2 (n=8).

(Brillinger & Segundo, 1979). If, instead of a deterministic threshold, the threshold was a normally distributed variable, the firing probability function would become a sigmoid function of the internal variate.

Figure 9A shows the firing probability function for a leaky integrator model, the internal variate being the convolution of the ACT and the input noise. The firing probability shows the expected step, but the firing probability at high values of the internal variate does not equal one. This is so because the first-order estimate of the model omits the resseting mechanism of the leaky integrator. Figure 9B illustrates the effect of incorporating the effect of the reset mechanism. Again, the input was convolved with the ACT, but now the internal variate was set to zero whenever a spike occurred. The firing probability now shows the expected step-like response. If the input current, which in this case is not the threshold variate, is used as the internal variate, the approximation of the firing probability to a step function is poor (Fig. 9C).

Figure 10 shows the firing probability function estimated from the response of a Rpr1 neurone to GWN. In all measured cases the firing probability showed the expected step-like response to the internal variate, however the firing probability rose more slowly than the leaky integrator model and the maximum firing probability was invariably less than one. Inclusion of a reset mechanism increased both the rate of rise and the maximum of the firing probability curves (see fig. 10B). Nevertheless, the firing probability curves were still broader than those of the leaky integrator. The failure of the firing probability to

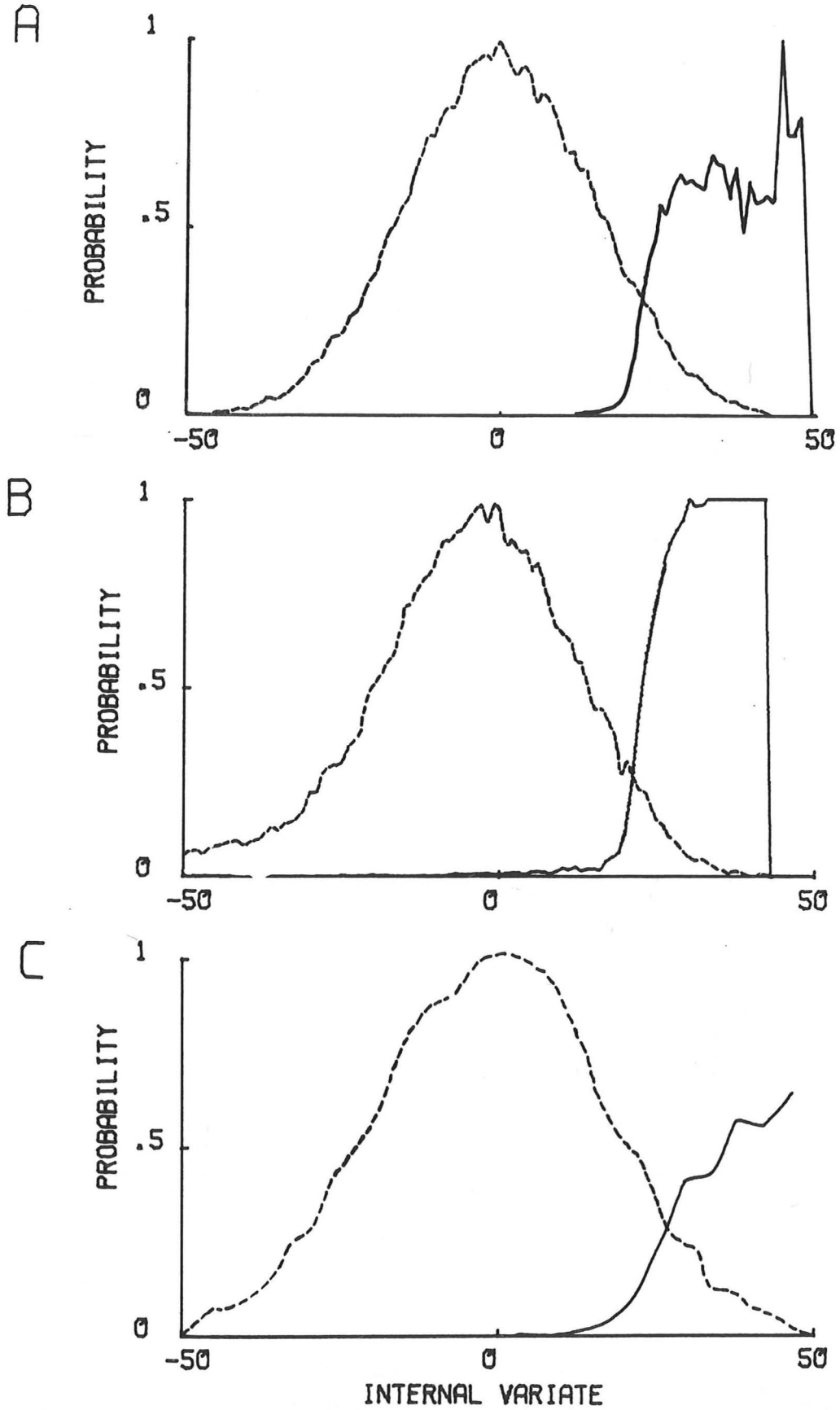

Figure 6.9. The firing probability (unbroken line) of a leaky integrator model as a function of the chosen internal variate. The dashed line is the normalized distribution of the internal variate. The scaling of the horizontal axis is arbitrary. The internal variate was; (A) the convolution of the measured ACT with the input signal (B) same as A, but with a reset mechanism (C) input current.

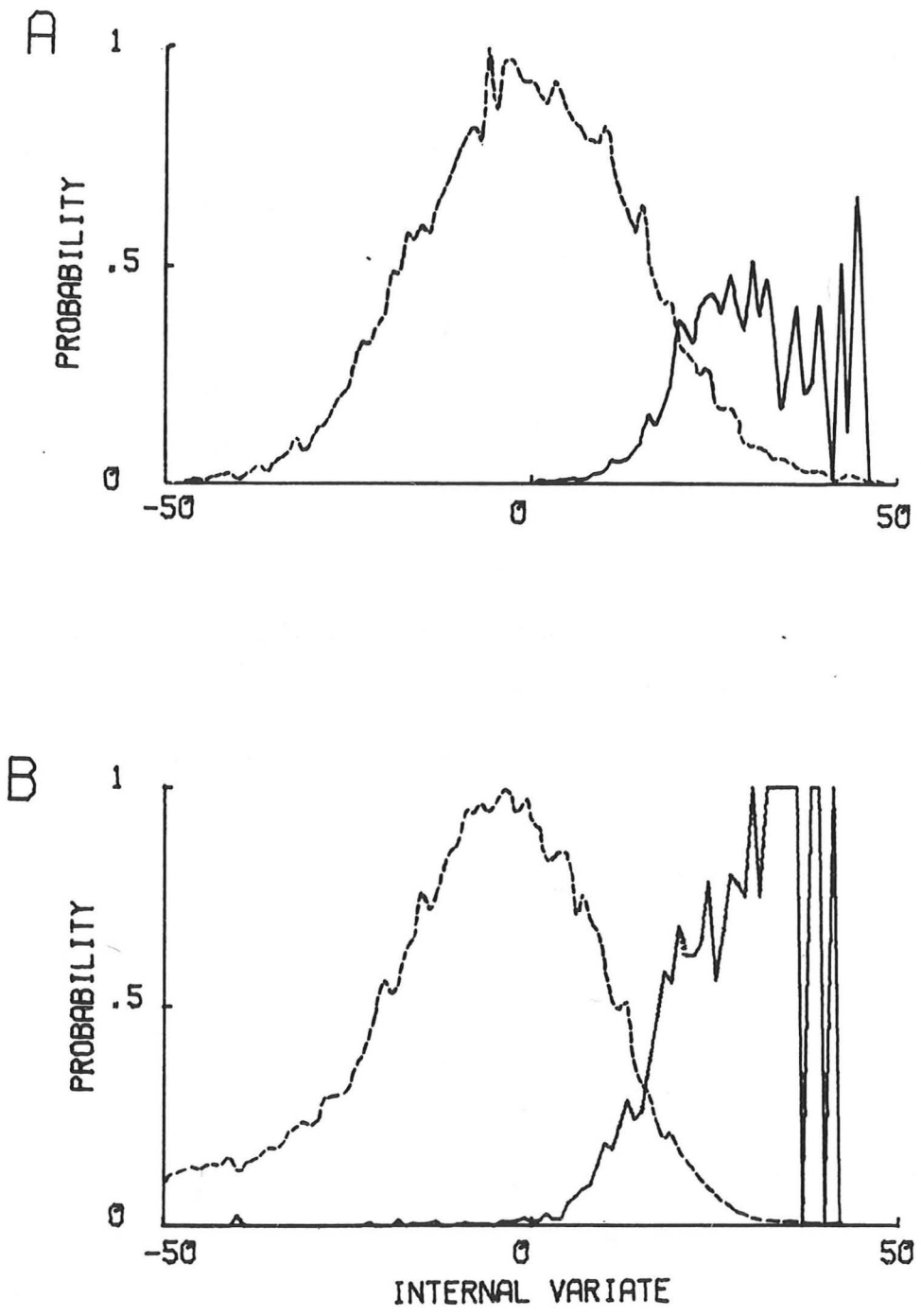

Figure 6.10. The firing probability (unbroken line) of a Rpr1 neurone as a function of the internal variate and the dashed line is the normalized distribution of the internal variate. The internal variate is the convolution of the input current and the measured ACT. (A) without reset mechanism (B) with reset mechanism.

approach a sharp step could be due either to the incompleteness of the functional model, in the sense that nonlinear contributions need to be added, or to fluctuation of the threshold or to both.

The first-order Wiener kernel in cascade with a threshold device, did however provide an good approximation of spike initiation, in that it predicted the timing of 60-80% of the observed action potentials elicited by a GWN input (see fig. 11).

6.4.4. ADAPTATION

All neurones studied in this chapter showed the classical adaptation response to a step current input. That is to say, the instantaneous frequency decreased asymptotically to a steady value. This decay could be approximated by a single exponential for the neurones Lpr1/2 and Rpr 76/77, except for a rapid phase occurring over the first three to six spikes (see fig. 12). The average time constants were; 2.5 $\pm$ 0.2 s for Lpr1/2 (n=22) and 2.1 $\pm$ 0.1 s for Rpr 76/77 (n=29). The decay time constants showed no dependence on the input amplitude in the range .25 to 20 nA. Furthermore, it was impossible to distinguish between left and right-hand cells on the basis of the dynamics of adaptation.

The impulse response of a linear system is equal to the time derivative of the step response. This relationship can be used to estimate the approximate form of the impulse response of a nonlinear system. To calculate the impulse response the interspike intervals were converted to instantaneous frequency, smoothed with a five point least-squares quadratic formula and differentiated with the central difference formula (see

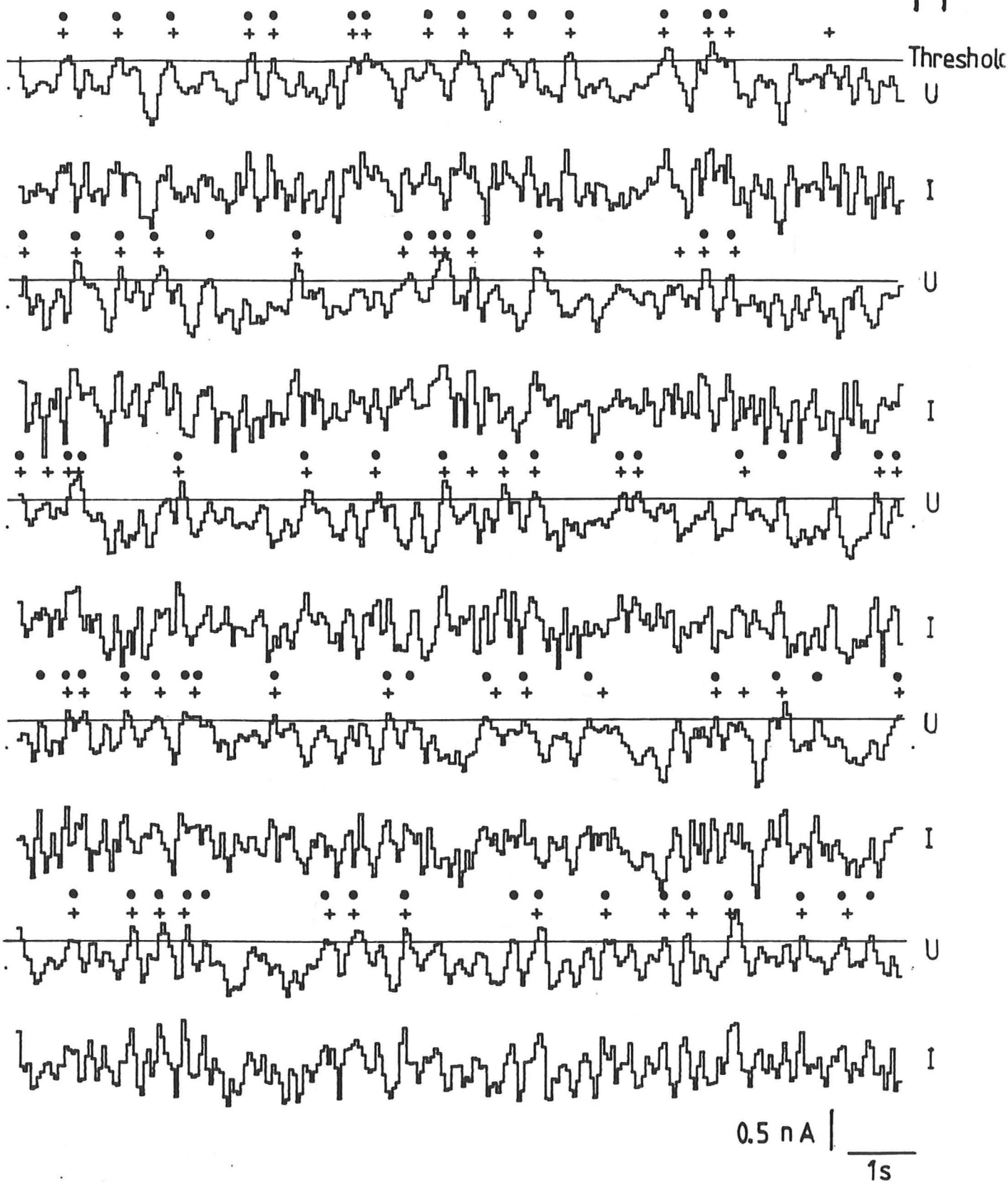

Figure 6.11. Response of Rpr1 neurone (+) to a continuous GWN signal and spikes predicted (●) from the convolution of the measured ACT and the input noise (I). The scaling of the output of the linear model (u) is arbitrary.

equations 3.11 & 3.12 respectively). Two typical impulse responses are illustrated in figure 12. Both have the characteristics of a system that responds to the rate of change of the input, that is to say, a sharp positive peak followed by a prolonged negative undershoot.

6.5. DISCUSSION

6.5.1. GWN EXPERIMENTS

It is noteworthy that the response of many of the neurones tested remained invariant during the repeated application of a segment of GWN. However it should be emphasized that the stationarity is not an invariant characteristic of a neurone: an apparently stationary neurone can be made non-stationary by increasing the average rate of firing.

The stationarity test is useful even when it is not coupled to a Wiener analysis, because if the system is stationary, it is in principle possible to find a model of spike initiation that shows no dependence on the rate of firing. Whereas if the system is non-stationary, a model of spike initiation will have to take into account the activity dependence of the spike threshold. This might arise through the accumulation of ions (Adelman & FitzHugh,1975) or the long term modification of membrane properties invoked by spiking (de Peyer et al, 1982) . Non-stationarity may of course indicate that the condition of the cell is declining.

The ACT as defined in this study represents the average of all current waveforms that lead to spike initiation. In most cases the shape of the ACT was similar to that of a leaky

integrator, in that it decays monotonically to zero. But in general its detailed time course was not that of a simple exponential.

Plots of the standard deviation of the ACT and the current distribution, show clearly that the neurones do not respond to a small set of stereotyped inputs. Action potentials were triggered by a variety of current trajectories of which the ACT was the average.

The strong dependence of the kernel shape on the DC bias and on the power of the input, raises again the question of the models tractability. To adequately represent the system up to first-order, estimates of the kernels are needed at a number of DC biases and, for each bias current, at a range of input powers. The number of kernels needed make the estimation and representation of the system difficult.

The early phase of the ACT was often in the form of a plateau. In a few cases increasing the power of the input led to a greater increase in the height of the plateau than of the height of the late phase. Guttman etal. (1974) observed a similar phenomenon in the space-clamped squid axon. They demonstrated that the plateau phase and its dependence on the input power could be reproduced by the Hodgkin-Huxley model, if account was taken of the spike latency distribution. The increase of the plateau phase with input power, is a consequence of the reduction of spike latency and its variance, as the threshold overshoot increases.

The value of a functional model for a bursting neurone like Rpr1 may be questioned. However, it has been shown for a similar

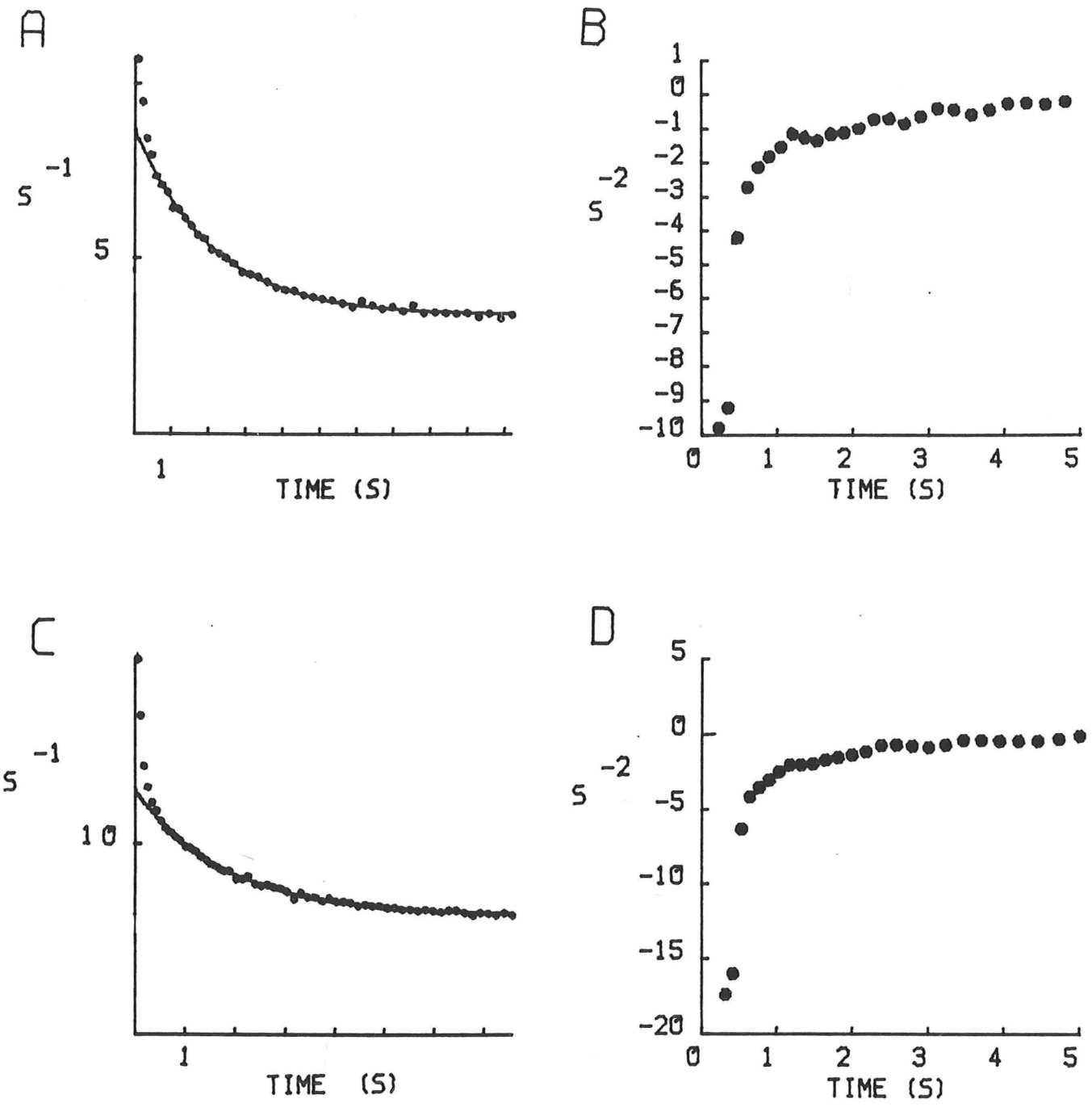

Figure 6.12. Response of neurones to step current inputs.
(A) Rpr 76/77 step input = 11.7 nA (B) time derivative of A.
(C) Lpr 1/2, step input = 9.5 nA (C) time derivative of C.

neurone in *Aplysia*, that in the intact animal, the neurone does not burst and appears to be driven synaptically (Stinnakre & Tauc, 1969). In this study it was found that the endogenous currents can be overridden to the extent that the cell responds identically to repeated applications of GWN. Furthermore, the functional model leads to good predictions of spike timing in response to a GWN input.

6.5.2. THRESHOLD

The white noise method reconstructs the form of the internal variate, but it does not unequivocally disclose the identity of the variate (the internal variate has dimensions of inverse seconds). It is incorrect, to do as Brillinger and Segundo (1979) do, to identify the internal variate automatically with the voltage at the impulse initiation zone. This is neither required by Wiener's theory, nor do excitable membranes necessarily behave like voltage-threshold devices. Noble and Stein (1966) have shown that an infinite cable with Hodgkin-Huxley kinetics, will not invariably initiate an action potential when the voltage exceeds the threshold for the space clamped axon. The threshold condition in this case is that the integral of membrane current have a net inward component.

If the soma-to-spike initiation zone transfer function were linear, and the neurone behaved like a voltage threshold device, the ACT would correspond exactly to the soma-to-spike initiation transfer function (this follows from the theorem stated in section 6.2.) To estimate the form of the soma-to-initiation zone transfer function of neurones Lpr1/2, the neurones were modelled as a lumped soma with two infinite cables of the same diameter attached to the soma. It can be shown using the B&C calculus that

the transfer function from the soma to one of the branches, is identical to that of an LSFC model with the same soma-to-dendrite conductance ratio, ρ_{∞}.

The transfer function of the LSFC model was calculated by using a fast Fourier transform algorithm to invert the transfer impedance (Norman, 1972), which was calculated by the B&C method (Fig. 13). If the ACT has the same shape as the transfer function, and τ_m and ρ_{∞} are known, the approximate position of the initiation zone could be estimated by finding the soma-to-dendrite distance that gives a transfer function with the same broadness at half height as the measured ACT.

The calculated transfer functions do not match the shape of the measured ACTs for neurones Lpr 1/2 and Rpr 76/77. In particular the transfer function does not match the complex shape of the early phase of the ACT (compare fig.13 with figs. 4 A&B). The failure of the simple voltage threshold model to account for the shape of the ACT could result from the ommission of spike latency fluctuations or from the misidentification of the threshold variate. Furthermore, it is likely that the linear membrane properties, estimated from the neurones response to small amplitude perturbation, does not correspond to the best first-order estimator for large amplitude inputs (see chapter 5).

The failure of the predicted soma-to-dendrite transfer function to match the ACT does not exclude the possibility that the neurones behave like voltage threshold devices, but it does suggest that modelling the input current-to-spike transformation on the basis of the estimated linear properties would be

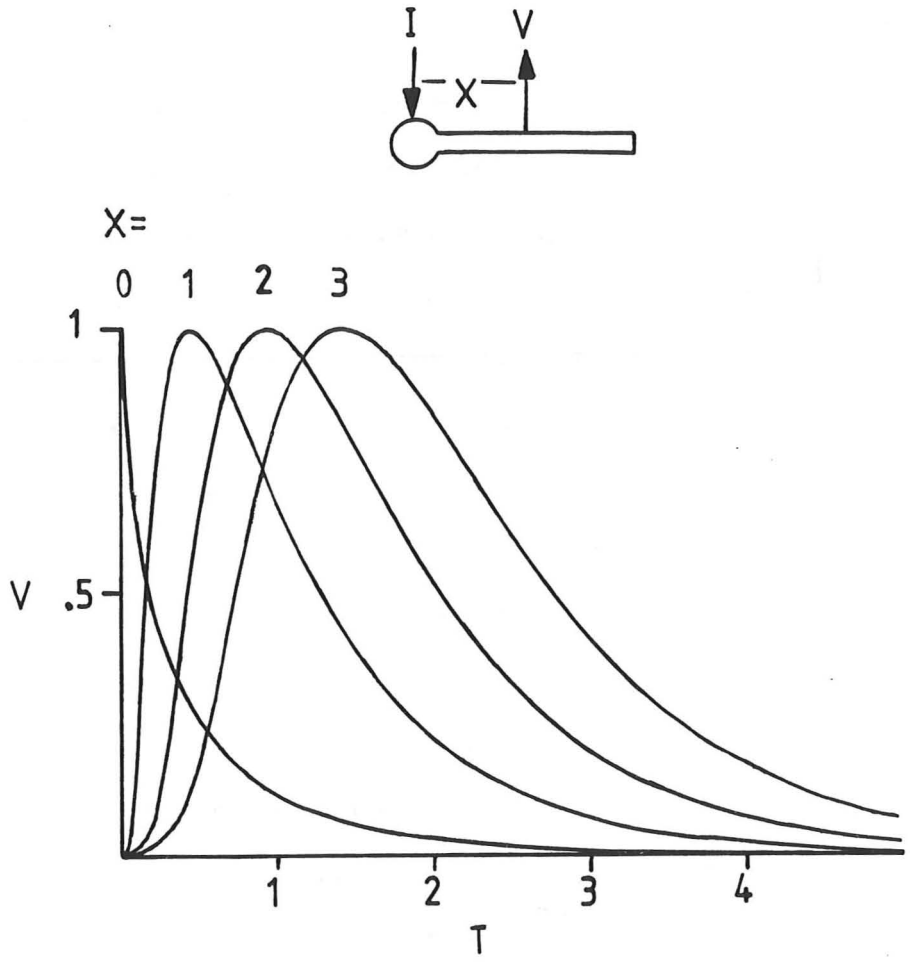

Figure 6.13. Transient voltage response of an LSFC model at a distance of Xλ from the soma, to an impulse applied at the soma. The responses have been normalized and are plotted as a function of dimensionless time T (= t/τ_m).

inadequate.

6.5.3. STIMULUS DEPENDENCE OF THE DYNAMICS

The Wiener functional representation estimated from the response of the system to a GWN signal with a particular power density, will only be the best functional model for that particular input (Schetzen, 1980). It will not in general be the best representation of the response of the system to any other input (eg. other sorts of noise signals and step inputs). If a stimulus-invariant functional representation is desired, the Wiener kernels must be transformed to the corresponding Volterra kernels. This transformation can be described analytically (Schetzen, 1980); however low-order Volterra kernels will have contributions from high-order Wiener kernels. Since in practice it is only feasible to measure Wiener kernels up to third-order, it will not be possible to transform Wiener to Volterra kernels.

A related problem is whether the behaviour of the system depends on the form of the input stimulus. Could the signal itself change the state of the system? Aertsen and Johannesma (1981) have suggested how this might be tested using inputs that are linear transforms of GWN. Wiener kernels could be estimated for two different signals using the Lee-Schetzen method, and if the system is not affected by the signal, the Volterra kernels should be identical. However, the problem of estimating enough Wiener kernels to accurately convert the kernels to Volterra kernels persists, and this makes the method impracticable.

Deterministic inputs were used both to explore alternative methods of measuring neuronal dynamics, and to test for the

possibility of the stimulus-dependence of the dynamics. From the adaptation response of a neurone to a step input it was possible to estimate the form of the impulse response. However, caution should be exercised in comparing the impulse response with the ACT because in the absence of details of the system's dynamics it is not possible to make explicit the precise relationship between these two first-order predictors. Only in the case of a first-order system will the ACT correspond exactly to the impulse response.

The difference between the dynamics estimated from the step response and that from the response to GWN, can be most clearly underlined by comparing the duration (i.e. the memory) of the first-order functions. In the case of neurones Lpr 1/2 and Rpr 76/77 the mean duration of the ACT was 505 ms while that of the impulse response was in all cases greater than 1.5 s. Furthermore only 2 of the 60 measured ACTs showed the characteristic negative undershoot of adaptation, which all the measured impulse responses exhibited. It might be argued that the method used to measure the ACT may in some way mask any ongoing adaptation. However, the fact that the ACT is a good predictor of the occurrence of action potentials in response to GWN, suggest that little adaptation occurs in response to GWN. This conclusion probably only holds good for low firing rates (i.e. less than .7 spikes per second). It was not possible to test this conjecture, because high firing rates were associated with output non-stationarity, and this rendered the Wiener method inapplicable.

It is worth emphasizing that adaptation is not necessarily associated with time-invariance. If adaptation results from an activity-related increase in threshold, and the threshold relaxes

back to its initial value after being perturbed, the system is stationary. However if the change in threshold is irreversible then the system is non-stationary.

In summary, the above findings suggest that steps and GWN signals appear to invoke different dynamics. Models estimated from the response to GWN serve as poor predictors of the response to step inputs and vice versa. Different phenomenological models are needed to account for each sort of input. However, it is possible that a Hodgkin-Huxley-like model, might encompass the response to both forms of input.

The demonstration of the dependence of the neuronal dynamics on the form of the input, raises the question of the appropriateness of an input in assaying neuronal dynamics. For example, it is known that neurones can be damaged by high amplitude current inputs (Zimmerman, 1982) or driven into exotic forms of behaviour (Holden & Ramadan, 1981). The latter may throw light on the underlying dynamics. However, in building up simple phenomenological models it may be useful to restrict inputs to some range that may be termed 'natural' for the neurone. To infer the range of natural inputs it would be necessary to measure spike patterns in an intact animal during a number of different behavioural acts. A natural current input could then be defined as one that does not give rise to spike patterns that do not occur in the intact animal.

6.5.4. A NOTE ON THE SECOND-ORDER WIENER KERNEL

The Wiener method has in this study only been taken as far as estimating the first-order Wiener kernel. The functional model was terminated at this stage because there are certain

theoretical and practical impediments to the measurement of the second-order Wiener kernel of the current-to-internal variate transformation, that can be explained as follows. If spike initiation can be represented by a cascade of an input current-to-internal variate transformation (termed here 'X') and a threshold device, then if X is a sandwich system, the first-order Wiener kernel of the whole system corresponds exactly to the linear part of X. However the second-order Wiener kernel of the whole system is not the same as the second-order component of X, but is a combination of the second order properties of both systems (Marmarelis & Marmarelis, 1978). The second-order Wiener kernel of X can only be calculated if the second-order *Volterra* components of both the whole system and the threshold device are known. As the arguments of section 6.5.4. show it will be difficult if not impossible to measure the relevant Volterra kernels.

The fact that the firing probability function of the measured first-order kernel, together with a reset mechanism, does not show a very sharp step, suggests that a nonlinear component may be needed to account for the current-to-internal variate transformation.

6.6. CONCLUSION

The Wiener method of system identification provides a useful first approximation of a neurone's input-output dynamics, however progress towards better neuronal models within the context of Wiener's theory is limited for two reasons. Firstly, it is seldom possible to measure kernels of order greater than two. Secondly

it is difficult to find stimulus invariant forms of the Wiener functional representation.

Both of these deficiencies of the functional representation could be met by parametric models. However, there is no automatic procedure for generating parametric models; they can only be found by the judicious interplay of physiological knowledge and mathematical intuition. If the task of explaining neuronal networks in terms of the properties of its component neurones is to prove feasible, models are needed that are mathematically simpler than detailed channel based models (Joyner et al., 1978), yet more robust than the functional series representation. (The models of FitzHugh (1969) and Krinskii & Kokoz (1973) may serve as useful starting points).

Wiener's system identification procedure is unlikely to prove useful in the specification of parametric models, because of the complex relationship between the system' dynamics and its Wiener kernels. However, given the form of the model, noise signals may provide a more rigorous test of the model than deterministic signals, because noise subjects the system to a greater range of input trajectories. Furthermore, once outside the formal framework of Wiener's theory, there is no restriction on the form of the noise, and one is free to use input signals that approximate more closely the fluctuations observed in biological systems (eg. 1/f noise, Verveen & DeFelice, 1974).

APPENDIX A

GENERALIZING THE B&C METHOD

The B&C calculus can be extended to include the case of a dendritic cylinder with a membrane that can be represented by any combination of linear elements (i.e. resistors, capacitors and inductors.)

Consider a cable of length 1 terminated with impedances $Z_o(s)$ and $Z_1(s)$, and with a current source at x=1. Let v(x,t) be the transmembrane potential measured relative to the resting potential. From Kirchoff's current law the spatial rate of change of the axial current, $i_a(x,t)$ is equal and opposite to the membrane current per unit length, $i_m(x,t)$ at all points on the cable except that at which the current is applied,

$$\partial i_a / \partial x = -i_m \qquad (1)$$

From Ohm's law the rate of change of voltage with distance is given by :

$$\partial v / \partial x = - r_a i_a \qquad (2)$$

Differentiating equation 2 with respect to x, and combining the result with equation 1,

$$\partial^2 v / \partial x^2 = r_a i_m \qquad (3)$$

Let y(s) be the admittance of the unit membrane, and V(s) and I(s) be the Laplace transforms of the voltage and current respectively, then the Laplace transform of the membrane current is :

$$I_m = y V \qquad (4)$$

Taking the Laplace transform of equations 2 and 4 and substituting equation 4 for the membrane current, the equations become respectively,

$$dV/dx + r_a I_a = 0 \qquad (5)$$

$$d^2V/dx^2 - r_a y V = 0 \qquad (6)$$

If we let $\gamma = (r_a y)^{1/2}$, then equations 5 and 6 are identical to equations 31 and 32 of B&C, which serve as the starting point for the derivation of the method. Since no other assumptions are introduced in the course of the derivation of the graphical calculus, the B&C method is applicable to a tree with an arbitrary unit membrane impedance, the only modification necessary is that $\gamma = (r_a y)^{1/2}$

APPENDIX B

INTRODUCING SYNAPSES

The B&C equations predict the voltage output for a constant current source, synapses are however not ideal current sources, as the amount of current delivered depends on the voltage at the synapse. Further the B&C equations predict that the transfer impedance is not altered by the interchange of current and voltage electrodes. In contrast, when current is injected through a synapse the amount of current delivered will depend on the input impedance. This can be illustrated by considering the attenuation of DC potentials between any two point i and j on an arbitrary dendritic tree, the synapse being located at site i. The current generated by a synapse with conductance g is :

$$i_i(t) = g(t)(E'_i - v_i(t)) \qquad (1)$$

where $E'_i = E_i - E_o$, and E_i is the reversal potential of the synapse and E_o the resting potential.

Considering only steady-state potentials, the potential at the site of current injection is,

$$v_i = K_{ii}\, i_i \qquad (2)$$

Substituting this into equation 1 and solving for i_i.

$$i_i = gE'_i/(1+gK_{ii}) \qquad (3)$$

The membrane potential at site j is then:

$$v_j = gE'_i K_{ij}/(1+gK_{ii}) \qquad (4)$$

For small changes in conductance the output is proportional to the synaptic conductance, however for large conductance changes the output saturates at a value of $E_i K_{ij}/K_{ii}$.

It is in general not possible to solve the time dependent case of equation 1 in closed form, however Poggio and Torre (1978) have described a simple graphical technique for deriving a Volterra series approximation.

APPENDIX C

Figure A.1. A wide-band microelectrode amplifier (designed by D.M. Unwin).

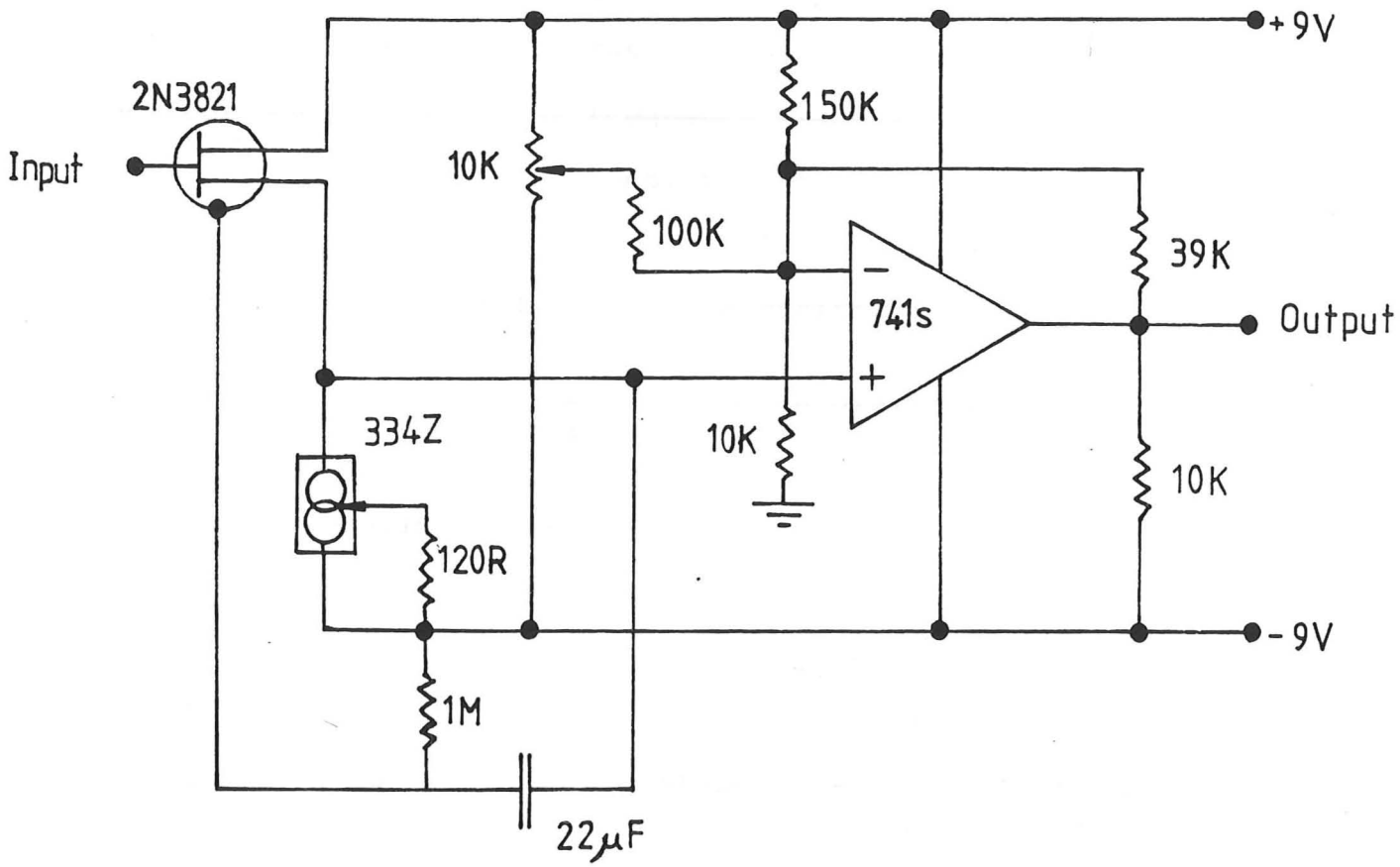

APPENDIX D

THE GOERTZEL ALGORITHM: a single frequency Fourier transform.

Assume that N+1 points of some wave form have been sampled at intervals of T seconds and stored in an array. The Goertzel algorithm (Gold & Rader, 1969) provides a way of extracting the magnitude and phase of any frequency component in the range k/NT Hz (k = 0, 1, 2, ... N/2) from the digitized record.

In what follows the algorithm is formalized in a BASIC-like language. Comments are denoted by a semicolon.

```
DIM X(N)                ;Array holding digitized waveform
                        ;starts at X(0)
FREQ = 2*π/N

INPUT "HARMONIC", K ;

A= 2*COS(FREQ*K)

Y1 = 0

Y2 = 0

FOR I = 1 TO N          ;note algorithm begins at the second
                        ;point in the array

Y = X(I) + A*Y1 - Y2

Y2 = Y1

Y1 = Y

NEXT I

RE = (2/N)*( Y1-((A*Y2)/2)))   ; real component at frequency
                               ; k/N*T

IM = (2/N)*Y2*SIN(FREQ*K)      ; imaginary component

AMP = SQRT( RE*RE + IM*IM)     ; amplitude of component

PHASE = ARCTAN( IM/RE )

PHASE = PHASE + 90*SGN( RE )   ; for phase convention see
                                 fig. 2.1.
```

APPENDIX E

THE GENERALIZED ADRIAN ALMERS METHOD

Eisenberg and Mathias (1980) outlined a method for estimating electrotonic parameters in such a way as to avoid exponential peeling. I have applied this method to the estimation of the electrotonic parameters of an LSFC model and have found the method to be so sensitive to noise as to render it inapplicable in most cases. Nevertheless the derivation is given here as it illustrates the usefulness of algebraic computer methods. Furthermore the derivation serves as a proof of the structural identifiablity of the LSFC model.

Consider an arbitrary linear circuit with an input admittance Y(s). If all derivatives of Y(s) with respect to the Laplace transform variable, s, exist at s=0, then the admittance can be represented by a Taylor series expansion (Adrian & Almers, 1974):

$$Y(s) = Y(0) + sY^{(1)}(0) + s^2/2!\ Y^{(0)}(0) + \ldots\ s^n/n!\ Y^{(n)}(0) \qquad (1)$$

where $Y^{(n)} = d^n\ Y(0)\ /\ d\ s^n$

Adrian and Almers (1974) showed that the term $Y^{(1)}$ is the effective capacity of the system, and for the special case of a parallel R-C circuit, corresponds to the real capacitance. Eisenberg and Mathias (1980) have generalized this approach to consider higher-order derivatives of the admittance. They demonstrated that for a linear system represented by an impedance Z(s), for a step current input i_∞, the nth derivative of Z(s) at s=0 is given by :

$$Z^{(n)}(0) = n/i_\infty \int_0^\infty (-t)^{(n-1)}\ [\ v(t)-v(\infty)\ ]\ dt \qquad (2)$$

All the terms on the right hand side of equation 2 can be measured, therefore $Z^{(n)}(0)$ can be calculated. The derivatives

of the admittance can then be calculated from the derivatives of the impedance. The admittance is by definition the inverse of the impedance (Y(s)= 1 / Z(s)) and from this it follows that:

$$Y^{(1)} = - Z^{(1)} / Z^2 \qquad (3)$$

$$Y^{(2)} = - Z^{(2)}/Z^2 + 2(Z^{(1)})^2/Z^3 \qquad (4)$$

$$Y^{(3)} = -Z^{(3)}/Z^2 + (6Z^{(1)}Z^{(2)})/Z^3 - 6(Z^{(1)})^3)/Z^4 \qquad (5)$$

$$Y^{(4)} = -Z^{(4)}/Z^2+(8Z^{(1)}Z^{(3)}+6(Z^{(2)})^2)/Z^3 - 36(Z^{(1)})^2Z^{(2)}Z/Z^4 + 24(Z^{(1)})^4/Z^5 \qquad (6)$$

A correspondence is now set up between the measured derivatives of the admittance and the parameters of the LSFC model.

For the LSFC model the admittance is:

$$Y(s) = \frac{1 + s\tau_m + \rho_\infty Q \tanh(QL)}{R_{inp}(1 + \rho_\infty \tanh(L))} \qquad (7)$$

where: $Q=(1+s\tau)^{1/2}$

The analytic expressions for the derivatives of the admittance of this expression at s=0, were calculated using the algebraic language CAMAL (Fitch, 1975). The equations are represented in fig.2.

These equations cannot be solved analytically, so a graphical method is used. Combining equations 9,10 & 11 of fig.2..

$$\frac{2!4!Y^{(3)}}{3!Y^{(2)}Y^{(4)}} = \frac{F(3)}{F(2)F(4)} \qquad (13)$$

The left-hand side of equation 13 can be derived from the measured values of the derivatives of the admittance, while the right-hand side is a function of L only (see fig.2). The electrotonic length of the cable can be found from a table of

Appendix figure 2

Algebraic expansion of the input admittance of an LSFC model

Key to symbols of CAMAL program

$a = s T_m$; $b = L$. ; $c = \rho_\omega$

$d = 1 / (R_{inp} (1 + \rho_\omega \tanh (L)))$

$f = \tanh (L)$

CAMAL program (comments denoted by '|')

```
A=1
FOR I=1:1:N
  A = (A+(1+a)/A)/2          | expand sqrt(1+a)
REPEAT
B=f
FOR I=1:1:N
  B=f+$((1-BB)b(dA/da)) da
REPEAT                       | expand tanh(b sqrt(1+a))
                             | $ = integral sign
 C = d(1+a+cAB)
F[20]                        | input admittance of LSFC
EXPAND(C,a,F[N])
FOR I=0:1:N
  PRINT[F[I]]
REPEAT
```

Output of CAMAL program.

Where, $F[n] = Y^{(n)} / n!$ and '↑' denotes exponentiation.

$$F[0] = (d + f c d) \quad (8)$$

$$F[1] = (d + (1/2) b c d + (1/2) f c d - (1/2) f\uparrow 2 b c d) \quad (9)$$

$$F[2] = ((1/8) b c d - (1/8) f c d - (1/4) f b\uparrow 2 c d - (1/8) f\uparrow 2 b c d + (1/4) f\uparrow 3 b\uparrow 2 c d) \quad (10)$$

$$F[3] = -((1/16) b c d - (1/16) f c d + (1/24) b\uparrow 3 c d - (1/16) f\uparrow 2 b c d - (1/6) f\uparrow 2 b\uparrow 3 c d + (1/8) f\uparrow 4 b\uparrow 3 c d) \quad (11)$$

$$F[4] = ((5/128) b c d - (5/128) f c d + (1/96) b\uparrow 3 c d + (1/64) f b\uparrow 2 c d - (5/128) f\uparrow 2 b c d + (1/24) f b\uparrow 4 c d - (1/24) f\uparrow 2 b\uparrow 3 c d - (1/64) f\uparrow 3 b\uparrow 2 c d - (5/48) f\uparrow 3 b\uparrow 4 c d + (1/32) f\uparrow 4 b\uparrow 3 c d + (1/16) f\uparrow 5 b\uparrow 4 c d) \quad (12)$$

values of the right hand side of equation 13.

From equation 9 & 10,

$$\tau_m = \left(\frac{2!\ Y^{(3)}}{3!\ Y(2)}\right)\left(\frac{F(2)}{F(3)}\right) \qquad (14)$$

The second term in brackets is a function of L only and so the membrane time constant can be calculated.

From equation 8 & 9,

$$\rho_\infty = \frac{Y^{(1)} - \tau_m Y^{(0)}}{\tau_m Y^{(0)} (0.5L + 0.5 \tanh (L) - 0.5 L \tanh^2 (L)) - Y^{(1)} \tanh(L)} \qquad (15)$$

REFERENCES

Adelman, W. J. & FitzHugh, R. (1975) Solutions of the Hodgkin-Huxley equations modified for potassium accumulation in a periaxonal space.
Fed. Proc., 34, 1322-1329.

Adrian, R.H. & Almers, W. (1974) Membrane capacity measurements on frog skeletal muscle in media of low ion content
J. Physiol. 237: 573-605.

Aertsen, A. M. H. J. & Johannesma P. I. M. (1981) The spectro-temporal receptive field: a functional characteristic of auditory neurons.
Biol. Cybern. 42: 133-143.

Akaike, N., Brown, A. M., Dahl, G., Higashi, H., Isenberg, G., Tsuda, Y. & Yatani, A. (1983) Voltage-dependent activation of potassium current in *Helix* neurones by endogenous cellular calcium.
J. Physiol. 304: 309-324.

Amari, S. I. (1974) A method of statistical neurodynamics.
Kybernetik. 14: 201-215.

Baker, C. L. & Hartline D. K. (1978) Nonlinear systems analysis of repetitive firing behaviour in the crayfish stretch receptor.
Biol. Cybern. 29: 105-113.

Barrett,J.N., and W.E.Crill (1974) Specific membrane properties of cat motoneurones
J.Physiol.(Lond.). 239:301-324.

Bellman, R. & Astrom, K. J. (1970) On structural identifiability.
Math. Biosc. 7: 329-339.

Bendat, J. S. & Piersol, A. G. (1971) Random data: analysis and measurement procedures.
New York: Wiley Intersciences.

Bracewell, R. N. (1965) The Fourier transform and its applications.
New York : McGraw-Hill.

Brillinger, D. R. & Segundo, J. P. (1979) Empirical examination of the threshold model of neuron firing.
Biol. Cybern. 25:213-220.

Brown, T.H., Perkel, D.H., Norris, J.C. & Peacock, J.H. (1981) Electrotonic structure and specific membrane properties of mouse dorsal-root-ganglion neurons.
J. Neurophysiol. 45: 1-15

Bryant, H. L. & Segundo, J. P. (1976) Spike initiation by transmembrane current: a white noise analysis. J. Physiol. 260: 279-314.

Butz,E.G., and J.D.Cowan. (1974) Transient potentials in dendritic systems of arbitrary geometry. Biophys.J. 14:661-689.

Calvin, W. H. (1978) Setting the pace and pattern of discharge: do CNS neurones vary their sensitivity to external inputs via their repetitive firing processes? Fed. Proc. 37 2165-2170.

Calvin, W. H. & Graubard, K. (1979) Styles of neuronal computation. In: The neurosciences fourth study program, ed. Schmitt, F. O. & Wordon, F. G., pp. 513-524. Cambridge, Massachusets: MIT Press.

Calvin, W.H. (1975) Generation of spike trains in cns neurons. Brain. Res., 84, 1-22.

Carius, W.J. (1979) Generation of 2-nd harmonic due to dielectric saturation at the modified lipid bilayer. Dipicrylamine in lecithin membranes. Ber. Busenges. Phys. Chem., 83, 905-911.

Chandler, W. K., FitzHugh, R. & Cole, K. S. (1962) Theoretical stability properties of a space-clamped axon. Biophys. J. 2: 105_127.

Christensen, B.N. & Teubl, W.P. (1979) Estimates of the cable parameters in the lamprey spinal cord neurones. J. Physiol., 297, 299-318.

Clausen, C., Lewis, S. A. & Diamond, J. M. (1979) Impedance analysis of a tight epithelium using a distributed resistance model. Biophys. J. 26: 291-318.

Cole, K. S. (1968) Membranes, ions and impulses. Berkeley & Los Angeles: University of California Press.

de Boer, E. (1967) Correlation studies applied to the frequency resolution of the cochlea. J. Aud. Res. 7:209-217.

de Boer, E. & de Jongh, H. R. (1978) On Cochlear encoding: potentialities and limitations of the reverse correlation technique. J. Acoust. Soc. Am. 63: 115-135.

de Boer,E (1976) Cross-correlation function of a band-pass nonlinear network. Proc. IEEE 64: 1443-1446.

de Jongh, H. R. & Kernell, D. (1982) Limits of usefulness of electrophysiological method for estimating dendritic length in neurones.
J. Neurosci. Methods. 6: 129-138.

de Peyer, J. E., Cachelin, H. B., Levitan, I. B. & Reuter, H. (1982) Ca^{2+} activated K^{+} conductance in internally perfused snail neurons is enhanced by protein phosphorylation.
Proc. Natl. Acad. Sci. USA., 79, 4207-4211.

DeFelice, L.J., Adelman, W.J., Clapham, D.E. & Mauro, A. (1981) Second-order admittance in the squid axon.
In: The Biophysical Approach to Excitable Systems , ed. W.J.Adelman , Plenum Press ,37-63.

Diamond, J. M. & Machen T. E. (1983) Impedance analysis in epithelia and the problem of gastric acid secretion.
J. Membrane Biol. 72: 17-41.

Dworsky, L. N. (1979) Modern transmission line theory and its applications.
New York: John Wiley & sons.

Eckhorn, R. & Popel, B. (1979) Generation of Gaussian noise with improved quasi white properties.
Biol. Cybern. 32: 243 - 248.

Eisenberg, R. S. & Johnson E. A. (1970) Three dimensional electric field problems in physiology.
Prog. Biophys. Mol. Biol., 20, 1-65.

Eisenberg, R. S. & Mathias, R. T. (1980) Structural analysis of electrical properties of cells and tissues.
Crit. Rev. Bioeng. 4: 203-232.

Eisenberg, R.S. & Engel, E. (1970) The spatial variation of membrane potential near a small source of current in a spherical cell.
J. Gen. Physiol. 58: 736-757.

Endrenyi, L. (1980) Kinetic models: uncertain identification but some robust parameters .
Adv. Physiol. Sci. Vol 34. Mathematical and computational methods in physiology, ed. Fedina, L., Kanyar, B., Kocsis, B. & Kollai M. 205-213. Budapest: Pergamon Press.

Eykhoff, P. (1974) System identification.
London : John Wiley and sons.

Falk, G. & Fatt, P. (1964) Linear electrical properties of striated muscle fibres observed with intracellular electrodes.
Proc. R. Soc. B 160: 69-123

Fatt, P. (1957) Sequence of events in the synaptic activation of a motoneurone.
J. Neurophysiol., 20, 61-80.

Fitch, J. (1975) CAMAL user's manual.
University of Cambridge Computer Laboratory.

FitzHugh, R. (1969) Mathematical models of excitation and propagation in nerve.
In: Biological Engineering, ed. H. P. Schwan., pp 1-85. New York: Mc Graw Hill.

FitzHugh, R. (1982) Nonlinear sinusoidal currents in the Hodgkin-Huxley model.
In: The Biophysical Approach to Excitable Systems., ed. W.J. Adelman ,Plenum Press, 25-35.

FitzHugh, R. (1983) Sinusoidal voltage clamps of the Hodgkin-Huxley model.
Biophys. J. 42: 11-16.

Foster, K. R., Bidinger, J. M. & Carpenter, D. O. (1976) The electrical resistivity of cytoplasm.
Biophys. J., 16, 991-1001.

French, A. S. (1976) Practical nonlinear system analysis by Wiener kernel estimation in the frequency domain.
Biol. Cybern. 24: 111-119.

French, A. S. & Di Caprio, R. A. (1975) The dynamic electrical behaviour of the electrotonic junction between Retzuis cells in the leech.
Biol. Cybern. 17: 129-135.

Gerald, C.F. (1978) Applied numerical analysis.
Addison - Wesley Publishing Company.

Gibson, J. (1983) Properties of glial cells in the leech nervous system.
Ph.d. thesis. University College London.

Gold, B. & Rader C. M. (1969) Digital processing of signals.
New York: McGraw Hill Book Co.

Gorman, A.L.F. & Mirolli, M. (1972) The passive electrical properties of the membrane of a molluscan neurone.
J. Physiol., 227, 35-49.

Graubard, K. (1975) Voltage attenuation within *Aplysia* neurons: the effect of branching pattern.
Brain Res. 88: 355-332.

Graubard, K. & Calvin, W. H. (1979) Presynaptic dendrites: implications of spikeless synaptic transmission and dendritic geometry.
In: The neurosciences fourth study program, ed. Schmitt, F. O. & Worden, F. G., pp. 317-331. Cambridge, Massachusetts: MIT Press.

Grove, T. M., Bekey, G. A. & Haywood, L. J. (1980) Analysis of errors in parameter estimation with applications to physiological systems.
Am. J. Physiol. 8: 390-400.

Guttmann, R., Feldman, L. & Lecar, H. (1974) Squid axon membrane response to white noise stimulation . Biophys. J. 14: 941-955.

Hamming, R. W. (1977) Digital Filters. Englewood Cliffs: Prentice-Hall.

Haydon, P. G. & Winlow, W. (1981) Morphology of the giant dopamine-containing neurone, R. Pe. D.1 in *Lymnaea Stagnalis* revealed by Lucifer yellow CH. J. Exp. Biol. 94: 149-157.

Haynes, L. W. & Kerkut, G. A. (1978) Passive and *active electrical properties of two giant neurones in Helix aspersa* Comp. Biochem. Physiol. 60A: 133-138.

Holden, A. V. (1976) Models of the stochastic activity of neurones. Lecture notes in Biomathematics 12. Berlin: Springer Verlag.

Holden, A.V. & Ramadan, S. M. (1981) Repetitive activity of a molluscan neurone driven by maintained currents: a supercritical bifurcation. Biol. Cybern. 42, 79-85.

Horwitz, B. (1983) Unequal diameters and their effects on time-varying voltages in branched neurons. Biophys. J., 41, 51-66

Horwitz, B. (1983) An analytic method for investigating transient potentials in neurones with branching dendritic trees. Biophys. J. 36, 155-192.

Iansek, R. & Redman, S.J. (1973) An analysis of the cable properties of spinal notoneurones using a brief intracellular current pulse. J. Physiol. 234: 613-636.

Jack, J. J. B., Noble, D., & Tsien, R. W. (1975) Electric current flow in excitable cells. Oxford: Clarendon Press.

Jack, J.J.B. (1979) An introduction to linear cable theory. In: The neurosciences fourth study program, ed. Schmitt, F. O. & Worden, F. G., pp. 423-437. Cambridge, Massachusetts: MIT Press.

Jack,J.J.B., and S.J.Redman. (1971) An electrical description of the motoneuron, and its application to the analysis of synaptic potentials. J.Physiol.(Lond.). 215:321-352

Johnston, D. (1981) Passive cable properties of hippocampal CA3 pyramidal neurones. Cell. Molec. Neurobiol. 1: 41-55.

Joyner, R. W., Westerfield, M., Moore, J. W. & Stockbridge. (1978) A numerical method to model excitable cells. Biophys. J. 22: 155-170.

Kerkut, G. A., Lambert, J. D. C., Gayton, R. J., Laker, J. A. & Walker, R. J. (1975) Mapping of nerve cells in the suboesophageal ganglia of *Helix aspersa*. Comp. Biocham. Physiol. 50A: 1-25.

Kerkut, G. A. & Meech, R. W. (1966) The internal chloride concentration of H and D cells in the snail brain. Comp. Biochem. Physiol 19: 819-832

Koch, C., Poggio, T. & Torre, V. (1982) Retinal ganglion cells: a functional interpretation of dendritic morphology. Phil. Trans. R. Soc. Lond. B. 298: 227-264

Krinskii, Y.I. & Kokoz, Yu.M. (1973) Analysis of excitable membranes - I. Reduction of the Hodgkin- Huxley equations to a second order system. Biofizika, 18, 506-541.

Lanczos, C. (1956) Applied Analysis. Englewood Cliffs, N.J.: Prentice-Hall.

Lane, N.J. & Swales, L.S. (1976) Interrelationship between golgi, gerl and synaptic vesicles in the nerve cells of insect and gastropod ganglia. J. Cell Sci. 22: 435-453.

Lapique, L. (1907) Recherches quantitives sur l'excitation electriques des nerfs, traitee comme un polarization. J. Physiol. Paris. 9: 622-635

Lederer, W. J., Spindler A. J. & Eisner, D. A. (1979) Thick slurry bevelling: a new technique for bevelling extremely fine microelectrodes & micropipettes. Pfluger Archiv. 381: 287-288.

Lee, Y.W. & Schetzen, M. (1966) Measurement of the Wiener kernels of a nonlinear system by cross- correlation. Int. J. Control, 2, 237-254.

Lucas, K. (1917) The conduction of the nervous impulse. Cambridge: Cambridge University Press.

Magchielse, T., Hooisma, J. & Muijser, H. (1981) Measurement of the electrotonic length constant in cultured muscle fibres. J. Neurosci. Methods. 4: 157-161

Maiskii, V. A. (1965) Electrical characteristics of surface membranes of the giant nerve cells of *Helix pomatia* Fiziol. Zh. SSSR. 49: 1468-1471.

Marmarelis, P.Z. & Marmarelis, V.Z. (1978) Analysis of physiological systems: the white-noise approach. N.Y.: Plenum.

Marr, D. C. & Poggio, T. (1977) From understanding computation to understanding neural circuitry. Neurosciences. Res. Prog. Bull. 15: 470-488.

Mars, P. & Poppelbaum, W. J. (1981) Stochastic and deterministic averaging processes. Peter Peregrinus.

McCulloch, W. S. & Pitts, W. H. (1943) A logical calculus of ideas immanent in nervous activity. Bull. of Math. Biophys. 5: 115-133.

Meech, R. W. (1979) Membrane potential oscillations in molluscan "burster" neurones. J. Exp. Biol. 81: 93-112.

Meves, H. (1968) The ionic rquirements for the production of action potentials in *Helix pomatia* neurones. Pflugers Arch. 304: 215-241.

Nelson, P.G. & Lux, H.D. (1970) Some electrical measurements of motoneuron parameters. Biophys. J., 10, 55-73.

Nguyen, V. V. & Wood, E. F. (1982) Review and unification of linear identifiability concepts. SIAM Rev. 24: 34-51

Nicola, V. F., van de Ven, H. H. & Eykhoff, P. (1980) Influences of the input signal in non-linear parameter estimation Int. J. Systems Sci. 8: 961-984.

Noble, D. & Stein, R.B. (1966) The threshold condition for initiation of action potentials by excitable cells. J. Physiol., 187, 129-162.

Norman, R.S. (1972) Cable theory for finite length dendritic cylinders with initial and boundary conditions. Biophys. J. 12, 25-45.

Palm, G. (1978) On representaion and approximation of nonlinear systems. Biol. Cybern. 31: 119-124.

Poggio, T. & Torre, V. (1978) A new approach to synaptic interaction. In: Theoretical approaches to complex systems. Lecture notes in biomathematics, vol 21., ed. Heim, R. & Palm, G. 89-115. Springer Verlag.

Rall, W. (1962) Theory of physiological properties of dendrites. Ann. N.Y. Acad. Sci. 96: 1071-1092.

Rall,W. (1959) Branching dendritic trees and motoneuron membrane resistivity. Exp. Neurol. 1:491-527

Rall,W. (1960) Membrane potential transients and membrane time constant of motoneurons.
Exp. Neurol. 2:503-532

Rall,W. (1969) Time constants and electrotonic length of membrane cylinders and neurons.
Biophys.J. 9:1483-1508

Rall,W. (1977) Core conductor theory and cable properties of neurones
In Handbook of Phsiology (Sect.1) The Nervous System.I. Cellular Biology of Neurons. E.R.Kandel, editor .Am.Pysiol.Soc.,Bethesda, Md. 39-97

Roberge, F. A., Jacob, R., Gulrajani, R. M. & Mathieu, P.A. (1977) A study of isopotentiality in *Aplysia* neurons.
Can. J. Physiol. Pharnacol. 55: 1162-1169.

Roberts, A. & Bush, B. M. H. (eds.) (1981) Neurones without impulses.
Cambridge: Cambridge University Press.

Schetzen, M. (1980) The Volterra and Wiener theories of nonlinear systems.
New York: Wiley.

Siegler, M. V. S. & Burrows, M. (1979) The morphology of local non-spiking interneurones in the metathoracic ganglion of the locust.
J. Comp. Neurol., 183, 121-148.

Sigvardt, K. A., Hagiwara, G., & Wine, J. J. (1982) Mechanosensory integration in the crayfish abdominal nervous system: structural and physiological differences between interneurones with single and multiple spike initiation sites.
J. Comp. Physiol., 148, 143-157.

Skaugen, E. & Walloe, L. (1979) Stochastic activity of a Hodgkin-Huxley membrane with a finite number of ionic channels.
Acta. Physiol. Scand., 107, 343-363.

Stewart, W. W. (1978) Functional connections between cells as revealed by dye-coupling with a highly fluorescent napthalmide tracer.
Cell, 14, 741-759.

Stinnakre, J. & Tauc, L. (1969) Central neuronal response to the activation of osmoreceptors in the osphradium of *Aplysia*
J. Exp. Biol., 51, 347-361.

Swadlow, H. A., Kocsis, J. D. & Waxman, S. G. (1980) Modulation of impulse conduction along the axonal tree.
Ann. Rev. Biophys. Bioeng. 9: 143-179.

Swanson, G. D. (1977) Biological signal conditioning for system identification.
Proc. IEEE 65: 725-740.

Tauc, L. (1962) Site of origin and propagation of spike on giant neuron of *Aplysia*.
J. Gen. Physiol., 45, 1077-1097.

Valdiosera, R., Clausen, C. & Eisenberg, R. S. (1974) Measurement of the impedance of frog skeletal fibers.
Biophys. J. 14: 295-315.

Verveen, A. A. & De Felice, L. J. (1974) Membrane noise.
Prog. Biophys. Mol. Biol. 28: 189-265.

Victor, J. and Shapley, R. (1980) A method of nonlinear analysis in the frequency domain.
Biophys. J., 29, 459-484.

Wiener, N. (1959) Nonlinear problems in random theory.
The Technology Press of MIT. and Wiley, New York

Winlow, W. A. & Kandel, E. R. (1976) The morphology of identified neurones in the abdominal ganglion of *Aplysia Californica*.
Brain Res. 112: 221-249.

Zierler, K. (1981) A critique of compartmental analysis.
Ann. Rev. Biophys. Bioeng. 10: 531-562.

Zimmerman, U. (1982) Electronic field-mediated fusion and related electrical phenomena.
Biochem. Biophys. Acta. 684, 227-277.